

UNIVERSITÀ POLITECNICA DELLE MARCHE

Facoltà di Ingegneria

Corso di Laurea Magistrale in Environmental Engineering

Dipartimento di Scienze ed Ingegneria della Materia, dell'Ambiente ed  
Urbanistica



A TRANSIENT DENSITY DEPENDENT TRANSPORT MODEL TO  
ELUCIDATE SALINIZATION PATTERNS IN THE VOLTURNO RIVER  
AQUIFER

Master Thesis of:  
**Ofori Abraham**

Relator:  
**Dott. Nicolò Colombani**

Corelator:  
**Prof. Matteo Postacchini**

Academic year 2023/2024

# INDEX

1.0 INTRODUCTION.....	5
2.0 MATERIALS AND METHODS .....	8
2.1 Study Area .....	8
2.2 Model Setup .....	11
2.3 HEC-RAS Setup .....	12
2.4 Processing MODFLOW.....	16
2.5 MODFLOW.....	16
2.6 SEAWAT.....	19
2.7 Model Setup .....	21
2.8 The Models Menu   MODFLOW Menu .....	31
2.9 SEAWAT.....	47
3.0 RESULTS AND DISCUSSION .....	60
3.1 HEC-RAS Results .....	60
3.2 River Salinization by Tidal Forcing and Seawater Ingression .....	60
3.3 SEAWAT Results .....	63
3.4 Heads contours results.....	63
3.5 Maps and Heads in selected piezometers.....	69
3.6 Water Fluxes.....	77
3.7 Seawater Intrusion Assessment .....	84
4.0 CONCLUSION.....	98
5.0 REFERENCES.....	99

## LIST OF ACRONYMS

BCF	Block Centred Flow
CA	Cancello ed Arnone
CC	Climate Change
CFM	Centro Funzionale Multirischi
CI	Campanian Ignimbrite
CMDS	Copernicus Marine Data Store
CV	Castle Volturno
DTM	Digital Terrain Model
FRC	Flood Rating Curve
GCSM	General Constituent Simulation Model
HEC-RAS	The Hydrologic Engineering Centre's– River Analysis System
ISPRA	Istituto Superiore per la Protezione e la Ricerca Ambientale
LPF	Layer Property Flow
MODFLOW	Modular Finite-Difference Flow Model
NYT	Neapolitan Yellow Tuff
PM	Processing MODFLOW
RS	Remote Sensing
SWI	Seawater Intrusion
VAP	Volturno Alluvial Plain
VE	Volturno Estuary
VR	Volturno River

## ABSTRACT

Aquifer salinization is a widespread problem that affects groundwater quality and its usage in coastal areas. The main mechanisms of aquifer salinization are: the classical seawater wedge along the coasts, preferential pathways through rivers and canals or by paleo salinity. To assess the salinization of the final reach of the Volturno river aquifer, surface water modelling coupled with density dependent groundwater modelling were employed to determine the predominant cause of the aquifer salinity. HEC-RAS numerical model was used to determine the salinity along the river channel and the river stages from the river mouth to Cancellone ed Arnone (approximately 13 km) for a hydrologic decade (2010 to 2020). Salinity and river stages results obtained from the HEC-RAS simulations were thereafter used as input data in addition to gridded recharge and evapotranspiration data from ISPRA into a SEAWAT numerical model. The SEAWAT model was downscaled from a validated MODFLOW model for the entire Campania Region. The SEAWAT model domain extended from the Agnena and Regi Lagni channels covering an area of approximately 91 km<sup>2</sup>. The direction of flow and piezometric heads within the aquifer during the period of study were directed towards the wetlands and swampy areas along the sides of the Volturno river channel, moreover hydraulic heads within the aquifer were observed to be gradually declining due to low recharge events and increased evapotranspiration due to global warming. The SEAWAT model balance determined that the rate of freshwater inflow into the river by the aquifer is gradually declining, whereas the aquifer salinization is increasing mainly by the Volturno river leakage during droughts. A numerical scenario was implemented in SEAWAT using the results of recent study that characterized the groundwater salinity distribution in the area, comparison between the aquifer salinization by actual seawater intrusion and paleo salinity were made and quantified. It was ascertained that the main cause of aquifer salinization is due to paleo salinity, and the relative importance of the various salinizing mechanisms is: paleo seawater presence >> seawater ingress in the Volturno river >> seawater wedge along the coast > evapoconcentration via evapotranspiration processes.



## 1.0 INTRODUCTION

Groundwater resources play a crucial role in sustainable development and effective water resource management, serving as the primary source of freshwater (Mirzavand et al., 2014; Mirzavand and Ghazavi, 2015). Nearly half of the world's drinking water and a large portion of the world's irrigated water supply come from groundwater (Simlandy, 2015). Many regions rely on groundwater for irrigation, especially during dry seasons, enhancing crop yields and ensuring food security. Furthermore, industries often utilize groundwater for manufacturing processes, emphasizing its economic importance (Roy, 2015; Simlandy, 2015). Moreover, groundwater sustains ecosystems by maintaining base flow in rivers and wetlands, even during dry periods (Yao et al., 2018).

While groundwater is a valuable resource, over-extraction and contamination pose significant challenges. The increasing demand for water, driven by population growth and exacerbated by climate change (CC), has led groundwater quantity and quality to decrease in many aquifers in the world during the last decades (Aeschbach-Hertig & Gleeson, 2012; Lal et al., 2018). More specifically, these effects are emphasized in the semi-arid zones and delta areas along which many human activities are concentrated (Vaux, 2011). The current groundwater resources are already insufficient in many areas to meet the constant demand of industries, agriculture, urbanization, and the environment.

One of the most important reasons of diminishing groundwater quality in coastal aquifers is groundwater salinization (Vengosh et al., 2003). The infiltration of ocean water into fresh groundwater, which results in the groundwater becoming contaminated with salt, is called seawater intrusion (SWI). SWI occurs in virtually all coastal aquifers worldwide because of the differences in density between fresh and saltwater. This is because seawater is denser than freshwater due to its higher mineral content (Johnson, 2007; Xu et al., 2021).

Although it is a natural process, human activity has the potential to exacerbate this process. In many coastal areas, SWI has risen due to human activity, particularly groundwater pumping from freshwater wells along the coast (Johnson, 2007; Parisi et al., 2018; Xu et al., 2021). A multitude of wells drilled for irrigation can increase the wide cone of depression created by the massive water overdraft, which can lead to water quality deterioration (Teatini et al., 2001).

On the other hand, CC is likely to reduce freshwater resources by causing meteorological droughts that propagate to groundwater systems, leading to below-normal groundwater levels which can possibly initiate or worsen SWI phenomena (Eswar et al., 2021; Richardson et al., 2024).

SWI may occur directly within coastal aquifers or through surface water bodies connected to the sea. In fact, rivers together with agricultural, and drainage canals are additional factors that could trigger SWI since they offer preferential pathways for saltwater to flow inland. Interaction between groundwater and surface water bodies is considered to have significant effects on aquifer salinization (Ferguson and Gleeson, 2012; Hussain et al., 2019; Cao et al., 2020).

Since deltas and estuaries are typically regarded as the fast-evolving landforms because of their sensitivity to sea level changes during the postglacial period. Rapid sea level rise in the late Pleistocene led to marine transgression in river valleys and coastal areas, followed by a shift to regression after the mid-Holocene and the development of deltas and estuaries after sea-level rise ceased, which is a characteristic feature of the Mediterranean Sea, since the Mediterranean Sea is associated to the freezing and melting of ice shields during the Quaternary period (Gossel et al., 2010; Yu et al., 2023). For instance, during the Holocene, global eustatic changes and sediment supply drove the formation of the Volturno coastal plain along the Tyrrhenian Sea in the Mediterranean (Ruberti et al., 2022). The primary processes of salinization in the Quaternary delta involve the salinization of open waterways and fresh groundwater. Furthermore, lateral, and vertical SWI and infiltration are the primary mechanisms by which coastal aquifers become salinized (Paldor & Michael, 2021).

Mixing behaviours in estuaries are complex and influenced by several factors, including the river discharge, wind and tidal currents, and the geographical features of the estuary. Stronger tidal currents due to storm surge and reduced river discharge due to droughts are associated with severe SWI events and consequently with thicker saltwater wedges (McLusky & Elliott, 2004; Tarolli et al., 2023)

To ensure the sustainable use of groundwater, integrated water management practices are crucial. This involves monitoring several surface- and ground-water parameters, implementing water conservation measures, and establishing regulations to prevent over-extraction and pollution.

Nowadays, numerical models represent a valuable tool for hydrogeologists to better understand SWI and predict saltwater contamination in coastal aquifers. Models are employed to evaluate the existing conditions of groundwater and surface water resources, forecast their responses to alterations in land use and climate, and create management strategies to preserve and safeguard both types of water resources (Bonumà et al., 2015).

To simulate SWI numerically, a groundwater flow model that considers density-dependent conditions is necessary. This model tracks the movement and evolution of the transition zone between fresh and saltwater (Lu et al., 2013; Kourgialas et al., 2016).

Various models, such as SUTRA, FEFLOW, MT3DMS and SEAWAT, aid in forecasting groundwater flow and contaminant transport (Anderson et al. 2015). These models address either groundwater flow and contaminant transport equations (Bear & Cheng, 2010).

In this study, the coastal aquifer of the Volturno alluvial plain (VAP) in the Campania Region (Italy) was modelled to better characterize the salinization processes involved. The model was implemented in Processing Modflow 11 (PM11) graphical user interface. A transient groundwater flow simulation was carried out using the MODFLOW 2005 code over a simulation period of 10 years (2010-2020). Then, to simulate the salt transport within the aquifer the SEAWAT code was employed. MODFLOW and SEAWAT are used in a wide variety of applications, including investigating the effects of CC on groundwater resources and modelling the movement of solutes in groundwater systems (Guo & Langevin, 2002).

Recent developments in remote sensing (RS) have provided new opportunities to create spatially distributed input parameter sets and constrain groundwater models (Thakur et al., 2016). Both in situ and RS high-resolution transient observation datasets (including groundwater recharge, evapotranspiration, sea, and river levels etc..) were used to inform and calibrate the model.

Water quality models such as MIKE, Delft 3D, EFDC and Tuflow are widely used and very important to predict the changes in surface water quality for environmental management. HEC-RAS and QUAL 2K water quality models were integrated to simulate the impact of tidal effects on water quality (Wang et al., 2013). Water surface profiles of a river can be estimated with HEC-RAS simulations for different storm events and the inundation of flood prone areas can also be predicted (Yang et al., 2006; Tamiru & Dinka, 2021).

In addition, the Volturno River (VR) contribution to SWI was estimated by performing a one-dimensional hydrodynamic and water quality analysis. The Hydrologic Engineering Centre's River Analysis System (HEC-RAS) developed by USACE (2016) was used to model the hydrodynamic of the final reach of the river. While the general constituent simulation module (GCSM) was used to simulate salinity as a single parameter and evaluate its distribution along the river reach. Results of such a simulation were used to feed the SEAWAT three-dimensional model, allowing for a better characterization of the surface- ground-water salt exchange.

Furthermore, Manfreda et al (2023) examined flood processes in Southern Italy, by reconstructing the time-series of peak flood discharges utilizing flood rating curves (FRC). The

FRC obtained from statistical data and analysis from the final reach of the VR was calibrated with HEC-RAS simulations. In addition, Gaiolini et al (2023) assessed the salinisation of the final reach of the VR by combining HEC-RAS modelling and spectral analysis for a hydrologic year.

The implemented transient numerical model helped to have a comprehensive understanding of the salinization dynamic of the analysed coastal aquifer, enabling for an accurate groundwater and mass balance calculation. As global water challenges intensify, having such a tool is crucial in supporting authorities to make informed decisions and minimize the impact on water quality and public health.

## 2.0 MATERIALS AND METHODS

This study deals with density-dependent transient groundwater flow simulations to assess the level of salinization of the final reach of the Volturno aquifer using numerical models. To achieve this goal, several parameters (hydrometric heights, sea heights, river recharge, evapotranspiration, etc) were implemented in the model using RS from 2010 to 2020.

To obtain the river salinity along the river reach, HEC-RAS was used to model the hydrodynamics of the river reach under consideration whereas the GCSM was used to simulate the river salinity as a single parameter and evaluate its distribution along the river reach.

To numerically simulate the groundwater flow, PM 11 produced by Simcore Software (2022) which also incorporates SEAWAT codes to simulate density-dependent groundwater flow variations was utilized. With this at hand, the model for the coastal aquifer for the Volturno was created. Details of the materials and methodologies that were employed for this study are fully described in this section in addition with the model characterisations analysing all the inputs.

### 2.1 Study Area

Originating at an elevation of approximately 1,300 meters, the VR starts flowing from the province of Isernia in, Molise, (Italy), in the Mount Serra Grande massif. Before emptying into the Tyrrhenian Sea at Castel Volturno (CV), Campania, Italy, the river flows for a total of 149 kilometres. Approximately 41°05'10"N 14°04'42"E are the coordinates of the river mouth (Rapporto sullo stato dell'ambiente (2020); Autorità di Bacino del Fiume Volturno, 2018).

Tectonic activity has shaped the final reach of the VR's complicated geology over a long period of time. The river passes through several geological formations, such as the Neapolitan Basin, the Phlegraean Volcanic District, and the Campanian Ignimbrite (CI). High-angle faults that

run at the base of carbonate slopes and have offsets of thousands of meters surround the plain of the VR, which is housed in a graben-like structure (Corrado et al., 2020; Gaiolini et al., 2022).

Since the beginning of an extensive volcanic activity and the localized development of extensional tectonics across the continental margin in the mid-late Pleistocene, the area has been mostly buried by sea water. Approximately 55 m deep, the CI is a vast region of volcanic rock that originated about 39,000 years ago. A substantial ash dump from Mount Somma's eruption coated the surrounding area. The plateau that the VR passes over was formed by this extensively weathered ash deposit. A further eruption that occurred about 15,000 years ago resulted in the Neapolitan Yellow Tuff (NYT), another ignimbrite deposit. The majority of the Quaternary volcanoclastic products that are emerging in the Campania Plain are found in the Tuff units (NYT) and associated ash deposits. The paleo-VR severely degraded these deposits because of the sea level dip during the Last Glacial Maximum (Matano., 2018; Busico et al., 2021).

A prominent embayment formed near the mouth of the paleo Volturno estuary (VE), along with a landward enlargement of the continental shelf, were the results of the most recent Pleistocene-early Holocene sea-level rise, which also produced a rapid flooding of the lower paleo-Volturno incised valley. A wave-dominated delta system with flanking strand plains generating beach-dune systems that partially enclose shallow lagoons and marshes was made possible by a coastal pro-gradation phase that was developed at the end of the transgression phase. The Holocene sedimentary development essentially inherited the current morphology. The mouth of the VR is a low-lying region with semipermanent water bodies (wetlands and lagoons) with a mean ground elevation above sea level (a.s.l.) of roughly  $-2.0$  to  $4.0$  m. Here, silt lens is stacked between sand dunes and serves as the aquifer's host (Matano et al., 2018; Busico et al., 2021).



Figure 1 Satellite view showing the main features of the area of study (Source: Gaiolini et al., 2023).

Since most of the marshy coastal plain lands were reclaimed beginning in the sixteenth century, there has been a significant increase in farming and agriculture as well as urbanization along the coastal zone (Matano et al., 2018; Gaiolini et al., 2022).

For the purposes of this study, the lower VR alluvial plain was considered, comprising the last 13 km of the river reach, whereas longitudinally, the study area borders the Agnena and the Regi Lagni canals. Approximately the study area has a perimeter of 38.74 km and an area of 90.86 km<sup>2</sup>.

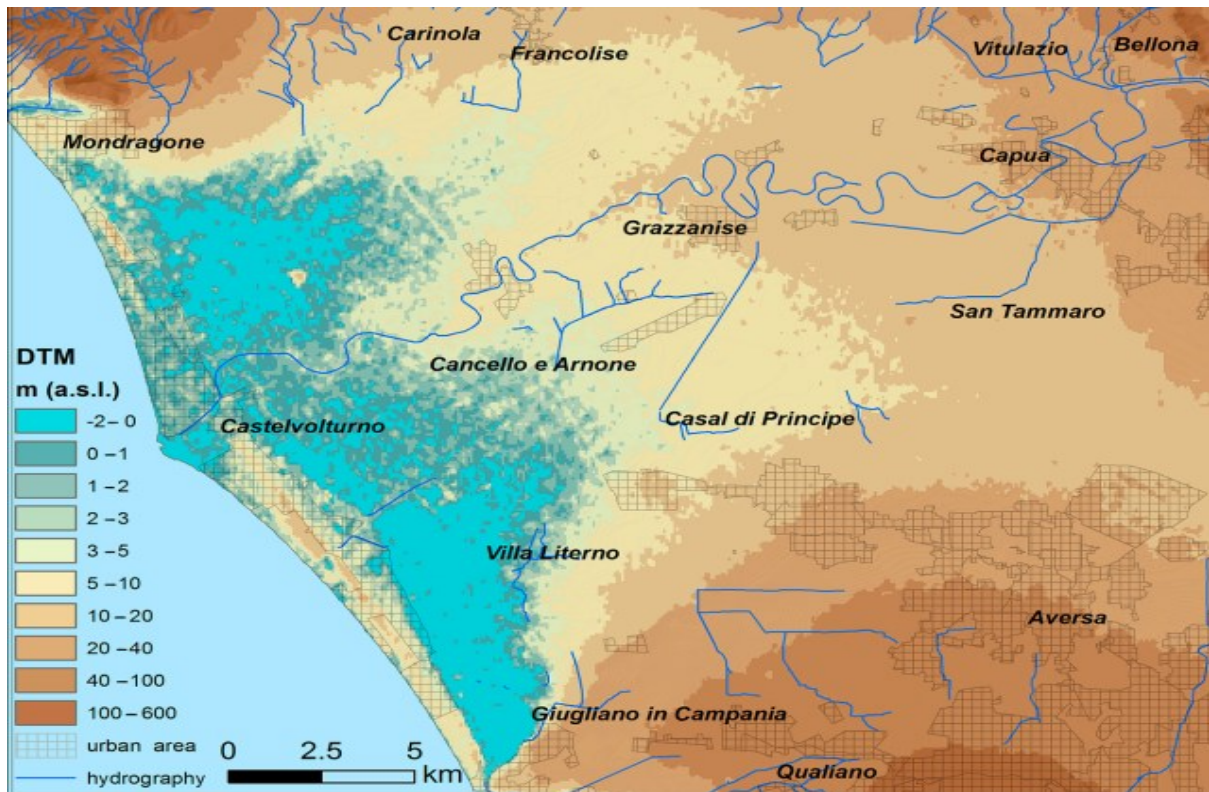


Figure 2 Altimetry classes of the Volturno Plain from Digital Terrain Model with 70-m cell size (Source: Matano et al., 2018).

## 2.2 Model Setup

To achieve a density-dependent model for the VR aquifer, the salinity along the river reach from Cancellone e Arnone (CA) to CV needed to be determined. Moreover, there exist no field salinity data from 2010 to 2020 for the final reach of the VR. For this reason, RS data were employed to obtain the salinity along the river with the help of HEC-RAS environment, the obtained salinity data from the HEC-RAS were thereafter inputted into the PM 11 model to further assess the salinisation of the VR aquifer.

## 2.3 HEC-RAS Setup

Hydrometric levels of the river at the CV and CA stations were obtained from the Centro Funzionale Multirischi (CFM, 2023) della Protezione Civile Regione Campania, spanning from 1st January 2010 to 31st December 2020. The daily data were monthly averaged according with the temporal resolution used in the MODFLOW simulation.

About RS, the daily averaged height of the sea from 1<sup>st</sup> January 2010 to 31<sup>st</sup> December was obtained from Copernicus Marine Data Store (CMDS). The MATLAB environment was used to read the Copernicus data (Ferris, 2020) and then transformed into monthly averages.



A digital terrain model (DTM) with a spatial resolution of 2x2 m cells was utilized to extract topographic data and depict the topography of the Volturno alluvial plain (Gaiolini et al., 2023). Projections relative to the EPSG: 32633 coordinate system were fixed in GIS environment and the merged DTM was imported in RAS-Mapper interface. EPSG:32633 is a coordinate reference system that is used in GIS to represent geographic data in the VE.

HEC-RAS supports either a single terrain model or multiple terrain files that cover the area of interest. Moreover, HEC-RAS increase the efficiency of model analysis and refinement by allowing the use and visualization of geospatial data, along with RAS simulation results, within a single modelling environment (Ackerman et al., 2010), permitting the model's setup using national open-access datasets.

The model geometry was formulated, sketching the final reach of the river, together with the left and right overbanks and cross sections in a RAS-Mapper environment. Actual cross-sections in the .dwg format that were retrieved from the local basin authority were processed in a GIS environment and imported as shapefiles into RAS-Mapper. Levees were placed on the topographical elevations according to the DTM and the Google Earth 2014 view. Bridges have been incorporated into the model, with uncertainty on the breadth of the bridge deck and the quantity and size of piers in the Google Earth 2014 perspective. In the bridge modelling, a value of 1.2 and 0.95 was assigned to drag and pier shape coefficients, respectively. Lastly, a value of 0.3 and 0.5, respectively, was assigned to the contraction/expansion coefficients in the upstream and downstream sections of each bridge. Since the bridge piers affect the flow motion both upstream and downstream, these coefficients are especially significant when there are bridges (Subedi et al., 2019).



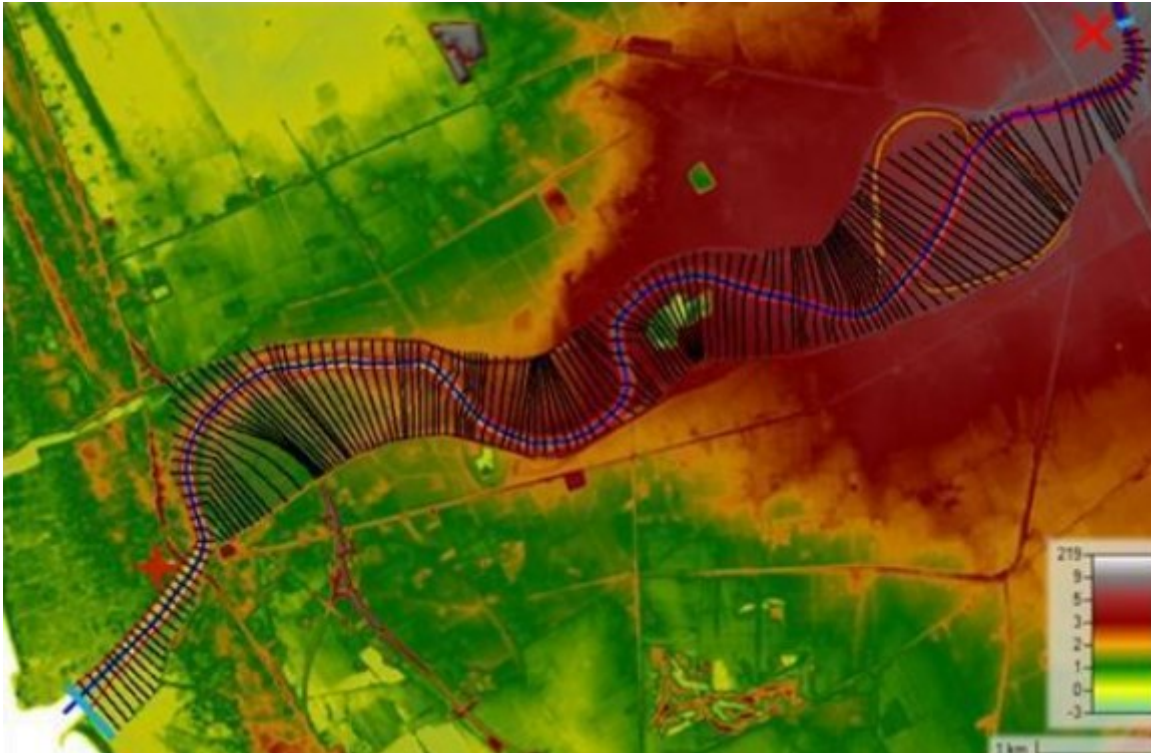


Figure 3 RAS-Map view of the model.

The estuarine salinity structure is caused by the effects of geometry, tidal variation, salinity difference between sea and river water, and freshwater discharge (Yoon & Woo, 2015). For this reason, the hydrodynamic regime was first studied performing a 1D unsteady flow simulation. In the hydrodynamics module, HEC-RAS solves the following 1D equations of continuity and momentum (Brunner, 2010):

$$\frac{\partial Q}{\partial x} + \frac{\partial A}{\partial t} - ql = 0, \quad (1)$$

$$\frac{\partial Q}{\partial t} + \frac{\partial \left( \frac{Q^2}{A} \right)}{\partial x} + gA \frac{\partial h}{\partial x} = gA \left\{ \left( \frac{n*Q^2}{A*R^{2/3}} \right)^2 - B \right\}, \quad (2)$$

where  $Q$  is the discharge;  $A$  is the cross-sectional area;  $x$  is the distance along the channel;  $t$  is the time;  $ql$  is the lateral inflow per unit length;  $g$  is the acceleration due to gravity;  $h$  is depth;  $B$  is the bottom slope;  $n$  is the Manning's roughness coefficient, and  $R$  is the hydrodynamic radius. The user of the software must define the bridge modelling approach and add boundary conditions to the model.

The stage hydrograph boundary conditions were assigned to the most upstream (CA river gauge) and the most downstream (at the mouth of the river) cross-sections as shown in the figure above. The hydrograph had daily resolution and were downloaded from CFM river gauges at CV and CA, the hydrograph was thereafter averaged for every month spanning from

2010 to 2020. Time series of Tyrrhenian Sea level data at VE were downloaded from CMDS with daily resolutions, and the monthly averages determined. The energy-based method (standard step method), which treats a bridge like a natural river cross-section except that the wetted perimeter is increased where the water encounters the bridge structure and the area of the bridge below the water surface is subtracted from the total area, was selected to calculate losses through the bridge (HEC, 2022). The simulation plan was designed to run the model over the whole hydrologic decade (2010–2020) while choosing a monthly output temporal resolution based on the boundary conditions.

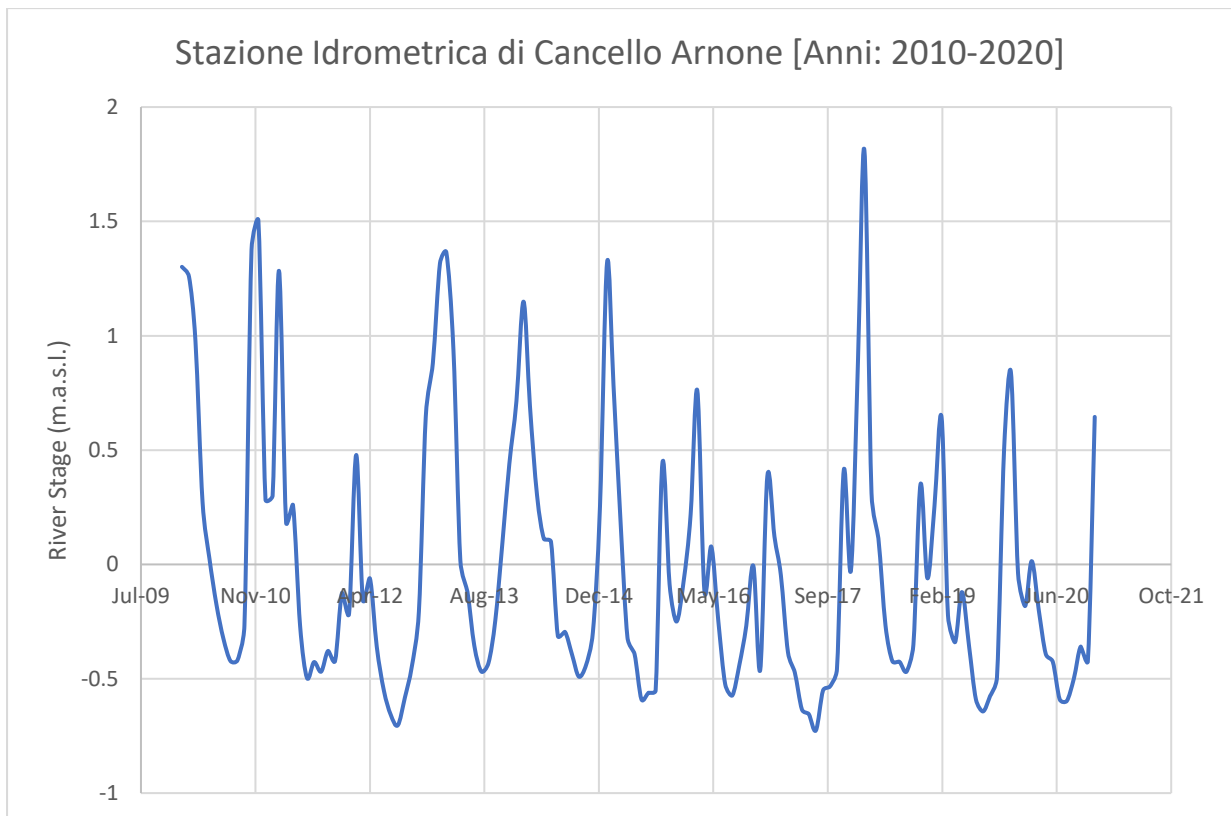


Figure 4 Averaged Hydrograph at the CA Station (Source: CFM, 2023).

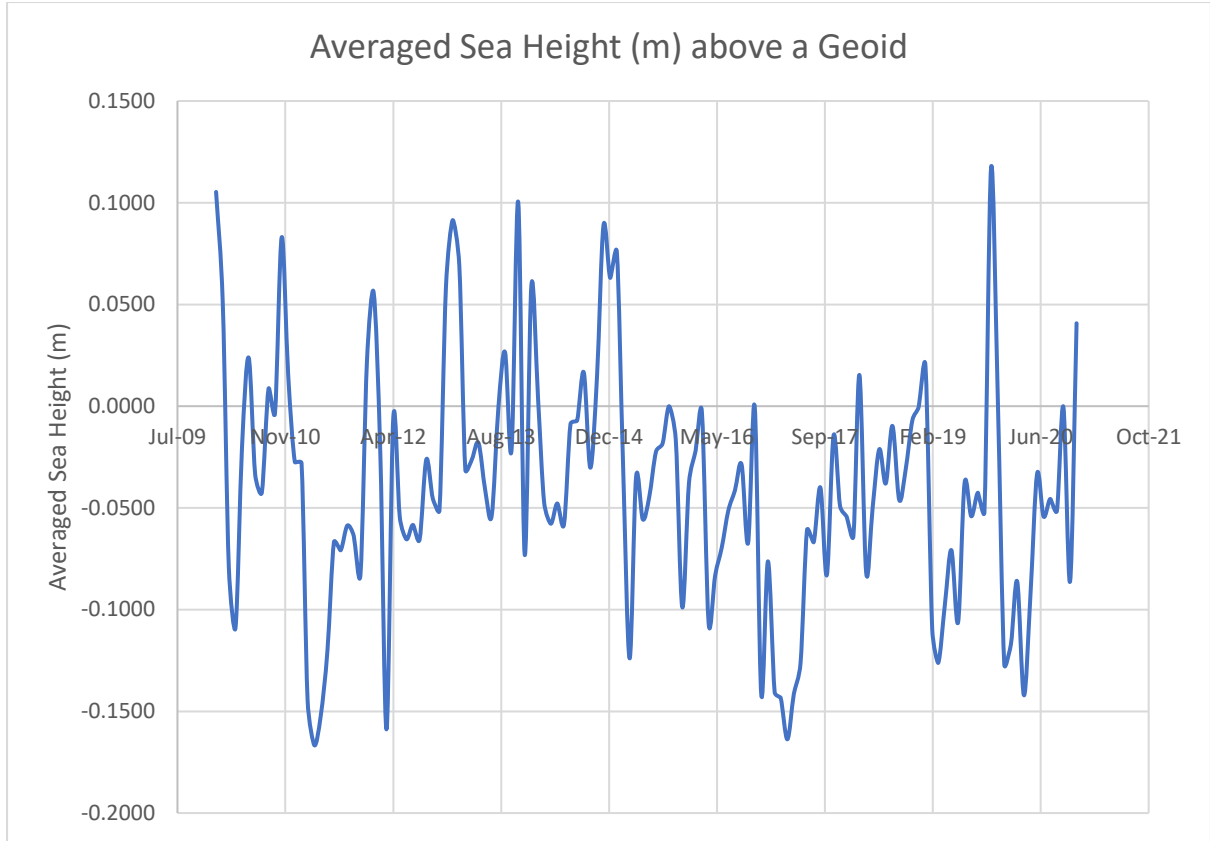


Figure 5 Averaged Sea Height (m) at the Estuary (Source: CMDS, 2023).

The HEC-RAS Water Quality module, which is based on the one-dimensional transport equation (advection-dispersion equation) of a conservative element, was used to model the evolution of salinity (Brunner, 2010):

$$\frac{\partial(AC)}{\partial t} + \frac{\partial}{\partial x}(VAC) = \frac{\partial}{\partial x} \left[ D_x A \frac{\partial C}{\partial x} \right] \quad (3)$$

where C is the salinity concentration;  $D_x$  is the longitudinal dispersion coefficient; V is the flow velocity. In the hydrodynamic analysis module, which is connected to the water quality model, velocity and water level were previously estimated. The longitudinal dispersion coefficient (D), which is determined by the equation below, and the boundary and initial conditions values of salinity concentrations must be entered by the user for the salinity concentration to be simulated as a single parameter in the GCSM.

$$D = 0.011 * \frac{v^2 w^2}{dv \sqrt{dg}} \quad (4)$$

where v is the longitudinal velocity; w is the stream top width; d is the hydraulic depth; and g is the acceleration due to gravity.

A freshwater salinity concentration value of 0.4 g/L, based on the analysis of the historical major ions concentrations at the Capua measuring station (ARPAC, 2023) was assigned to the

upstream boundary CA and a seawater salinity value of 38 g/L was assigned to the downstream boundary at the river mouth (Zhang et al., 2009; Sorgente et al., 2020). Values of  $8 \times 10^{-11}$  m<sup>2</sup>/s & 50 m<sup>2</sup>/s were assigned as upper and lower limits of D, estimated using Equation (4). The minimum value is representative of the sole molecular diffusion coefficient in water and the maximum value was sourced from Zheng & Huai (2014) that compiled a series of representative D values for rivers. Based on the unsteady flow simulation, the simulation plan was scheduled to run for the whole hydrologic decade (2010–2020).

## 2.4 Processing MODFLOW

PM 11, a Simcore Software was used for the numerical simulation of the salinity transformation from the surface water to the groundwater after the salinity variations along the river reach was simulated with HEC-RAS.

PM 11 was developed by Simcore Software in response to the need for a user-friendly graphical user interface (GUI) for MODFLOW (Simcore Software, 2022). During the early 2000s, Simcore Software started working on PM 11. The initial objective was to develop a GUI that would relieve the burden of writing code for users to build, run, and post-process MODFLOW models. In 2005, PM 11 was initially made available to the public. PM 11 now supports a wide range of MODFLOW features, including variable-density flow (SEAWAT), solute transport (MT3DMS), and heat transport (NWT). PM 11 also includes several features that make it easy to calibrate and post-process MODFLOW models.

The next paragraphs provide a description of every supporting program and set of codes utilized in the modelling of this case study, including the theoretical underpinnings.

## 2.5 MODFLOW

MODFLOW is the U.S. Geological Survey Modular Finite-Difference Flow model, which is a computer code that solves the groundwater flow equation. The program is used by hydrogeologists to simulate the flow of groundwater through aquifers. The software can model both steady and transient flow in a system where aquifer layers can be either unconfined, confined, or a combination of the two. The governing partial differential equation for a confined aquifer used in MODFLOW according to McDonald & Harbaugh (1988):

$$\frac{\partial}{\partial x} \left[ K_{xx} \frac{\partial h}{\partial x} \right] + \frac{\partial}{\partial y} \left[ K_{yy} \frac{\partial h}{\partial y} \right] + \frac{\partial}{\partial z} \left[ K_{zz} \frac{\partial h}{\partial z} \right] + W = S_s \frac{\partial h}{\partial t} \quad (5)$$

Where:

- $K_{xx}$ ,  $K_{yy}$  and  $K_{zz}$  are the values of hydraulic conductivity along the x, y, and z coordinate axes (L/T),
- $h$  is the potentiometric head (L) or hydraulic head (L),
- $W$  is a volumetric flux per unit volume representing sources and/or sinks of water, where negative values are extractions, and positive values are injections ( $T^{-1}$ ),
- $S_s$  is the specific storage ( $L^{-1}$ ) and
- $t$  is the time (T).

This, in conjunction with initial and boundary conditions, represents transient three-dimensional ground-water flow in an anisotropic and heterogeneous medium, assuming that the coordinate directions and principal axes of hydraulic conductivity are aligned (Harbaugh et al., 2000). MODFLOW solves the above equation (5) by means of the finite-difference method, the hydraulic head is calculated for each node of the model domain. To accomplish this, it requires the values specific storage and hydraulic conductivity in both the vertical and horizontal directions as inputs. It requires the boundary conditions characterization (i.e., the interaction between the domain area and its external environment), together with the initial conditions (i.e., values of the variable at initial time) to obtain a unique solution.

Three general types of boundary condition are considered in MODFLOW:

- *Specified head (Dirichlet Condition)*, in which heads are specified along the boundary for the entire duration of the stress period. It acts as a source or sink of water entering or leaving the model domain,
- *Specified flow boundary (Neumann Condition)*, which is implemented when the flow exchanged in the model domain is known,
- *Head-dependent flow or General Head Boundary (Cauchy Condition)*, which is a kind of combination of the previous ones, in which both heads and flow along the boundary are known.

The finite difference form of the partial differential in a discretized aquifer domain (represented using rows, columns and layers) is;

$$\begin{aligned}
& CR_{i,j-1/2,k}(h_{i,j-1,k}^m - h_{i,j,k}^m) + CR_{i,j+1/2,k}(h_{i,j+1,k}^m - h_{i,j,k}^m) \\
& + CC_{i-1/2,j,k}(h_{i-1,j,k}^m - h_{i,j,k}^m) + CC_{i+1/2,j,k}(h_{i+1,j,k}^m - h_{i,j,k}^m) \\
& + CV_{i,j,k-\frac{1}{2}}(h_{i,j,k-1}^m - h_{i,j,k}^m) + CV_{i,j,k+\frac{1}{2}}(h_{i,j,k+1}^m - h_{i,j,k}^m) \\
& + P_{i,j,k} * h_{i,j,k}^m + Q_{i,j,k} \\
& = SS_{i,j,k} * (\Delta r_j * \Delta c_i * \Delta v_k) * \frac{(h_{i,j,k}^m - h_{i,j,k}^{m-1})}{t^m - t^{m-1}} \quad (6)
\end{aligned}$$

Where:

- $h_{i,j,k}^m$  is the hydraulic head at cell  $i,j,k$  at time step  $m$ ,
- $CV$ ,  $CR$  and  $CC$  are the hydraulic conductances, or branch conductances between node  $i,j,k$  and a neighbouring node,
- $P_{i,j,k}$  is the sum of coefficients of head from source and sink terms,
- $Q_{i,j,k}$  is the sum of constants from source and sink terms, where  $Q_{i,j,k} < 0.0$ , is flow out of the groundwater system (such as pumping) and  $Q_{i,j,k} > 0.0$ , is flow in (such as injection),
- $SS_{i,j,k}$  is the Specific Storage,
- $\Delta r_j * \Delta c_i * \Delta v_k$ , are the dimensions of cell  $i,j,k$ , which, when multiplied, represent the volume of the cell and,
- $t^m$ , is the time at time step  $m$ .

MODFLOW is based on the following assumptions:

- a. Darcy's law, therefore, the flow is laminar,
- b. the standard expression for specific storage in a confined aquifer is applicable,
- c. the porous medium is assumed to be fully saturated with water and isothermal conditions prevail and,
- d. for a single, fully miscible liquid phase of very small compressibility is also assumed.

## 2.6 SEAWAT

SEAWAT is a computer program that simulates variable-density groundwater flow and transport. It is a companion model to MODFLOW and uses the same finite-difference method to solve the groundwater flow equation (Guo & Langevin, 2002).

The governing equation for flow and transport is:

$$\nabla * \left[ \rho \frac{\mu_0}{\mu} K_0 \left( \nabla h_0 + \nabla_z \frac{\rho - \rho_0}{\rho_0} \right) \right] = \rho S_{s,0} \frac{\partial h_0}{\partial t} + \theta \frac{\partial \rho}{\partial C} \frac{\partial C}{\partial t} - \rho_s q'_s \quad (7)$$

Where:

- $\rho_0$  is the fluid density ( $ML^{-3}$ ) at the reference concentration and reference temperature,
- $\mu$  is dynamic viscosity ( $ML^{-1}T^{-1}$ ),
- $K_0$  is the hydraulic conductivity tensor of material saturated with the reference fluid,
- $h_0$  is the hydraulic head ( $L$ ) measured in term of the reference fluid of a specific concentration and temperature,
- $t$  is Time ( $T$ ),
- $S_{s,0}$  is the specific storage ( $L^{-1}$ ),
- $\theta$  is the porosity,
- $C$  is salt concentration ( $ML^{-3}$ ),
- $q'_s$  is a source or sink ( $T^{-1}$ ) of fluid with density  $\rho_s$ .

This equation of state, which relates the fluid density to solute concentration, temperature, and pressure, is typically written as a function of the volumetric expansion coefficient for solute concentration ( $\beta_C$ ), temperature ( $\beta_T$ ), and pressure ( $\beta_P$ ), which are:

$$\beta_C = \frac{1}{\rho} \left( \frac{\partial \rho}{\partial C} \right)_{T, P}; \quad \beta_T = \frac{1}{\rho} \left( \frac{\partial \rho}{\partial T} \right)_{C, P}; \quad \beta_P = \frac{1}{\rho} \left( \frac{\partial \rho}{\partial P} \right)_{C, T} \quad (8)$$

where T is temperature (K) and P is pressure ( $ML^{-2}T^{-1}$ ) (Langevin et al., 2008).

To couple the solute-transport equation with the ground-water flow equation, SEAWAT employs either an explicit or implicit methods. Using the explicit method, the solute-transport equation is solved by using the advective velocity field that is obtained from solving the flow equation for each timestep. This procedure for alternately solving the flow and transport equations is repeated until the stress periods and simulation are complete. The flow and transport equations are solved repeatedly for the same timestep using the implicit approach for

coupling until the maximum difference in fluid density between successive iterations is less than a tolerance that the user specifies (Guo & Langevin, 2002).

SEAWAT is based on the assumptions that (a) Darcy's law is valid (laminar flow), (b) the standard expression for specific storage in a confined aquifer is applicable, (c) the diffusive approach to dispersive transport based on Fick's law can be applied, and (d) isothermal conditions prevail. The porous medium is assumed to be fully saturated with water. A single, fully miscible liquid phase of very small compressibility also is assumed (Guo & Langevin, 2002).

For a layer in which the storage coefficient remains constant during the simulation, the storage formulation is based on a direct application of the storage expression that applies to an individual cell,  $(i,j,k)$ . In MODFLOW, the storage expression has the form:

$$\frac{\Delta V}{\Delta t} = SS_{i,j,k} * (\Delta r_j * \Delta c_i * \Delta v_k) * \frac{(h_{i,j,k}^m - h_{i,j,k}^{m-1})}{t^m - t^{m-1}} \quad (9)$$

where:

- $\Delta V/\Delta t$  is the volumetric rate of accumulation of water in the cell,
- $SS_{i,j,k}$  is the specific storage of the material in cell  $i,j,k$ , and
- $\Delta r_j, \Delta c_i, \Delta v_k$  are the cell dimensions.

In SEAWAT, the storage formulation has the form:

$$\frac{\Delta m}{\Delta t} = \rho_{i,j,k} SS_{i,j,k} * (\Delta r_j * \Delta c_i * \Delta v_k) * \frac{(h_{i,j,k}^m - h_{i,j,k}^{m-1})}{t^m - t^{m-1}} \quad (10)$$

where  $\Delta m/\Delta t$  is the rate of mass accumulation of water in the cell. Using the storage concept defined in MODFLOW, mass storage capacity,  $SC1_{i,j,k}$ , can be defined as:

$$SC1_{i,j,k} = \rho_{i,j,k} SS_{i,j,k} * (\Delta r_j * \Delta c_i * \Delta v_k) \quad (11)$$

The Equation above can be rewritten as follows:

$$\frac{\Delta m}{\Delta t} = SC1_{i,j,k} * \frac{(h_{i,j,k}^m - h_{i,j,k}^{m-1})}{t^m - t^{m-1}} \quad (12)$$



## 2.7 Model Setup

The initial steps in the groundwater modelling process requires defining the objectives of the model (salinization), choosing the computer code “PM11” and, after gathering the necessary data, creating a conceptual model of the system. Following the grid, the parameters and the model menu, it is possible to implement the various input needed in the simulation. Beneath are the brief descriptions of all the tools employed on the menu taskbar.

### 2.7.1 Units

PM and its supported numerical models, except for GSFLOW, require the use of consistent units throughout the modelling process. For example, if you are using length [L] units of meters and time [T] units of seconds, hydraulic conductivity will be expressed in units of [m/s], pumping rates will be in units of [m<sup>3</sup>/s] and dispersivity will be in units of [m]. The values of the simulation results are also expressed in the same units. However, inconsistent units may be used for concentration values. For example, you may use [mg/l] in a model with the length unit of [m]. In this case, the calculated concentration will be expressed in [mg/l] and the calculated mass (= volume x concentration) will be expressed in [m<sup>3</sup> x mg/l]. For this study meters (m) and seconds (s) were used for both length and time respectively.

### 2.7.2 Temporal Discretization

MODFLOW divides the total time length of a simulation into discrete stress periods, which are, in turn, divided into time steps. Once a model is created or imported, the stress periods and time steps can be edited in *Discretization > Time*. The model input parameters are assumed to be constant during a given stress period. For transient flow simulations involving multiple stress periods, the user has the option of changing parameters associated with most flow packages, such as River or Well, from a stress period to another. For transport simulations, the user may change mass-loading rates and source concentrations associated with the fluid sources and sinks. For the purposes of this study, 132 stress periods were utilized with each stress period representing a particular month within the period of 11 years of study with each year also having 3-time steps also representing a four-month period within a year.

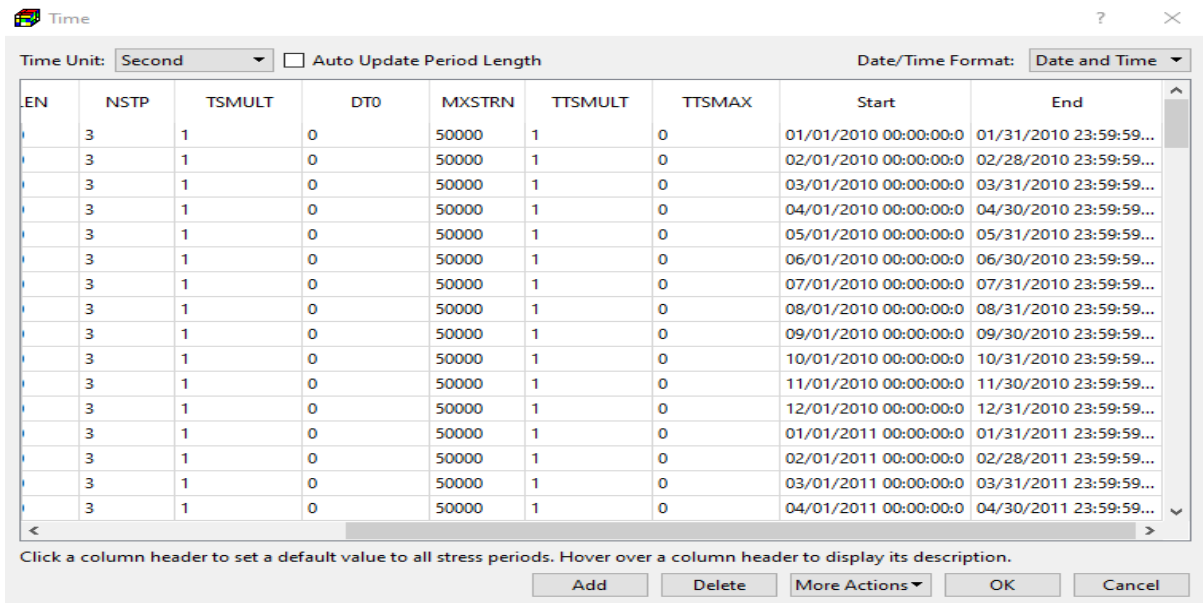


Figure 6 Dialog box indicating settings of Stress Periods

### 2.7.3 Spatial Discretization

In a MODFLOW model, an aquifer system is represented by a discretized domain consisting of an array of nodes and associated finite difference blocks (model cells). Hydrostratigraphic units can be represented by one or more model layers and the layer thickness may vary from cell to cell. The nodal grid forms the framework of the finite-difference numerical model. Once the head values are computed, they are used to calculate the cell-by-cell flow terms. The calculated head values and flow terms are the basis for water budget calculation, particle tracking, transport models, and visualization, such as flow vectors and contours.

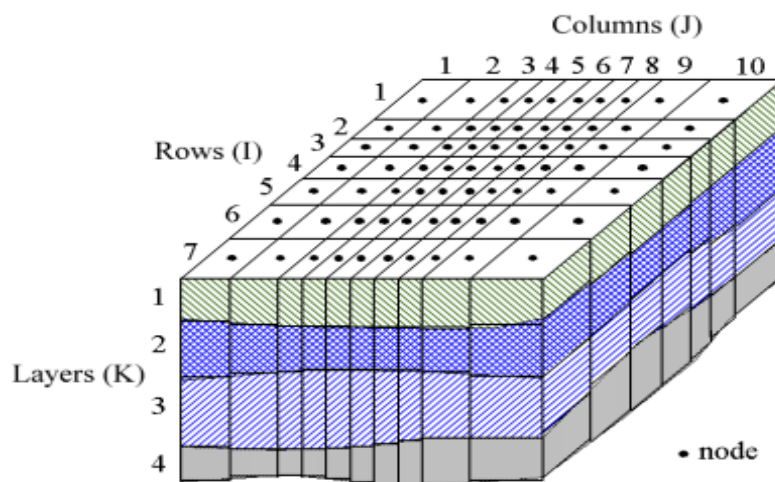


Figure 7 Spatial Discretization of a Modflow Model.

PM uses the index notation [Layer, Row, Column] to describe the location of a cell in a 3D array. For example, the cell located in the first layer, 6th row, and 2nd column is denoted by [1, 6, 2]. For 2D arrays, the index notation [Row, Column] is used. The numbers of layers, columns, and rows as well as column and row widths are defined when creating a new model or importing an existing model. These values can be modified with the Grid Editor. Model parameters (such as hydraulic conductivity or initial head) and features (such as well or river) are assigned to individual cells with the Data Editor. For this model, 7 equally layers thick, 90 rows, and 90 columns were employed [7, 90, 90].

#### 2.7.4 Grid Editor

The Grid Editor is used to adjust the finite difference model grid. By separating columns and/or rows, the user can refine the model grid or change the widths of the columns and/or rows, select *Discretization > Grid*. To adjust the width of a column or row and/or refine the grid, either right-click on the cell requiring modification or move the grid pointer to the cell using the arrow keys, then hit Enter. The dialog box for Grid Size is presented as seen in the figure below. To accept the modifications, make changes to the values in the Grid Size dialog box and click OK. To end the Grid Editor, click the Finish Edit button on the tool bar select *Tools > Finish Edit*. For this study, the rows and columns had square sizes of 146.667 by 146.667 m.

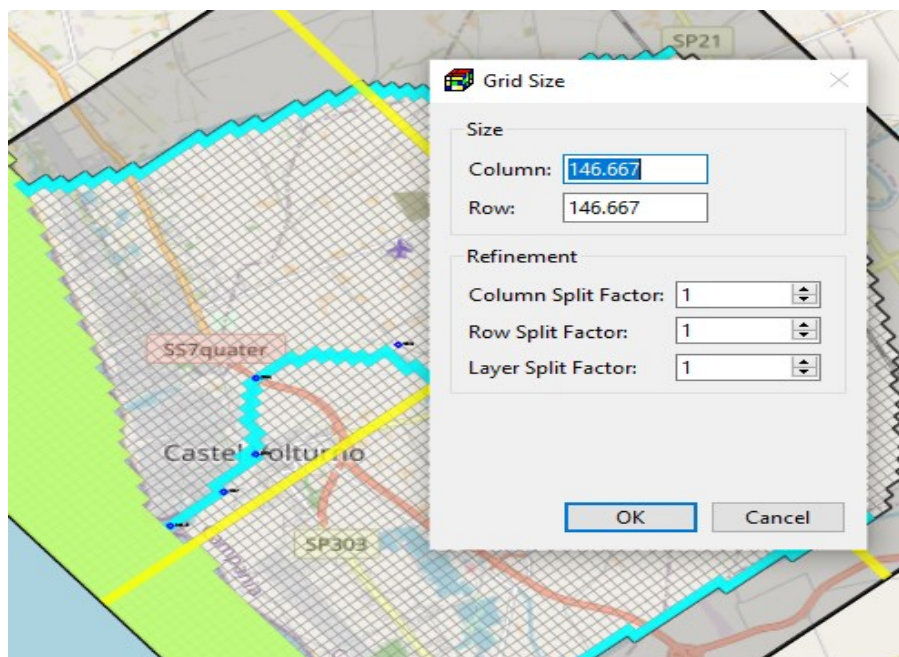


Figure 8 Grid Size dialog box.

### 2.7.5 Data Editor

The Data Editor is used to assign model parameters, such as HK, VK, drain, well, etc., to individual model cells. The Data Editor provides three input methods for most model parameters. The Cell-by-cell input method can be used to assign values to model cells directly or the Polyline or Polygon input methods can also be employed to help assigning model parameter to model cells. Regardless of the input methods being used, PM always use the cell-by-cell model parameters in the simulation. To start the Data Editor, select a menu item from the Discretization, Parameters, or Models menu and to end the Data Editor, click the Finish button on the toolbar or select *Tools > Finish Edit*.

### 2.7.6 Polyline Input Method

To activate this input method, select *Tools > Polyline Tool* or click the Polyline button on the toolbar and if the Pan tool is not activated, activate it too by clicking on the Pan button on the toolbar or selecting *Tools > Pan Tool*. The use of this input method is straightforward. Firstly, add polylines to the Map Viewer, assign data to one or more vertices of the polylines, and then apply the vertex data to model cells along the polylines by means of linear interpolation. To assist in editing polylines, the Polyline Tool has two popup menus, the Polylines menu, and Polyline Data menu. The Polylines menu contains functions related to all polylines and can be opened by right-clicking on the Map Viewer. The Polyline Data menu contains functions related to an existing polyline and can be opened by right-clicking on a vertex of that polyline.

### 2.7.7 Layer Property

The layer properties are defined the Layer Property dialog box in the figure below, Layer Type affects the numerical formulation of the groundwater flow equation. The available options and required parameters depend on the select internal flow package. It should be note that S, Ss, and Sy are used only in transient flow simulations. The settings of the dialog box depend on the selection of the Block Centred Flow (BCF) and Layer Property Flow (LPF) packages, when the LPF packages are selected, the columns of Transmissivity (T), Vertical Leakance (VCONT), and Storage Coefficient (S) are dimmed indicating that their settings or parameters aren't significant because the LPF package utilizes the HK, VK, Ss & Sy. Whereas, when the BCF package is selected, the column for Vertical Anisotropy is dimmed because it is not supported by the BCF package.

BCF Package supports the following layer types: (a) Confined; (i) required input parameters: T and S, (ii) Interblock conductance is calculated based on input values of T, and therefore

remains unchanged for the entire simulation. (b) Unconfined (valid for only layer 1): (i) required input parameters: HK and Sy, (ii) Interblock conductance is calculated based on HK and saturated thickness that may vary during a flow simulation. (c) Limited Convertible between confined and unconfined: (i) requiring input parameters: T, S, and Sy. (ii) Interblock conductance is calculated based on input values of T, and therefore remains constant for the entire simulation regardless of the saturated thickness. (iii) If the layer is fully saturated, the storage is calculated based on S; otherwise Sy and saturated thickness are used. (iv) Vertical flow from above is limited if the layer desaturates. (d) Full Convertible between confined and unconfined; (i) required input parameters: HK, S, and Sy. (ii) If the layer is not fully saturated, the storage is calculated based on Sy and the saturated thickness; and the interblock conductance is calculated based on HK and the saturated thickness. (iii) If the layer is fully saturated, the storage is calculated based on S; and the interblock conductance is calculated based on HK and the layer thickness. (iv) Vertical flow from above is limited if the layer desaturates.

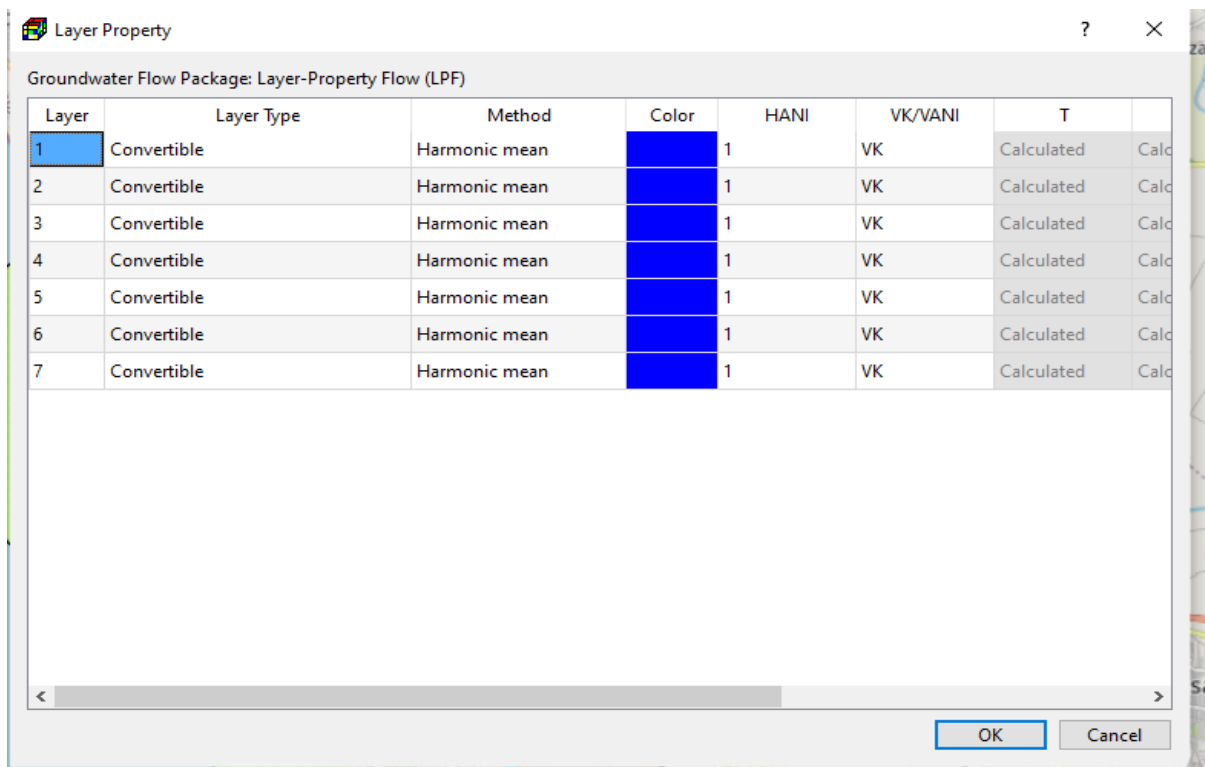


Figure 9 Layer Property Dialog box.

LPF Package supports the following layer types: (a) Confined: (i) required input parameters: HK, Ss, and VK or VANI (ii) Interblock conductance is calculated based on HK and layer thickness, and therefore remains constant for the entire simulation. (iii) The storage is

calculated based on  $S_s$  and layer thickness. (iv) VK or VANI is used for calculating vertical conductance between layers (b) Convertible between confined and unconfined: (i) required input parameters: HK,  $S_s$ ,  $S_y$ , and VK or VANI. (ii) If the layer is not fully saturated, the storage is calculated based on  $S_y$  and the saturated thickness; and the interblock conductance is calculated based on HK and the saturated thickness. (iii) If the layer is fully saturated, the storage is calculated based on  $S_s$  and the layer thickness; and the interblock conductance is calculated based on HK and the layer thickness. (v) VK or VANI is used for calculating vertical conductance between layers.

IBS: When the Interbed Storage package is activated, this option turns on/off the calculation of storage changes and compaction for specific layers.

TRPT is the ratio of the horizontal transverse dispersivity to the longitudinal dispersivity. TRPT is used by MT3D and SEAWAT

TRPV is the ratio of the vertical transverse dispersivity to the longitudinal dispersivity. TRPV is used by MT3D and SEAWAT.

Select *Discretization > Layer Top Elevation* or *Discretization > Layer Bottom Elevation* to define, respectively, the top or bottom elevations of the model cells with the Data Editor. For this study, all the layers were set as convertible layers.

### 2.7.8 Cell Status

MODFLOW requires an IBOUND array, which contains a value for each model cell. A positive value in the IBOUND array defines a variable-head (i.e., active) cell where the hydraulic head is computed, a negative value defines a constant head cell and the value 0 defines a no-flow cell (i.e., inactive) cell. It is suggested to use 1 for variable-head cells, 0 for no-flow cells and -1 for constant head cells. Any outer boundary cell, which is not a constant head cell, is automatically a zero-flux boundary cell. All the cells of the study area are active cells and were assigned a value of 1.

The transport models MT3D and SEAWAT require an ICBUND array, which contains a value for each model cell. A positive value in the ICBUND array defines an active concentration cell (the concentration varies with time and is calculated), a negative value defines a constant concentration cell (the concentration is constant) and the value 0 defines an inactive concentration cell (no transport simulation takes place at such cells). It is recommended to use the value 1 for an active concentration cell, -1 for a constant-concentration cell, and 0 for an inactive concentration cell. All cells in the model were assigned value 1, to allow the transport.



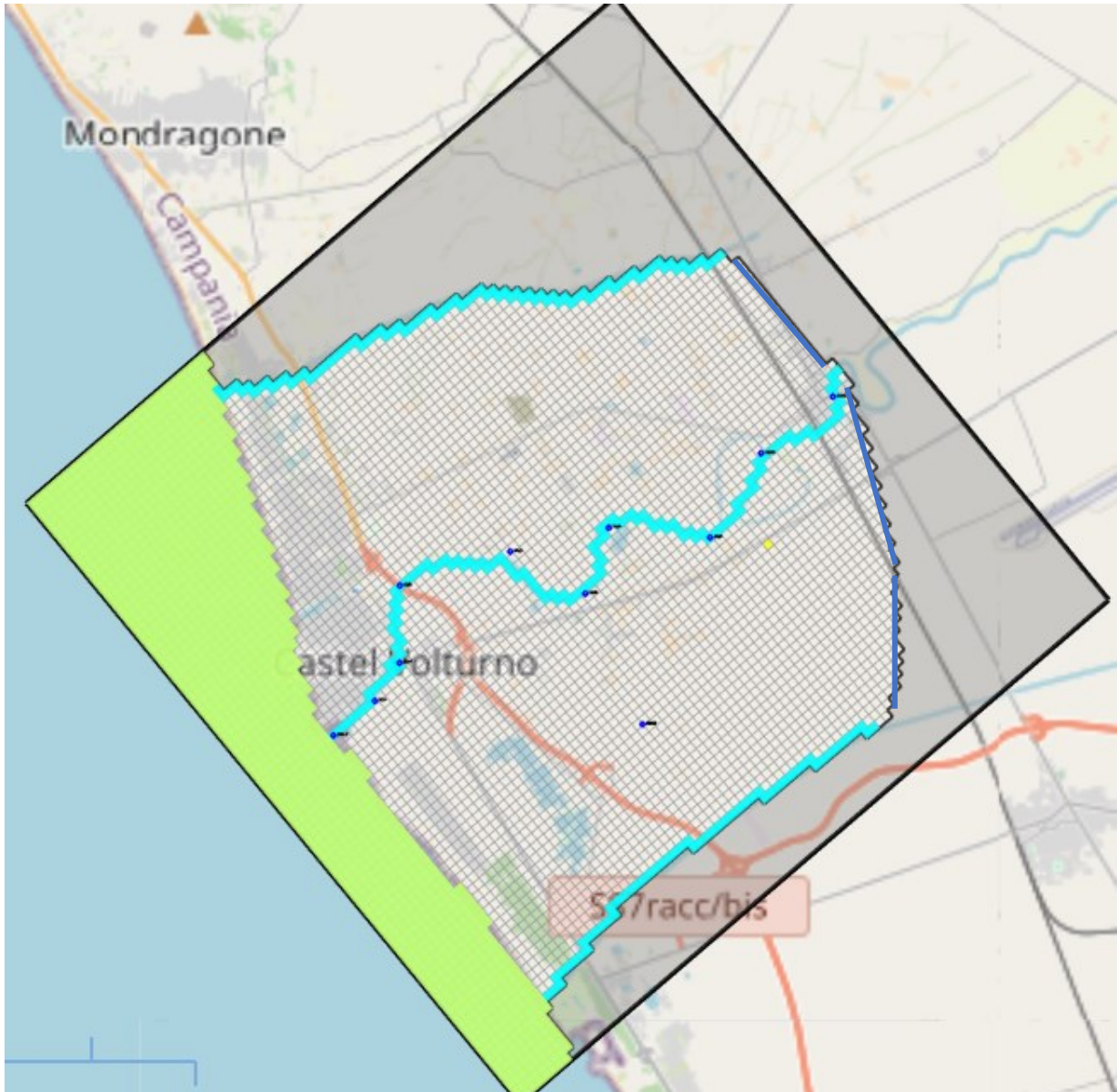


Figure 10 The Domain of the Model (the blue areas indicate the river and the canals as the boundaries of the area of study, the light green area represents the sea layer, the unshaded area represents the inactive cells for only the 1<sup>st</sup> layer).

### 2.7.9 Parameters Menu

This menu enables the input of time, initial hydraulic head values, and aquifer parameters. The requirement of an aquifer parameter for a model layer may vary depending on the layer properties set up, and it may not be needed for any model layer at all. Parameters utilised are illustrated below.

### 2.7.10 Starting Hydraulic Head

MODFLOW requires a starting hydraulic head value (starting head [L]) for each model cell at the beginning of a flow simulation. Starting heads at constant head cells are used as prescribed head values and remain constant throughout the flow simulation.

For steady-state flow simulations, the starting heads are used as initial values for the iterative equation solvers and should be set as close as possible to the final head solution. For an unconfined or a convertible layer, the starting head of a constant head cell must be higher than the elevation of the cell bottom. Otherwise, MODFLOW will write the message CONSTANT-HEAD CELL WENT DRY – SIMULATION ABORTED to its run listing file and then abort the simulation.

In a transient flow simulation, the starting heads provide a reference elevation for the solution. It is a standard practice to use heads generated by a steady-state model as the initial conditions for a transient model.

### 2.7.11 Horizontal Hydraulic Conductivity (HK)

Horizontal Hydraulic Conductivity (HK) [L/T] is the horizontal hydraulic conductivity along model rows. If the BCF package is selected as the internal flow package, HK is required for unconfined and full convertible layers. Whereas, if the LPF package is selected as the internal flow package, HK is required for all layer types. The horizontal hydraulic conductivity values range from  $1 \times 10^{-6}$  m/s in the coastal part of the VAP, where clay layers are present, to  $3.3 \times 10^{-4}$  m/s where fractured volcanic rocks are present. The model domain was divided into polygons whose extension corresponds to the extension of the different geological formations of the Campania region.



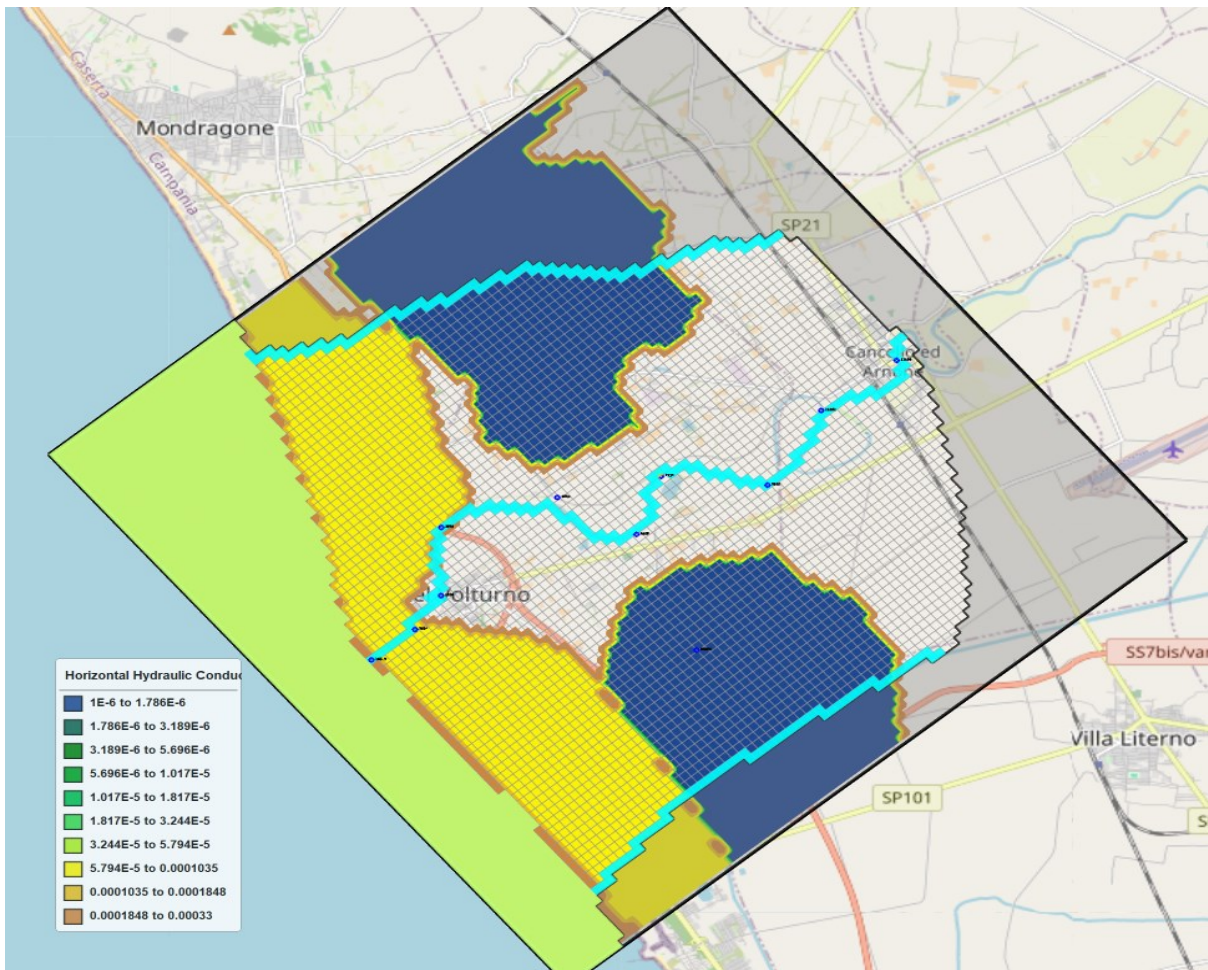


Figure 11 HK for layer 1, Stress Period 132 & Time Step 3.

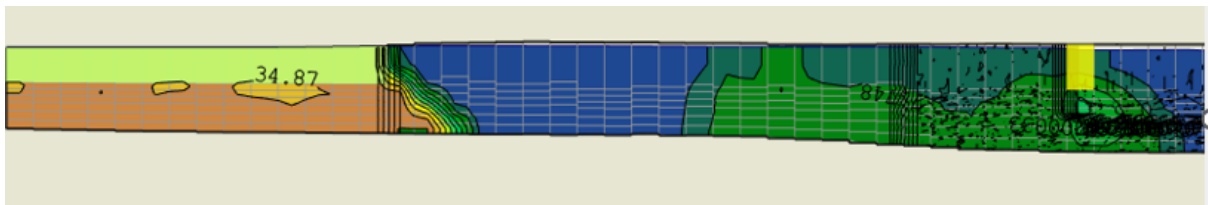


Figure 12 HK for Row Cross Section (layer 1, Row 33, Column 44) [Stress Period 132 & Time Step 3].

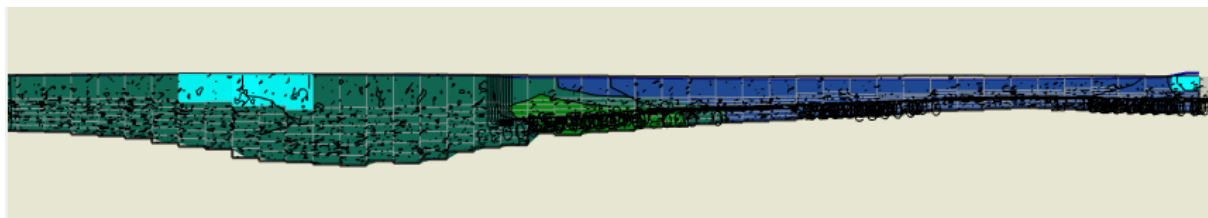


Figure 13 HK for Column Cross Section (layer 1, Row 33, Column 44) [Stress Period 132 & Time Step 3].

### 2.7.12 Vertical Hydraulic Conductivity (VK) and Vertical Leakance (VCONT)

The VCONT value is multiplied by cell area to obtain vertical conductance, which is used for formulating the vertical flow term by MODFLOW. If the LPF is selected as the internal flow package, VCONT is calculated for all layer types by LPF internally. The calculation is based on VK or Vertical Anisotropy and a direct input of VCONT is not possible.

The Layer-Property Flow (LPF) package supports the use of the cell-by-cell vertical hydraulic conductivity or vertical anisotropy, which is the ratio of horizontal hydraulic conductivity along rows to vertical hydraulic conductivity for the model layer. When Vertical Anisotropy of a layer in the Layer Property dialog box (Figure 10) is VK, the cell-by-cell vertical hydraulic conductivity of that layer is used in the simulation. When Vertical Anisotropy is VANI, the cell by-cell vertical anisotropy of the layer is used. For this study, to account for internal layering, the vertical hydraulic conductivity was set at a tenth of the horizontal hydraulic conductivity (Gaiolini et al., 2022).

### 2.7.13 Specific Storage (Ss) and Storage Coefficient (S)

For a steady state simulation, these menu items are not used and are deactivated. S is required by MODFLOW for confined or convertible layers. Specific storage [ $L^{-1}$ ] or specific storativity is defined as the volume fraction of water that a unit column of aquifer releases from storage under a unit decline in hydraulic head. The specific storage is a function of the compressibility of the water and the elastic property of the soil matrix and ranges in value from  $3.3 \times 10^{-6}[m^{-1}]$  of rock to  $2.0 \times 10^{-2}[m^{-1}]$  of plastic clay according to Domenico (1972). In a confined layer, the storage term is given by the storativity or storage coefficient (= specific storage [ $L^{-1}$ ]  $\times$  layer thickness [L]). The storativity is sometimes referred to as confined storage coefficient.

If the LPF package is selected as the internal flow package, Ss is required. A direct input of S is not possible. For this model, a Ss value of  $0.0001 m^{-1}$  was utilised.

### 2.7.14 Specific Yield (Sy)

Sy is required by MODFLOW for unconfined or convertible layers. Specific yield is defined as the volume of water that an unconfined aquifer releases from storage per unit surface area of aquifer per unit decline in the water table. Specific yield is a function of porosity (and is not necessarily equal to porosity), because a certain amount of water is held in the soil matrix and cannot be removed by gravity drainage according to Bear (1972). For the purposes of this study a Sy of 0.2 was used.

### 2.7.15 Effective Porosity ( $n_e$ )

Effective porosity is used by MODPATH, MT3D and SEAWAT for calculating the average velocity of the flow through the porous medium. If the total unit volume  $V$  of a soil matrix is divided into the volume of the solid portion  $V_s$  and the volume of voids  $V_v$ , the total porosity  $n$  is defined as  $n = V_v/V$ . Effective porosity (with the respect to flow through the medium) is always less than total porosity, sometimes (as in the case of clays) much less, because some of the pore spaces may be too small or too poorly connected so that part of the fluid is immobile or partially immobile. Mostly, good aquifers tend to have values of effective porosity in the range of 10-30%, which is characteristic of most perennial riverbeds (Buddemeier & Schloss, 2000). On a more macroscopic scale there's a drop in the value of the effective porosity that must be accommodate for, for the fact that unresolved conductivity variations lead to a reduction of effective porosity. An effective porosity of 0.2 was used for this model.

## 2.8 The Models Menu | MODFLOW Menu

A package of MODFLOW is the part of the program that deals with a single aspect of simulation. For example, the Well Package simulates the effect of wells, the River Package simulates the effect of rivers. To activate a package and edit its data, select the respective menu item. If the package is already activated, you will have the opportunity to edit its data or deactivate the package. The MODFLOW packages employed for the purposes of this study are Evapotranspiration (EVT), River (RIV), Recharge (RCH), Time-Variant Specified Head (CHD) & Well (WEL).

### 2.8.1 Flow Packages | Evapotranspiration (EVT)

The Evapotranspiration (EVT) Package simulates the effects of plant transpiration and direct evaporation by removing water from the saturated groundwater regime. Evapotranspiration can be drawn from only one cell in each vertical column of model cells. The evapotranspiration rate is calculated for a cell in each vertical column of model cells by,

$$R_{et} = ETVR \quad \text{if } h > SURF \quad (a)$$

$$R_{et} = ETVR \frac{h - (SURF - EXDP)}{EXDP} \quad \text{if } (SURF - EXDP) \leq h \leq SURF \quad (b)$$

$$R_{et} = 0 \quad \text{if } h < SURF - EXDP \quad (c)$$

Where:

$R_{et}$  [ $LT^{-1}$ ] is the rate of loss per unit surface area of water table due to evapotranspiration,

$h$  [L] is the calculated hydraulic head in the cell from which the evapotranspiration occurs,

$ETVR$  [ $LT^{-1}$ ] is the maximum possible value of  $R_{et}$  or potential evapotranspiration rate,

$SURF$  [L] is the ET surface elevation,

$EXDP$  [L] is the cutoff or extinction depth.

The evapotranspiration flow rate  $Q_{et}$  [ $L^3T^{-1}$ ] drawn from the model cell is,

$$Q_{et} = R_{et} * Area_c \quad (d)$$

where  $Area_c$  is the area of the model cell.

The package removes water from the saturated groundwater regime based on the following assumptions:

- a. when groundwater table is at or above the elevation of the ET surface  $h$ , evapotranspiration loss from the groundwater table is at the maximum ET Rate ( $R_{et}$ ),
- b. no evapotranspiration occurs when the depth of the groundwater table below the elevation of the ET surface exceeds the ET extinction depth ( $d$ ),
- c. in between these two extremes evapotranspiration varies linearly with the groundwater table elevation.

Input values that require specifications are:

- a. ET Option (NEVTOP): Three options are provided for designating the cell from which  $Q_{et}$  is drawn because  $Q_{et}$  is calculated for only one cell in each vertical column of model cells: (A) Only cells in the top grid layer are used for the computation of ET. (b) Cells in the layers specified by IEVT have their ET computed. (c) The highest variable-head cell in each vertical column is used to compute ET.
- b. Maximum ET Flux (EVTR) [ $LT^{-1}$ ]: potential evapotranspiration rate.
- c. Elevation of ET Surface (SURF) [L]: when head is higher than SURF,  $R_{et}$  equals to EVTR.
- d. ET Extinction Depth (EXDP) [L]: when head is lower than SURF - EXDP,  $R_{et}$  is zero.
- e. Layer Indicator (IEVT): This indicates the layer from which  $Q_{et}$  is removed from the groundwater system.
- f. Parameter Number is used to group cells, where the EVTR value is to be estimated by PEST.

Evapotranspiration data were retrieved using the BIGBANG model developed by ISPRA using RS technique. QGIS was used to process the data by trimming the files based on the model area, change coordinates and format.



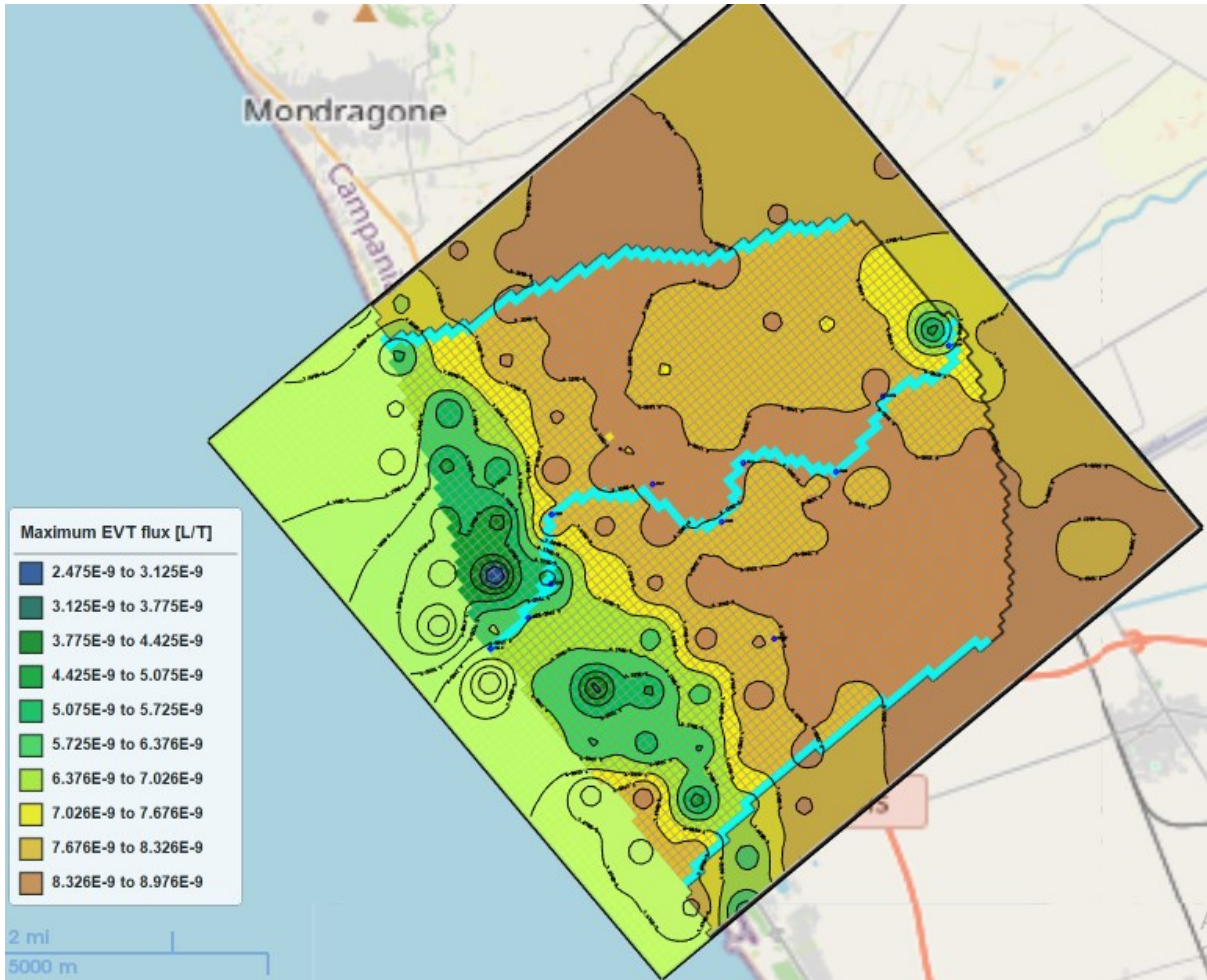


Figure 14 Maximum Evapotranspiration Flux (m/s).

### 2.8.2 Flow Packages | Recharge (RCH)

The Recharge (RCH) Package is designed to simulate distributed recharge to the ground-water system. The RCH Package does not allow for recharge to occur simultaneously at multiple depths in the same vertical column because natural recharge enters the ground-water system at the top, and therefore a value of the recharge flux  $RECH [LT^{-1}]$  is assigned to a cell in each vertical column of model cells. The recharge rate to the groundwater system  $Qrch [L^3T^{-1}]$  is calculated by,

$$Qrch = RECH * Area_c \quad (e)$$

Where:  $RECH [LT^{-1}]$  is the recharge flux at the cell, and  $Area_c$  is the area of the cell.

The required input parameters for all input methods are identical and listed below. Although these parameters are to be assigned to each vertical column of model cells, you may move between layers within the Data Editor to examine the grid configuration in each layer.

- a. Recharge Option (NRCHOP): Since  $Qrch$  is calculated for only one cell in each vertical column of model cells, three options are available for specifying the cell where  $Qrch$  is

applied to: (a) Recharge is only applied to the top layer. (b) Vertical distribution of recharge is specified in IRCH. (c) Recharge is applied to the highest variable-head cell in each vertical column.

- b. Recharge Flux (RECH) [ $LT^{-1}$ ].
- c. Layer Indicator (IRCH): This indicates the layer from which  $Qrch$  is added to the groundwater system.
- d. Parameter Number is used to group cells, where the RECH value is to be estimated by PEST.

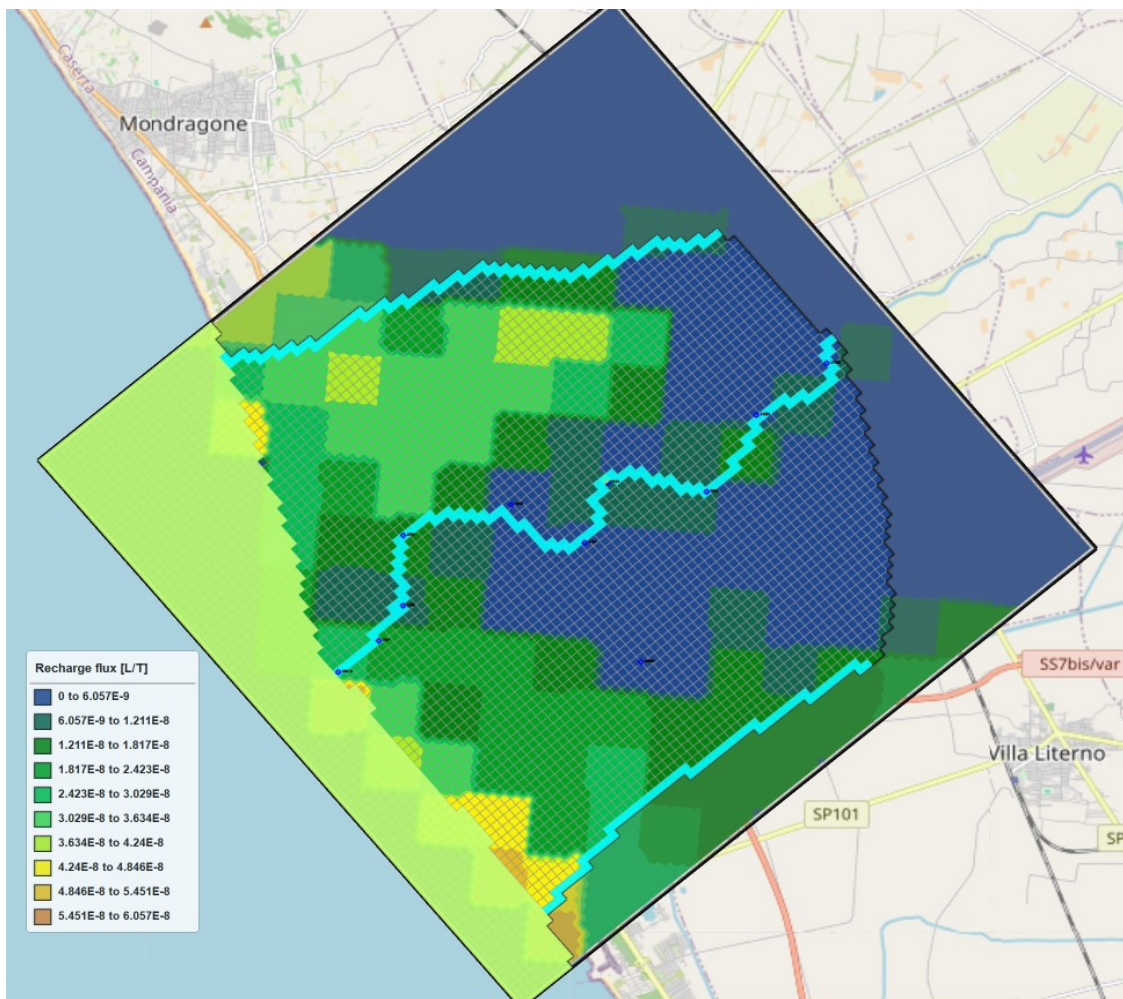


Figure 15 Recharge Flux (m/s).

Moreover, Recharge data were retrieved using the BIGBANG model developed by ISPRA. QGIS was used to process the data by trimming the files based on the model area, change coordinates and format.

### 2.8.3 Flow Package | River (RIV)

The purpose of the River (RIV) Package is to simulate the effects of flow between surface-water features and groundwater systems. Rivers and streams contribute water to or drain water from the groundwater system, depending on the head gradient between the river and the groundwater regime. A river is implemented by dividing into reaches so that each reach is completely contained in a single model cell. Multiple reaches may be assigned to a model cell. For each reach, the flow rate  $Q_{riv}$  [ $L^3T^{-1}$ ] between the reach and the model cell is calculated by the following equations,

$$Q_{riv} = C_{riv} * (h_{riv} - h) \quad \text{if } h > B_{riv} \quad (f)$$

$$Q_{riv} = C_{riv} * (h_{riv} - B_{riv}) \quad \text{if } h < B_{riv} \quad (g)$$

Where:  $Q_{riv}$  [ $L^3T^{-1}$ ] is the flow rate between the reach and the model cell (i.e., the groundwater system). A positive value means that water flows from the river to aquifer,

$h$  [L] is the calculated hydraulic head in the cell containing the reach,

$h_{riv}$  [L] is the head in the reach,

$B_{riv}$  [L] is the elevation of the riverbed bottom of the reach, and

$C_{riv}$  [ $L^2T^{-1}$ ] is the riverbed conductance of the reach.

Methods of inputting the River data parameters into the model include:

- a. All input methods: The data entry dialog boxes of all input methods include a Simulation Settings group that contains the option, Include Concentration Data in the SSM Package of MT3D/SEAWAT, if this box is checked, the values entered to Concentration (MT3D/SEAWAT) [ $ML^{-3}$ ] are used as source water concentration. If this box is not checked, the concentration of the source water is assumed to be zero.
- b. Cell-by-cell input method: For each reach, the following properties need to be assigned,
  - (i) Riverbed conductance  $C_{riv}$  [ $L^2T^{-1}$ ], which relates flow rate to the head differences between the reach and the aquifer. The value of  $C_{riv}$  depends on the material and characteristics of the riverbed and the immediate environment.
  - (ii) River Stage  $h_{riv}$  [L] is the hydraulic head of the reach.
  - (iii) Elevation of the Riverbed Bottom  $B_{riv}$  [L] is the elevation of the bottom of the riverbed.
  - (iv) Parameter Number is used to group cells, where the  $C_{riv}$  value is to be estimated by PEST.

- (v) Thickness of Riverbed Sediments (SEAWAT) [L], this value is used by SEAWAT to appropriately include the effects of variable-density river leakage and is used only if RBDTHK.
- (vi) River Water Density (SEAWAT) [ML<sup>-3</sup>] is the water density of the river. This is used by SEAWAT only if it is running in the uncoupled mode.
- (vii) Concentration (MT3D/SEAWAT) [ML<sup>-3</sup>], by clicking the Edit button to open a Concentration dialog box that allows you to specify the source water concentration of up to 100 species to the river. The entered concentration values may be used by the SSM Package of MT3D or SEAWAT.
- c. Polyline input method: The specified vertex data is interpolated to model cells.
- (i) Simulation Setting: (a) If this box is checked, the layer number of a reach along the polyline is determined by comparing its elevation of the riverbed bottom (Briv) with the top/bottom elevations of the cells in the same vertical model column as the reach: (1) if Briv is higher than the top elevation of the highest cell, the reach is assigned to the cell in Layer 1. (2) if Briv is lower than the bottom elevation of the lowest cell, the reach is assigned to the cell in Layer NLAY. (3) if Briv lies between top and bottom elevations of a cell, the reach is assigned to that cell.
- (b) If this box is not checked, the reaches along the polyline are assigned to the layer where the polyline is located.
- (ii) The data of this group are assigned to one or more vertices of a polyline. These vertex is interpolated to model cells by:
- (1) Riverbed conductance per unit length  $C_{rivl}$  [LT<sup>-1</sup>] is interpolated to the cells along the polyline. For each of those cells, the interpolated cell value  $C_{rivl}$  is multiplied with the length of the river within the cell to obtain the riverbed conductance  $C_{riv}$ :
- $$C_{riv} = C_{rivl} * l_c \quad (h)$$
- where  $C_{rivl}$  is the riverbed conductance per unit length at a given cell, and  $L_c$  is the length of the river within the cell.
- (2) All other parameters, parameter already described for the cell-by-cell input method above.
- d. Polygon input method: By using the Polygon input method, data may be applied to model cells by,
- (i) Simulation settings as already indicated for the above polyline method.
- (ii) Polygon Properties,



(a) Riverbed conductance per unit area  $C_{riva}$  [ $T^{-1}$ ]. For each cell within the polygon, the specified value ( $C_{riva}$ ) is multiplied with the cell area to obtain the riverbed conductance  $C_{riv}$ :

$$C_{riv} = C_{riva} * Area_c \quad (i)$$

where:

$C_{riva}$  is the riverbed conductance per unit area, and  $Area_c$  is the area of the cell.

(c) All other parameters, parameter already described for the cell-by-cell input method above.

For this study, the river heads were imported with the polyline input method and the average monthly values for the heads were obtained from the HEC-RAS interpolations. The River reach from the estuary to CA was divided into ten sections, the cross sections where the inputted values are located at (166.9, 785, 1558, 2891, 4863, 6428, 7737, 9522, 11281, & 13158) m. The average monthly river heads across each section were determined from January 2010 to December 2020, and inputted into the model. The graph below depicts the River stages for each cross section along the river reach as simulated by the HEC-RAS.

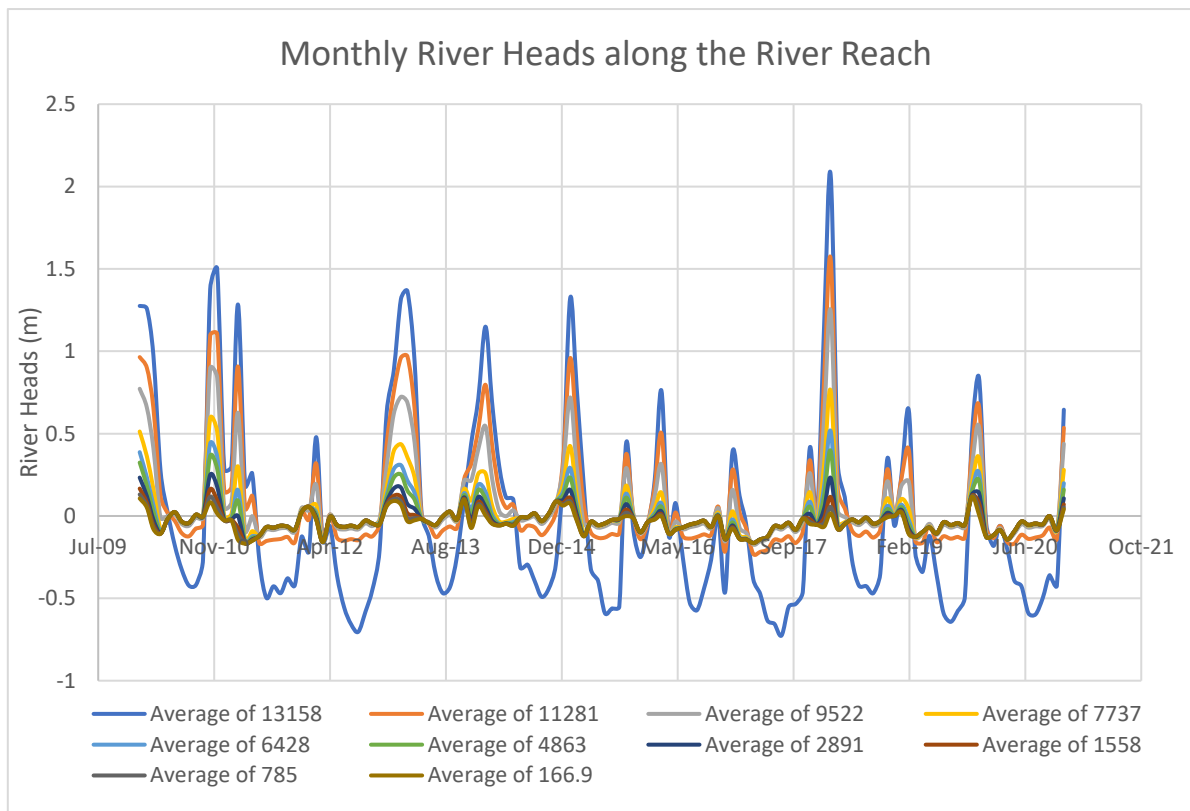


Figure 16 Averaged River Heads along the River Reach (CV- CA).

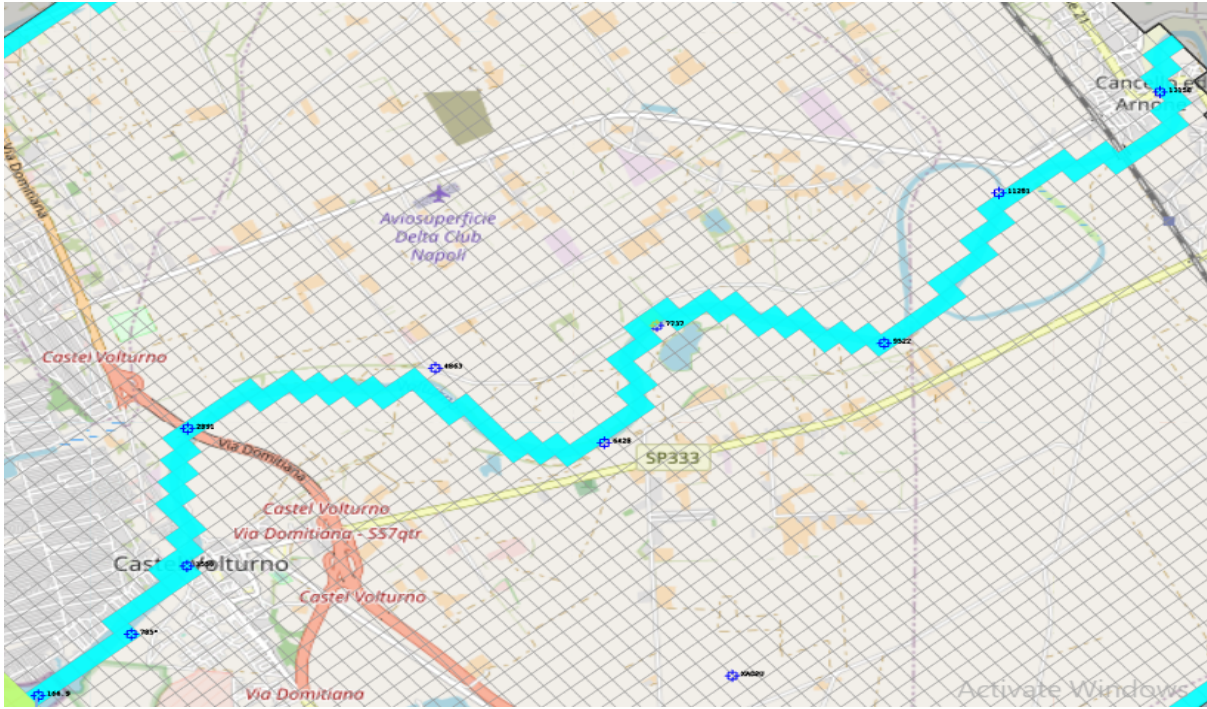


Figure 17 The Final VR Reach (light blue) & River Sections “Points of Inputted Heads” (blue).

#### 2.8.4 Flow Packages | Time-Variant Specified Head (CHD)

The Time-Variant Specified-Head (CHD) Package permits constant head cells to assume different head values at each time step for transient simulations. It offers a way to simulate fluctuations in the head over time that can be roughly represented by piecewise linear segments. The formulation of constant-head boundaries in MODFLOW is not changed by the CHD Package. All the input methods have the same set of needed input parameters, which are mentioned below.

- (i) Flag [-]: A non-zero value indicates that a cell is specified as a time-variant specified-head boundary.
  - (a) A no-flow cell cannot be converted to a CHD-cell.
  - (c) If a cell is specified as a time-variant specified-head boundary for a stress period and omitted in the specification for a subsequent period, it remains a constant-head boundary with a head equal to the end head of the last stress period for which it was specified.
- (i) Start Head (***h<sub>s</sub>***) [L] and End Head (***h<sub>e</sub>***) [L]: These values are the prescribed hydraulic head of the cell at the start and end of a stress period, respectively. For each time step within the stress period, the prescribed hydraulic head *h* at the cell is determined by,

$$h = h_s + (h_e - h_s) * \frac{PERTIM}{PERLEN} \quad (j)$$

where:

*PERTIM* is the starting time of the time step, and

*PERLEN* is the length of the stress period.

(ii) The interpolated head values remain constant during the time step.

Head Conversion (SEAWAT): This option determines how SEAWAT converts the specified values of *hs* and *he* to reference head. Four options are available:

(a) Use calculated water density at the cell.

(b) Use the specified water density value.

(c) Use the average of the calculated water density of the overlying cells.

(c) Input head values are reference head. No conversion

(iii) Water Density (d) [ $ML^{-3}$ ] (SEAWAT): Required only if the Head Conversion option is Use the specified water density value. SEAWAT uses this value to convert input head values to reference head.

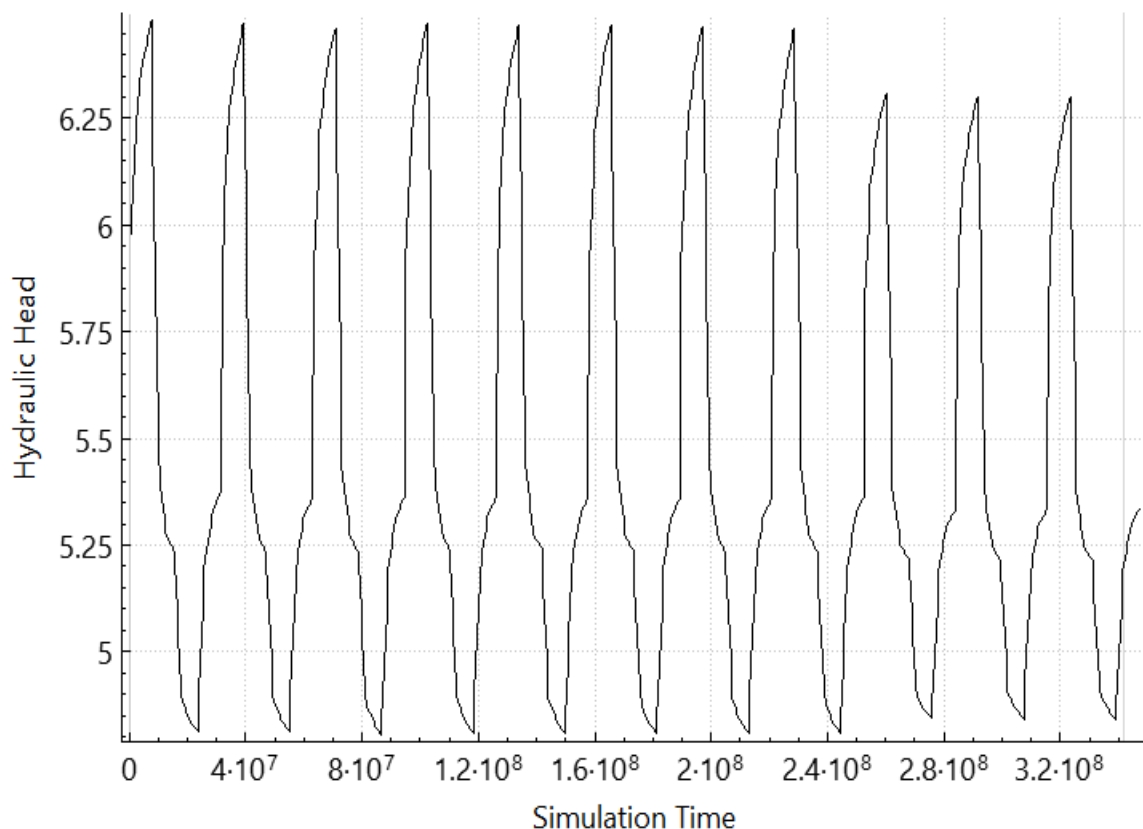


Figure 18 Time Variant head used at the eastern boundary (m a.s.l.).

### 2.8.5 Flow Package | Well (WEL)

The Well (WEL) Package is designed to simulate features such as wells that withdraw water from or add water to the aquifer at a constant rate during a stress period, where the rate is independent of both the cell area and the head in the cell. The Package can be used to simulate any features for which the recharge or discharge can be directly specified.

The area under study had a well which was included in the model at [7,47,71] depicting (layer 7, row 47 and column 71) as required by a 3D spatial discretization for a MODFLOW model. The well had a pumping rate of 0.02 m<sup>3</sup>/s, which is used in the summers (June, July & August). Therefore, the effects of the well in the model was only considered for the dry seasons.

All input methods include a Simulation Settings group that contains the following option: Include Concentration Data in the SSM Package of MT3D/SEAWAT, if this box is checked, the values entered to Concentration (MT3D/SEAWAT) [ML<sup>-3</sup>] are used as source water concentration. If this box is not checked, the concentration of the source water is assumed to be zero, as already described in the previous packages.

a) Cell-by-cell input method: Figure below shows the dialog box for specifying cell properties.

(a) Flow Rate (Q) [L<sup>3</sup>T<sup>-1</sup>]: Negative values are used to indicate pumping wells, while positive cell values indicate injection wells. The injection or pumping rate of a well is independent of both the cell area and the hydraulic head in the cell. MODFLOW assumes that a well penetrates the full thickness of the cell. To simulate wells that penetrate more than one model layer with the WEL Package, a flow rate must be specified for each penetrated layer. The total flow rate for a multi-layer well is equal to the sum of flow rates of individual layers.

For confined layers, the flow rate for each layer  $Q_k$  can be approximately calculated by dividing the total rate ( $Q_{total}$ ) in proportion to the layer transmissivities according to McDonald, et al., (1988).

$$Q_k = Q_{total} * \frac{T_k}{\sum T} \quad (k)$$

where  $T_k$  is the transmissivity of layer k, and  $\sum T$  is the sum of the transmissivity values of all layers penetrated by the multi-layer well.

(b) Parameter Number is used to group cells, where the Q value is to be estimated by PEST.

(c) Water Density (SEAWAT) [ $\text{ML}^{-3}$ ] is the density of injected water and is used by SEAWAT only if it is running in the uncoupled mode (i.e., the density-effect of all species are turned off).

(d) Well Name is an optional text string to identify the well and will appear in the Input File to the Well Package.

(e) Concentration (MT3D/SEAWAT) [ $\text{ML}^{-3}$ ]: Clicking the Edit button to open a Concentration dialog box that allows the user to specify the injected water concentration of up to 100 species. The user can either enter individual concentration values to the table directly or click the Set Value button to enter a uniform value for all species.

b) Polyline input method: Flow Rate per Unit Length [ $\text{L}^2\text{T}^{-1}$ ] is interpolated to the cells along the polyline. For each of those cells, the interpolated cell value  $Ql$  is multiplied with the length of the polyline within the cell to obtain the flow rate  $Q$ :

$$Q = Ql * l_c \quad (l)$$

where:

$Ql$  is the flow rate per unit length at a given cell, and

$l_c$  is the length of the polyline within the cell.

The other parameter values are interpolated to cells along the polyline and the interpolated values are used as the input data to those cells.

c) Polygon input method: Flow Rate per Unit Area [ $\text{T}^{-1}$ ] is assigned to the cells within the polygon. For each of those cells, the cell value  $Qa$  is multiplied with the cell area to obtain the flow rate  $Q$ :

$$Q = Qa * Area_c \quad (m)$$

where:

$Qa$  is the flow rate per unit area at a given cell, and  $Area_c$  is the area of the cell.

The other parameter values are used as the input data to the cells within the polygon.

## 2.8.6 Solvers

To calculate hydraulic heads, MODFLOW prepares one finite difference equation for each cell, expressing the relationship between the head at a node and the heads at each of the six adjacent nodes at the end of each time step. Because each equation may involve up to seven unknown values of head, and because the set of unknown head values changes from one equation to the next through the grid, the equations for the entire grid must be solved simultaneously at each

time step. The system of simultaneous finite difference linear equations can be expressed in matrix notation as,

$$A * x = b \quad (n)$$

where  $A$  is a coefficient matrix assembled by MODFLOW using user-specified model data;  $b$  is a vector of defined flows, terms associated with head-dependent boundary conditions and storage terms at individual cells;  $x$  is a vector of hydraulic heads at individual cells. During a MODFLOW run, the vector  $x$  is solved with one of the supported solvers.

For this study Preconditioned Conjugate Gradient (PCG) Solver package was utilised.

### 2.8.7 Preconditioned Conjugate Gradient (PCG) Solver Package

The PCG solver incorporates two forms of the Preconditioned Conjugate-Gradient method, that is (a) the Modified Incomplete Cholesky and (b) the Polynomial methods. The Modified Incomplete Cholesky method is almost always faster whereas the Polynomial method is potentially faster only on parallel computers where some of the work can be performed simultaneously on multiple processors.

a. Preconditioned Method:

(i) NPCOND; This is the matrix preconditioning method. The available options are (a) Modified Incomplete Cholesky (for use on scalar computers) and (b) Neuman series polynomial (for use on parallel computers).

(ii) NBPOL: This is used with the Neuman series polynomial preconditioning method. Checking this box to calculate the estimate of the upper bound on the maximum eigenvalue. If this box is cleared, the estimate is set as 2. Convergence is generally insensitive to this parameter.

b. Iterative Method:

(i) Maximum Number of Outer Iterations (MXITER): For a linear problem MXITER should be 1, unless more than 50 inner iterations are required, when MXITER could be as large as 10. A larger number (generally less than 100) is required for a nonlinear problem. For a linear problem, a single outer iteration with many inner iterations theoretically is adequate, but a few outer iterations should be used for large (greater than 10,000 cells) linear models.

(ii) Maximum Number of Inner Iterations (ITERI): ITERI typically varies from 10 to 30 for nonlinear problems; for most linear problems, a value of 30 will be enough. Five or more outer iterations and several inner iterations (20 or more) are typically the most efficient number of iterations for nonlinear situations. If the nonlinear terms are

reformulated frequently by having a small (less than 20) value for ITER1, the solution procedure becomes inefficient.

(iii) Relaxation Parameter (RELAX): This is the relaxation parameter used with the Modified Incomplete Cholesky preconditioning method. Usually, RELAX=1.0, but for some problems a value of 0.99, 0.98, or 0.97 will reduce the number of iterations required for convergence.

(iv) Damping Parameter (DAMPPCG): Values less than 1.0 can be used to aid convergence in nonlinear problems.

c. Convergence Criteria:

(i) Head Change (HCLOSE) [L] is the head change criterion for convergence. When the maximum absolute value of head change from all nodes during an iteration is less than or equal to HCLOSE, and the criterion for RCLOSE is also satisfied, iteration stops.

(ii) The residual criterion for convergence is called residual (RCLOSE) [L3T-1]. The iteration ends when the requirement for HCLOSE is met and the highest absolute value of the residual at every node throughout the iteration is less than or equal to RCLOSE. When the convergence requirements are met for the first inner iteration of a nonlinear problem, convergence is said to have occurred.

d. Printout from the Solver:

(i) Printout Option (MUTPCG) is a flag that controls printing of convergence information from the solver:

(a) 0: All available information: Print tables of maximum head change and residual each iteration.

(b) 1: The number of iterations only: Print only the total number of iterations.

(c) 2: None: No Printing.

(d) 3: Print as for 0, but only if solver convergence fails.

(ii) Printout Interval (IPRPCG): Whenever the time step is an even multiple of the printout interval, the extreme head change and residual (positive or negative) are printed for each repetition of a time step. Regardless of the value of the printout interval, the printout also happens at the conclusion of each stress phase.



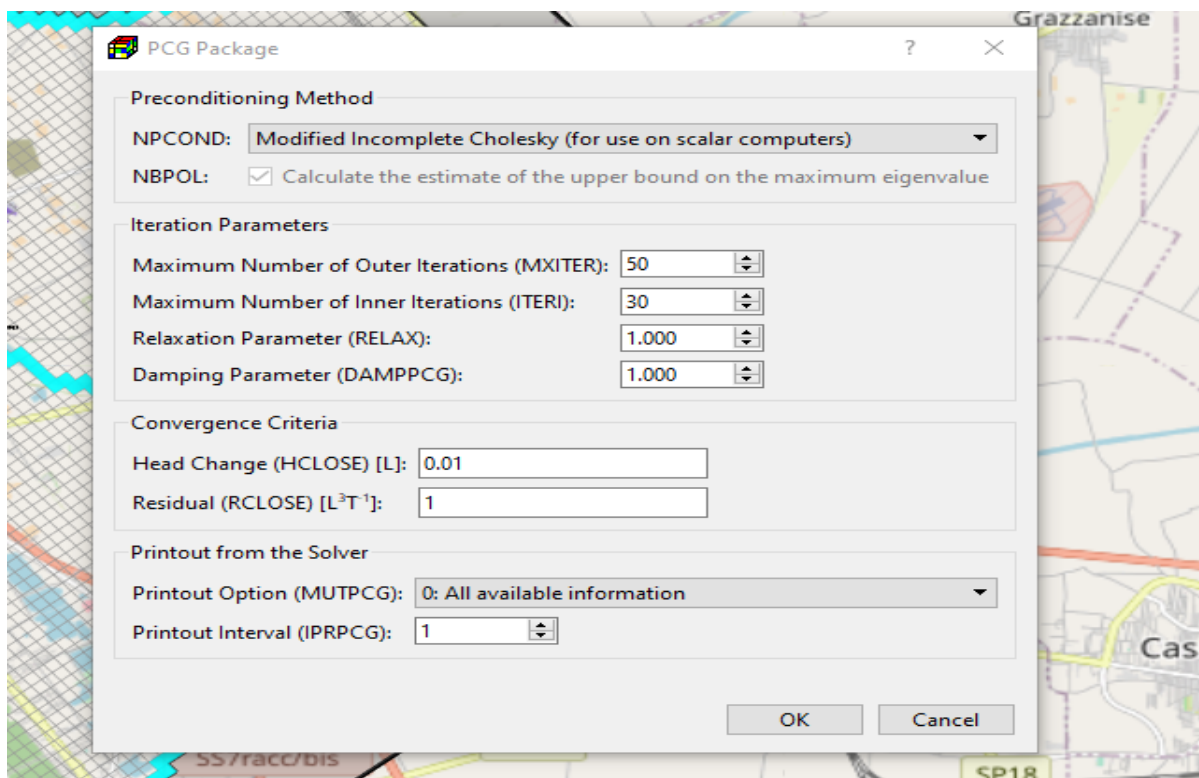


Figure 19 The PCG Package dialog box.

For this study, a Modified Incomplete Cholesky matrix preconditioning method was selected for the NPCOND, 50 and 30 were used for the MXITER and ITERI respectively, whereas 1 was used for both the Relaxing and Damping parameter. 0.01 m and 1 m<sup>3</sup>/s were assigned for both Head Change (HCLOSE) and Residual (RCLOSE) respectively, whereas 0 and 1 were assigned for the Printout Option (MUTPCG) and Printout Interval (IPRPCG).

### 2.8.8 Output Control

The primary output file of MODFLOW is the run listing file that can be found in *Models > Modflow > View > Run Listing File*. In addition to the run listing file, various simulation results can be saved by checking the corresponding output terms in the Modflow Output Control dialog box.

MODFLOW also calculates the volumetric water budget for the entire model at the end of each time step and saves it in the run listing file. An indicator of the numerical solution's general acceptability is given by the volumetric water budget. The system of equations solved by a model in numerical solution techniques typically has a flow continuity statement for each model; so, continuity between the total flows into and out of the model or a sub-region should exist, according to Simcore Software (2012).

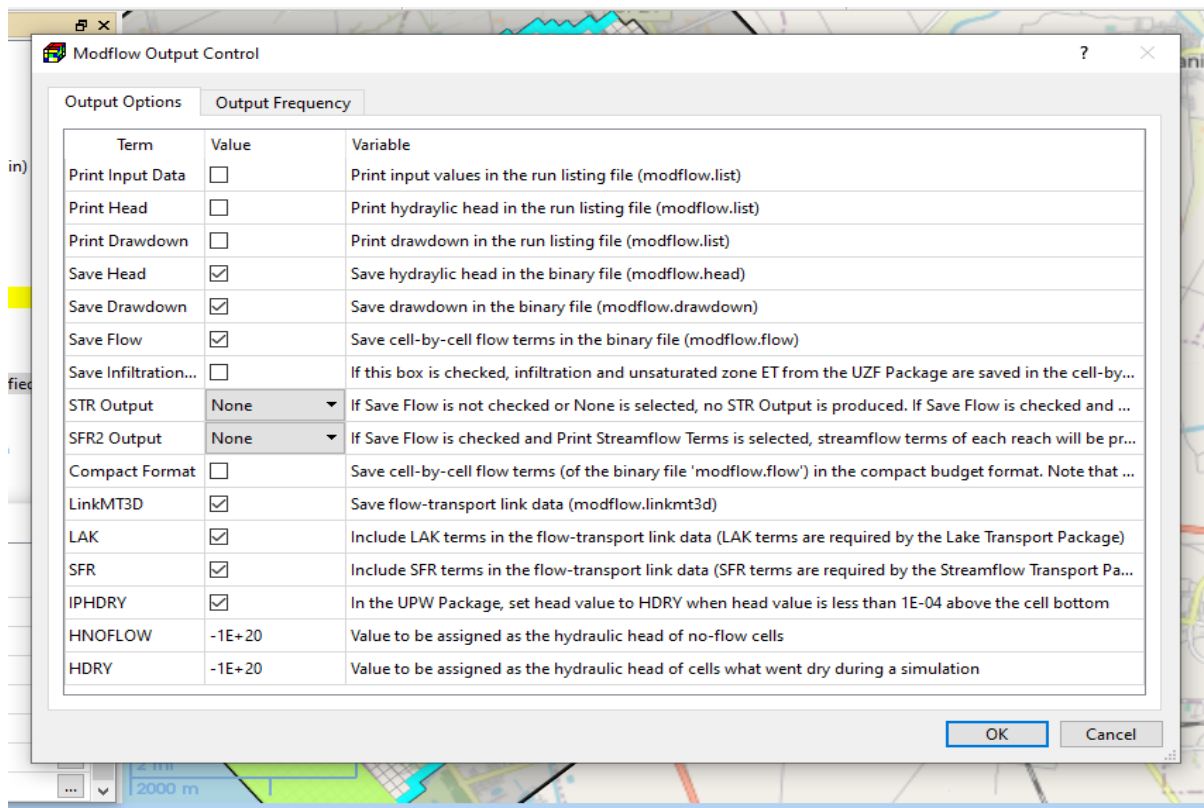


Figure 20 Modflow Output Control Dialog box.

## 2.8.9 Run

Select this menu item to open the Run Modflow dialog box. The dialog box can be used to start the flow simulation with MODFLOW, to build input files to MODFLOW, or to check the model data. The available settings of the dialog box are described below.

a. Table:

- (i) The build box. Prior to running a flow simulation, PM uses the user-specified data to build input files for MODFLOW. An input file will be built if its build box is checked. If an input file does not exist or the input data has been modified since the last build, its build box will be checked automatically. The input files will be saved in the Path displayed in the dialog box.
- (ii) Package is the name of the package of the flow model.
- (iii) Filename is the name of the input file.
- (iv) Status shows the status (such as Ready, Not Exist, etc.) of the input file.

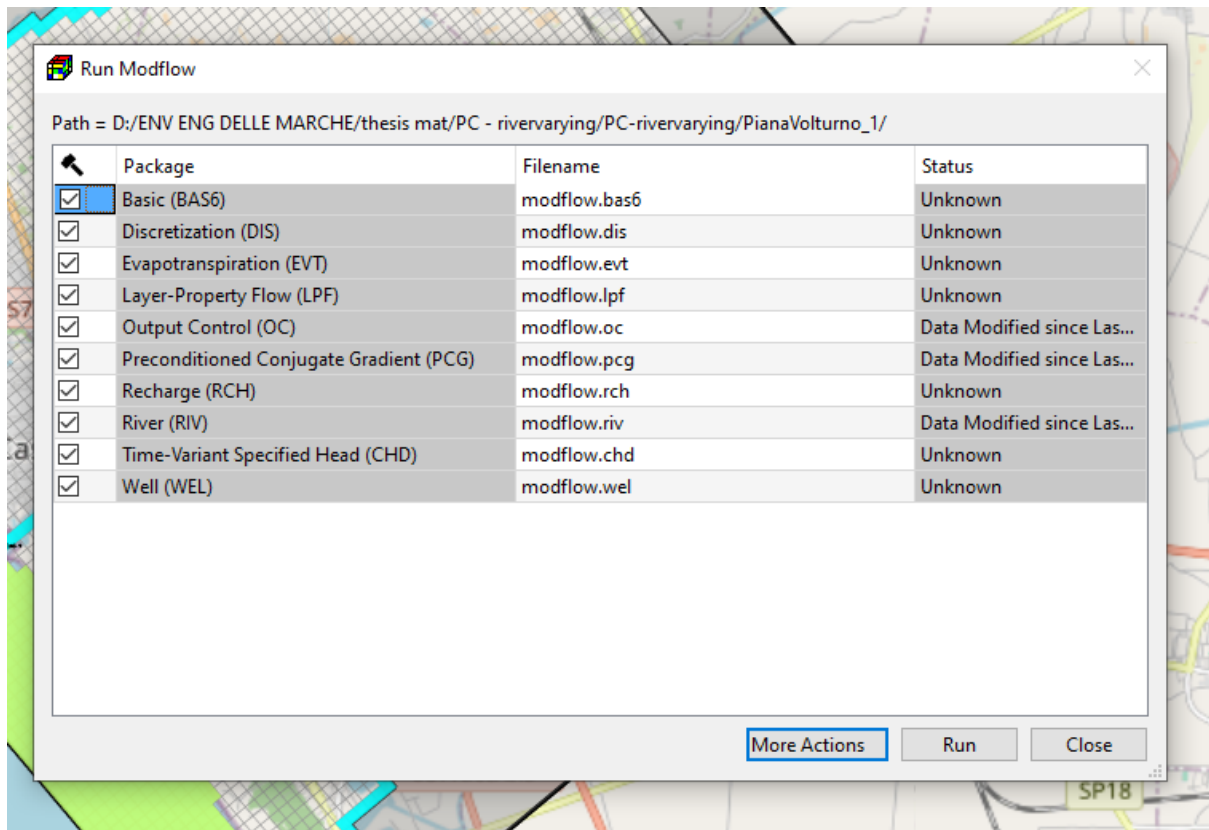


Figure 21 The Run Modflow dialog box.

a. More Actions:

(i) Inspect Model Data: Select this to check the geometry of the model and the consistency of the model data.

(ii) Build Input Files: Select this to build the input files with the checked build boxes.

(iii) Rebuild All Input Files: Select this to rebuild all input files, except for existing read only input files.

b. Run: Click this button to build input files with the checked build boxes and the start the flow simulation. If LPF or BCF is selected as the internal flow package, the flow simulation will be carried out by the executable file of MODFLOW-2005 defined in the Preferences dialog box.

### 2.8.10 ZoneBudget

There are situations in which it is useful to calculate flow terms for various zones (i.e., subregions) within the model domain. To facilitate such calculations, MODFLOW saves the computed flow terms for individual cells in the modflow.flow file (also known as the cell-by-cell budget file). The computed flow terms include (1) inflows or outflows due to external

stresses or boundaries, such as pumping well, recharge, or general-head boundary; (2) storage changes; (3) flows from or to constant-head boundary; and (4) flows across cell faces.

ZoneBudget according to Harbaugh (1990, 2009) is a program that reads flow terms from the cell-by-cell budget file and produces water budgets for user-defined zones within the model domain. The zones are defined by assigning zone numbers to model cells. For this study, the zone number was assigned as 1.

## 2.9 SEAWAT

This menu provides the interface to SEAWAT according to Langevin, et al., (2007). SEAWAT couples the flow and transport processes, therefore does not require a separate MODFLOW run.

### 2.9.1 Settings

The first step to use SEAWAT is to define the species, packages, and the reaction type in the Transport Settings dialog box. The features of this dialog box are detailed below.

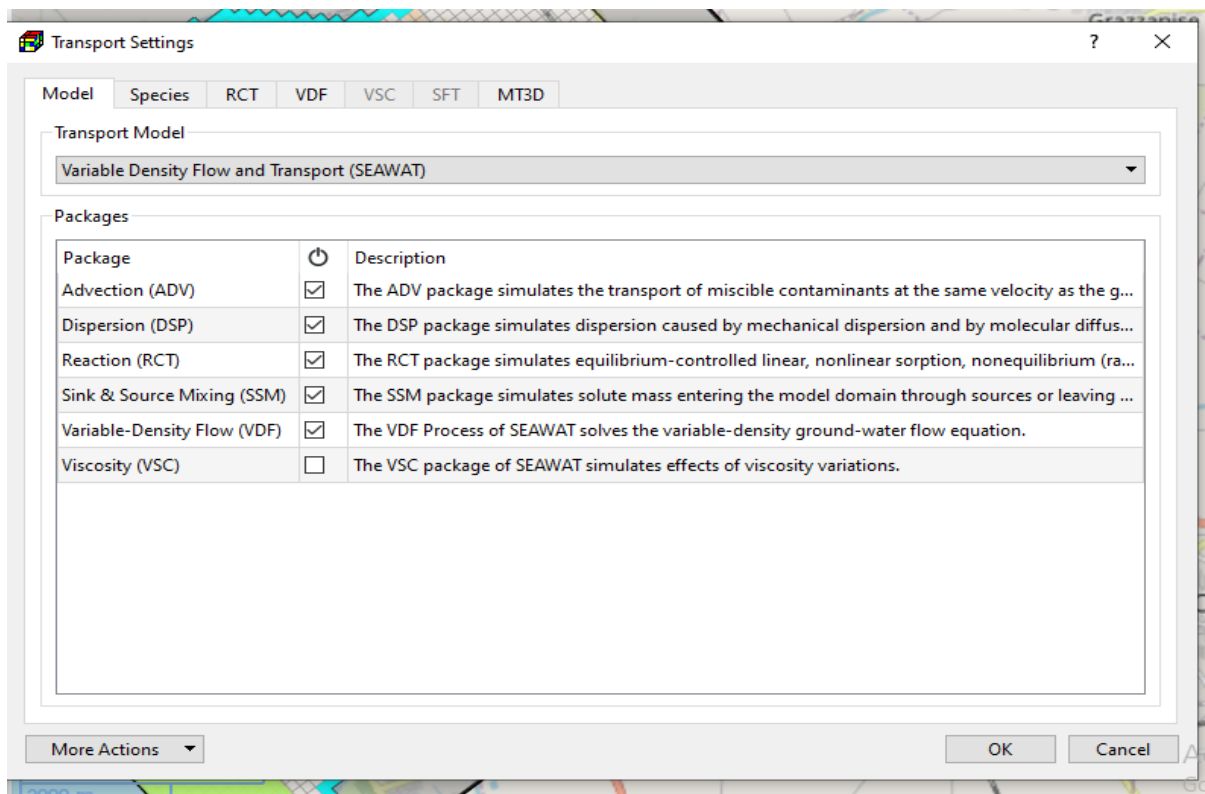


Figure 22 The Model tab of the Transport Settings dialog box.

The Model Tab above defines the transport model and packages to be used in the simulation. The Transport Model contains the Variable Density Flow and Transport (SEAWAT). If this

item is selected, the transport simulation will be carried out the executable file of SEAWAT. The transport process can be density dependent. For the purposes of this study, SEAWAT is selected since the model is density dependent.

Available packages of the selected transport model include:

- a) Advection (ADV): The ADV package simulates the transport of miscible contaminants at the same velocity as the groundwater. Advection (ADV) was selected for this study.
- b) Dispersion (DSP): The DSP package simulates dispersion caused by mechanical dispersion and by molecular diffusion driven by concentration gradients.
- c) Reaction (RCT): The RCT package simulates equilibrium-controlled linear, nonlinear sorption, nonequilibrium (rate-limited) sorption, and kinetic reactions.
- d) Sink & Source Mixing (SSM): The SSM package simulates solute mass entering the model domain through sources or leaving the model domain through sinks.
- e) Lake Transport (LKT): The Lake Transport (LKT) Package calculates solute concentrations in lakes.
- f) Variable-Density Flow (VDF): The VDF Process of SEAWAT solves the variable-density groundwater flow equation. Activate this package to include the density effect in the simulation.
- g) Viscosity (VSC): The VSC package of SEAWAT simulates effects of viscosity variations that are implemented in the LPF package.

Available packages of the selected transport model include:

- a) Advection (ADV): The ADV package simulates the transport of miscible contaminants at the same velocity as the groundwater. Advection (ADV) was selected for this study.
- b) Dispersion (DSP): The DSP package simulates dispersion caused by mechanical dispersion and by molecular diffusion driven by concentration gradients.
- c) Reaction (RCT): The RCT package simulates equilibrium-controlled linear, nonlinear sorption, nonequilibrium (rate-limited) sorption, and kinetic reactions.
- d) Sink & Source Mixing (SSM): The SSM package simulates solute mass entering the model domain through sources or leaving the model domain through sinks.
- e) Streamflow Transport (SFT): The SFT package of MT3D-USGS simulates one dimensional solute transport in the stream network that is defined by the SFR2 package.
- f) Lake Transport (LKT): The Lake Transport (LKT) Package calculates solute concentrations in lakes.

- g) Variable-Density Flow (VDF): The VDF Process of SEAWAT solves the variable-density groundwater flow equation. Activate this package to include the density effect in the simulation.
- h) Viscosity (VSC): The VSC package of SEAWAT simulates effects of viscosity variations that are implemented in the LPF package.

The Species Tab below defines the species to be used in the simulation. The table contains the species and related parameters such as:

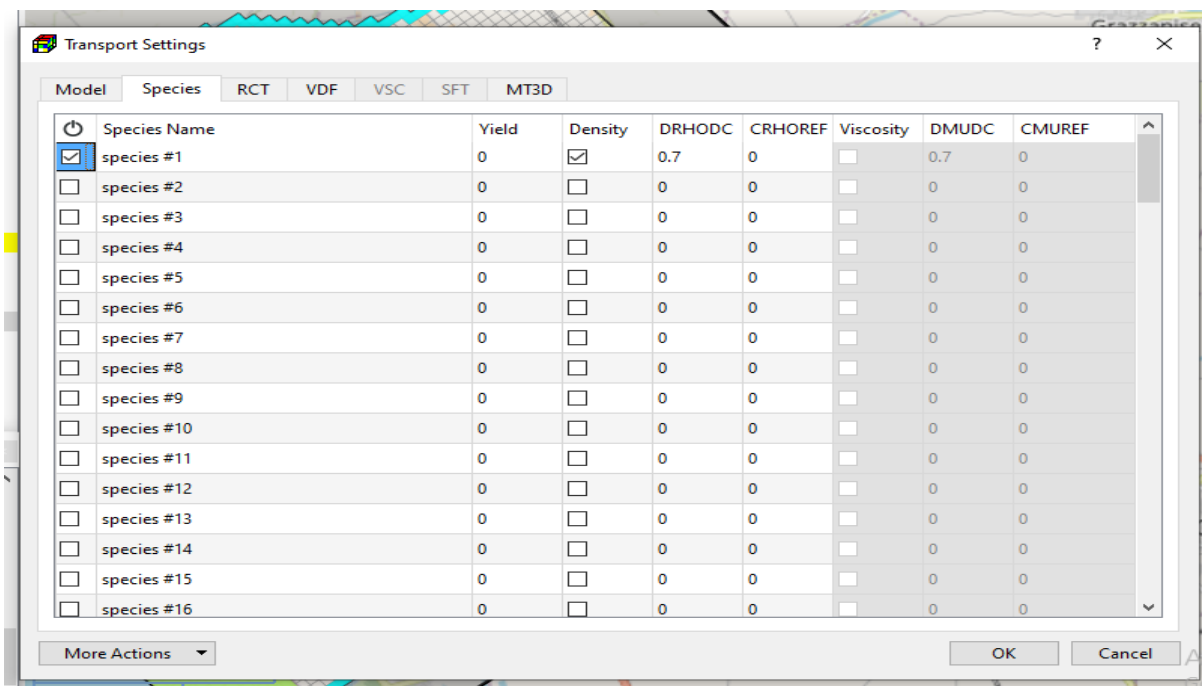


Figure 23 The Species Tab of the Transport Settings dialog box.

- a. Species Name: Name of the species.
- b. Yield: The value of the yield coefficient between the current species and the next species. This is used only if the first-order chain reaction is simulated.
- c. Density: This is used only if the Variable Density Flow (VDF) process of SEAWAT is turned on. If the Density box of a species is checked, the concentration of that species will affect the fluid density.
- d. DRHODC is the slope that relates fluid density ( $\rho$ ) to solute concentration (C), i.e.,  $\partial\rho/\partial C$ . This is used only if the Variable Density Flow (VDF) process of SEAWAT is turned on.

- e. CRHOREF is the reference concentration (i.e.,  $C_0$ ) for the species. For most simulations, CRHOREF should be specified as zero. This is used only if the Variable Density Flow (VDF) process of SEAWAT is turned on.
- f. Viscosity: This is used only if the Viscosity (VSC) package of SEAWAT is turned on. If the Viscosity box of a species is checked, the concentration of that species will affect the fluid viscosity.
- g. DMUDC is the slope that relates dynamic viscosity ( $\mu$ ) to solute concentration ( $C$ ), i.e.,  $\partial\mu/\partial C$ . This is used only if the Viscosity (VSC) package of SEAWAT is turned on.
- h. CMUREF is the reference concentration for the species. This is used only if the Viscosity (VSC) package of SEAWAT is turned on.

For the study, Species 1 was used, with the density section selected and both the DRHODC and DMUDC value set as 0.7.

### 2.9.2 Initial Concentration

At the beginning of a transport simulation, SEAWAT require the initial concentration of each active species at each active concentration cell, i.e.,  $ICBUND > 0$ . For the study, a scenario with average conditions was run for 100 years to reach the full development of the seawater wedge along the coast and the saline intrusion within the VR coastal reach. Then, the final heads and concentrations calculated by SEAWAT were imported as initial conditions in the transient model with variable boundary conditions using all the previously packages combined with the average monthly salinity obtained from the HEC-RAS simulations for the sections of the river reach (i.e., from section 166.9 m to 13158 m). Finally, to allow a more realistic representation of the salinization patterns, as initial concentrations were used the stochastic ensemble mean saline concentrations calculated by Schiavo et al. (2023) in the same area imported as shape file. Given that the stochastic ensemble was bidimensional, again the model was run for 100 years in mean conditions to allow the redistribution of salinities within the model domain.



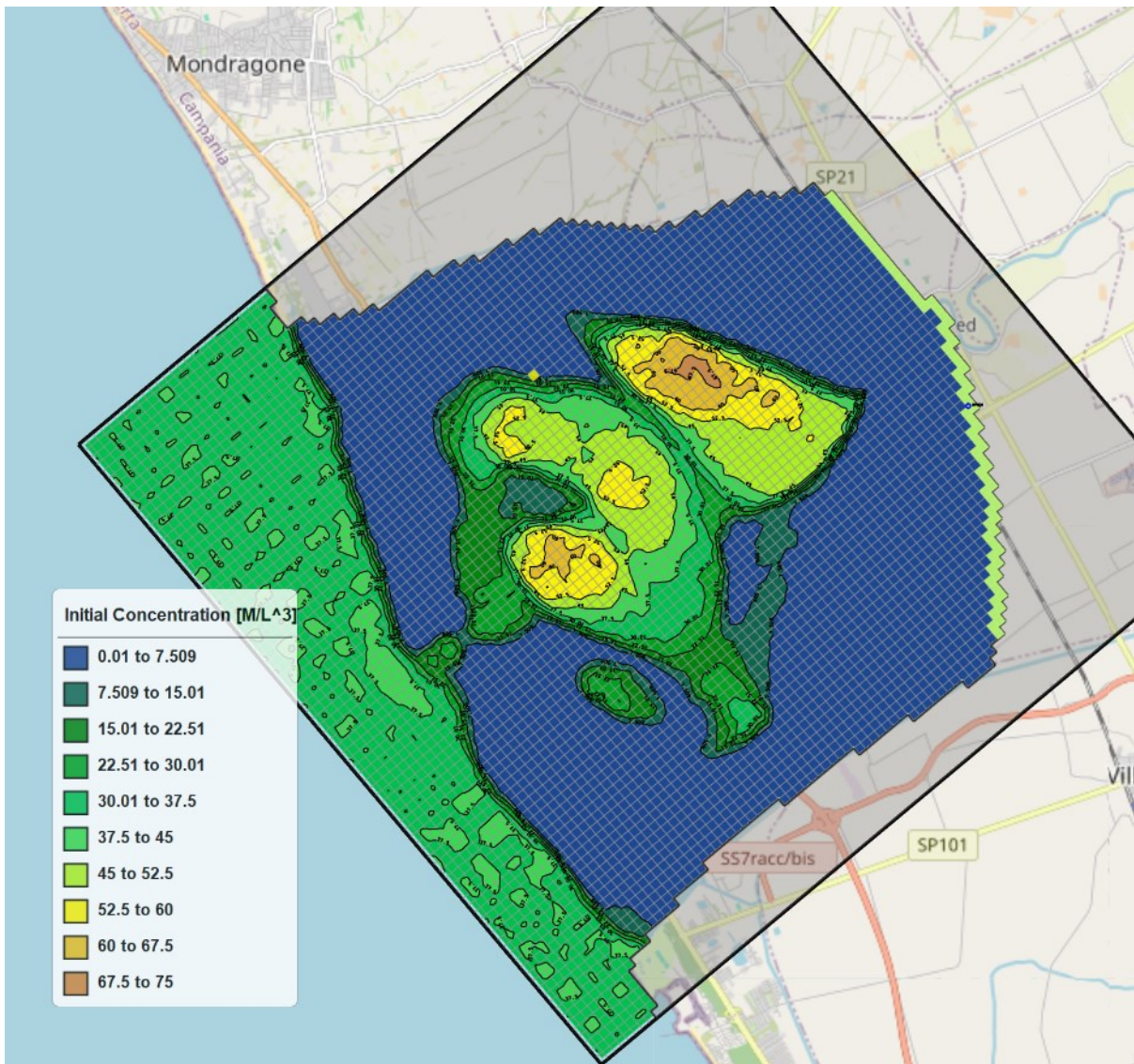


Figure 24 Paleo salinities in layer 7

### 2.9.3 Packages | Advection

The following parameters are defined in the Advection (ADV) Package dialog box:

Settings:

- a. Advection Solution Option (MIXELM):
  - i. Third-order TVD Scheme (ULTIMATE) is based on the ULTIMATE algorithm according to Leonard (1988), which is in turn derived from the earlier QUICKEST algorithm according to Leonard (1979). With the ULTIMATE scheme, the solution is mass conservative, without excessive numerical dispersion and artificial oscillation.
  - ii. Finite-Difference Method is implicit with the Generalized Conjugate Gradient solver (GCG) package. Due to the problems of numerical dispersion and artificial

oscillation, the upstream finite difference method is only suitable for solving transport problems not dominated by advection.

- iii. Forward Tracking Method of Characteristics (MOC) has been widely used. One of the most desirable features of the MOC technique is that it is virtually free of numerical dispersion that poses serious difficulty in many numerical schemes. However, it requires large computer memory when many particles are involved.
- iv. Backward Tracking Method of Characteristics (MMOC) uses one particle for each finite-difference cell and is normally faster than MOC. At each new time level, a particle is placed at the nodal point of each finite-difference cell. The particle is tracked backward to find its position at the old time. The concentration associated with that position is used to approximate the advection-relevant average concentration at the cell, where the particle is placed.
- v. Hybrid Method of Characteristics (HMOC) attempts to combine the strengths of the MOC and MMOC schemes by using an automatic adaptive scheme. When sharp concentration fronts are present, the advection term is solved by MOC with moving particles dynamically distributed around each front. Away from such fronts, the advection term is solved by MMOC. The criterion for controlling the switch between the MOC and MMOC schemes is given by DCHMOC.

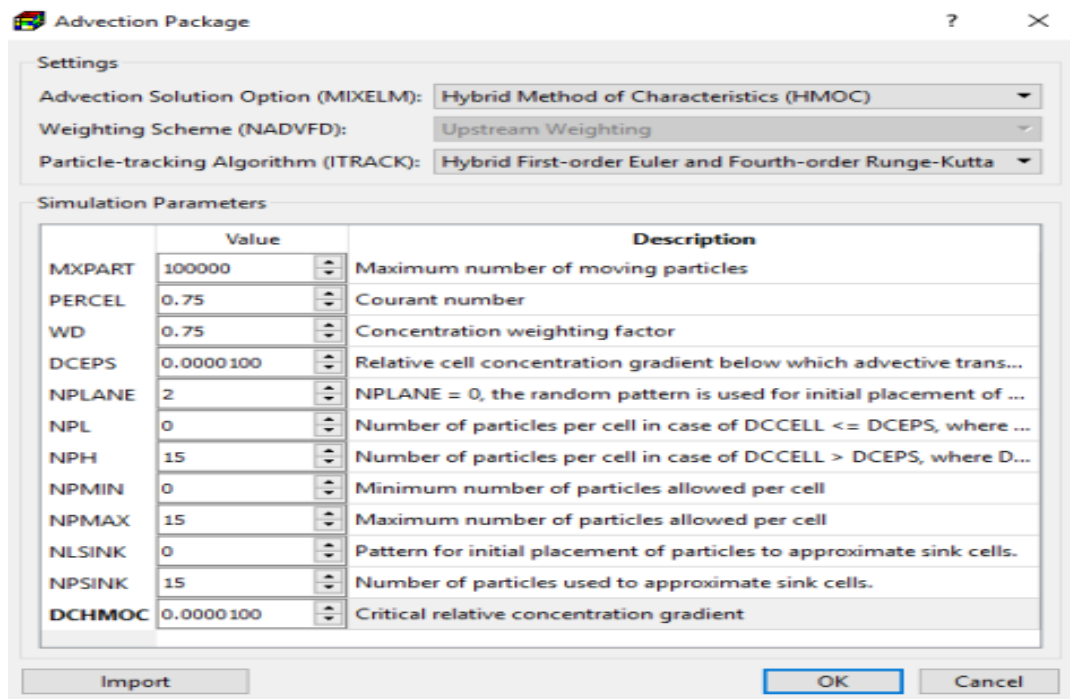


Figure 25 The Advection Package dialog box.

- b. Weighting Scheme (NADVFD) is needed only when the implicit finite-difference method is used. In the finite-difference method, when computing the mass flux into a model cell by advection, the concentration values at the cell interfaces between two neighbouring cells are used. For the upstream weighting scheme, the interface concentration in a direction is equal to the concentration at the upstream node along the same direction. For the central-in-space weighting scheme, the interface concentration is obtained by linear interpolation of the concentrations at the two neighbouring cells.
- c. Particle-tracking Algorithm (ITRACK) is used in combination with the method of characteristics:
  - i. First-order Euler: Using this algorithm, numerical errors tend to be large unless small transport steps are used. The minimum allowed transport step of all particles is determined by MT3D-USGS and is used in a transport step.
  - ii. Fourth-order Runge-Kutta: The basic idea of this method is to calculate the particle velocity four times for each tracking step: one at the initial point, twice at two trial midpoints, and once at a trial end point. A weighted velocity based on values evaluated at these four points is used to move the particle to a new position. This method permits the use of larger tracking steps.
  - iii. Hybrid First-order Euler and Fourth-order Runge-Kutta: The option is implemented by automatic selection of the fourth-order Runge-Kutta algorithm for particles located in cells which contain or are adjacent to sinks or sources, and automatic selection of the first-order Euler algorithm for particles located elsewhere.

Simulation Parameters: Depends on the selected Solution Scheme, one or more of the following parameters may be required.

- a) MXPART: Maximum number of moving particles in a simulation.
- b) PERCEL is the number of cells (or a fraction of a cell) any particle will be allowed to move in any direction in one transport step. Generally,  $0.5 \leq \text{PERCEL} \leq 1$ .
- c) WD is Concentration-weighting factor. WD lies between 0 and 1. The value of 0.5 is normally a good choice. This number can be adjusted to achieve better mass balance. Generally, it can be increased toward 1 as advection becomes more dominant.
- d) DCEPS is the relative cell concentration gradient below which advective transport is considered negligible. A value around  $10^{-5}$  is generally adequate.
- e) NPL, or number of initial particles per cell, is assigned to cells where the DCEPS is less than or equal to the relative cell concentration gradient  $DCCEL_{k,i,j}$ . Since advection is seen as insignificant when the  $DCCI_{k,i,j}$  is less than or equal to DCEPS, NPL can

typically be set to zero. Every cell throughout the grid has the same amount of particles in it when NPL and NPH are set equal.

- f) NPH is the number of initial particles per cell to be placed at cells where  $DCCELL_{k,i,j}$  is greater than DCEPS. The selection of NPH depends on the nature of the flow field and the computer memory limitation. Generally, a smaller number should be used in relatively uniform flow fields and a larger number should be used in relatively nonuniform flow fields.
- g) The lowest quantity of particles permitted per cell is known as NPMIN. To ensure that there are enough particles in a cell, additional particles are added if the number of particles in the cell at the conclusion of a transport step is less than NPMIN. In flow fields that are generally uniform, NPMIN can be set to zero; in flow fields that are diverging or converging, it can be set to a value greater than zero. A range of zero to four is usually suitable.
- h) The maximum number of particles per cell that are permitted is called NPMAX. A cell's contents are eliminated and replaced with a new set of particles equal to NPH if the number of particles within it are higher than NPMAX to maintain mass balance. Setting NPMAX to approximately two NPH is generally acceptable.
- i) In the MMOC system, the flag NLSINK indicates whether the fixed or random pattern is selected for the initial particle placement to mimic sink cells. It follows the same convention as NPLANE.
- j) In the HMOC solution scheme, the critical relative concentration gradient (DCHMOC) regulates the selective usage of either MOC or MMOC. The MOC solution is selected at cells where  $DCCELL_{k,i,j} > DCHMOC$ . The MMOC solution is selected at cells where  $DCCELL_{k,i,j} \leq DCHMOC$ .

#### 2.9.4 GCG Solver

Utilizing the generalized conjugate gradient method as its foundation, the GCG Solver is a versatile iterative solver designed to solve the transport equation system. This solver must always be activated. Without imposing any stability constraints on the transport step size, the dispersion, sink/source, and reaction terms are implicitly solved using this solution.

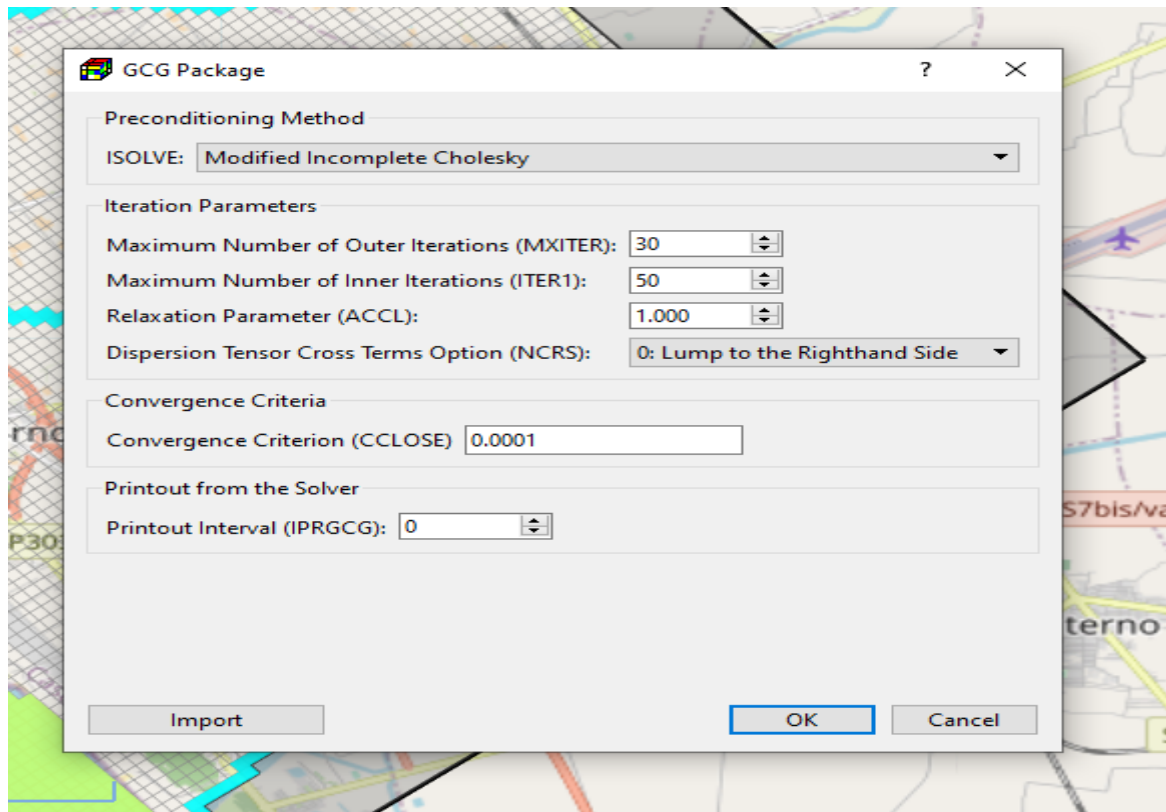


Figure 26 The GCG Package dialog box

1. Preconditioning Method (ISOLVE): The GCG package has three preconditioning options, Jacobi, SSOR, and Modified Incomplete Cholesky. The last one usually takes less iterations than the other methods, but it requires significantly more memory.
2. Iteration Parameters:
  - a. Maximum Number of Outer Iterations (MXITER) and Maximum Number of Inner Iterations (ITER1): The GCG solver has two iteration loops, an inner and an outer loop. Similar to the PCG solver of MODFLOW, all coefficients in the (transport-) matrix  $A$  and the right-hand-side vector  $b$  remain unchanged during inner iterations. The inner loop continues until ITER1 – iterations are executed, or the convergence criterion is met. If some of the coefficients in  $A$  are dependent on the concentration being solved, as in the case of nonlinear sorption, they must be updated in outer iterations.
  - b. Relaxation Factor (ACCL) is only used for the SSOR option; a value of 1.0 is generally adequate.
  - c. Dispersion Tensor Cross Terms Option (NCRS): NCRS is a flag for treatment of dispersion tensor cross terms. NCRS=0, lump all dispersion cross terms to the right-hand side of the system of transport equations. It is approximate but highly efficient.



3. Concentration Closure Criterion (CCLOSE) is the convergence criterion in terms of relative concentration. A value between  $10^{-6}$  and  $10^{-4}$  is generally adequate. Before solving the system of transport equations, it is normalized by dividing the concentration terms by the maximum concentration of all cells. When the change of the normalized concentration at all cells during an inner iteration is less than or equal to CCLOSE, iteration stops. When it takes only one inner iteration to converge, the solution is considered to have converged and the simulation proceeds to the next transport step.
4. Printout Interval (IPRGCG): The maximum concentration changes are printed out whenever the iteration number is an even multiple of this printout interval. Set it to zero for printing only at the end of each stress period.

For this study, Modified Incomplete Cholesky was selected for Preconditioning Method (ISOLVE) same as for the PCG Solver, other parameters were set as the PCG Solver. The Convergence Criterion (CCLOSE) was set at 0.0001.

### 2.9.5 Output Control

a. Output Options Tab:

- i. SAVUCN indicates whether the calculated concentration values should be saved in binary files which are used by PM for visualization. The default file names of the binary files are MT3Dnnn.UCN for the dissolved phase and MT3Dnnns.UCN for the sorbed phases, where nnn is the species number.
- ii. IFMTCN indicates whether the calculated concentration values should be printed to the Run Listing file.
- iii. IFMTNP indicates whether the number of particles in each cell should be printed to the Run Listing file.
- iv. IFMTRF indicates whether the model-calculated retardation factor should be printed to the Run Listing file.
- v. IFMTDP indicates whether the model-calculated, distance weighted dispersion coefficient should be printed to the Run Listing File.
- vi. CHKMAS indicates whether mass budget summary information should be printed to the mass budget file. The default file names of the mass budget summary files are MT3Dnnn.MAS, where nnn is the species number.
- vii. NPRMAS: Mass budget summary information is printed every NPRMAS transport step, if CHKMAS is checked.

- viii. NPRS: If  $NPRS < 0$ , simulation results are saved every NPRS transport steps (note that transport step counter starts at 0 within each flow time step.) If  $NPRS = 0$ , simulation results are saved at the end of each stress period. If  $NPRS > 0$ , simulation results are saved at the time points defined in Output Times.

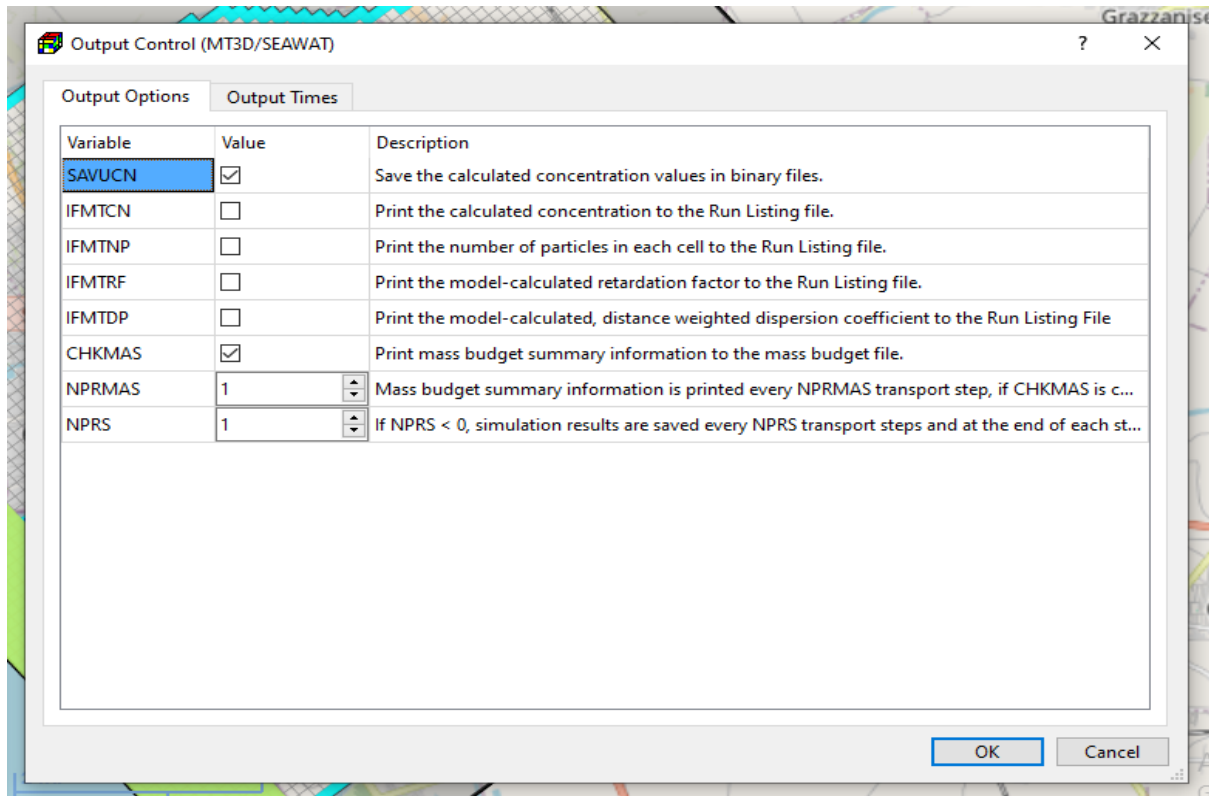


Figure 27 The Output Options tab of the Output Control (MT3D/SEAWAT) dialog box.

b. Output Times Tab:

- i. Table: The table contains the times at which the simulation results are saved and/or printed. Time values are expressed in the simulation time.
- ii. Start Time, End Time, and Time Interval: You can generate a list of output times by specifying the Start Time, End Time, and Time Interval, then clicking the Apply button. Once the list of output times is generated, you may modify the output time values on the table. Those time values will be sorted in ascending order when you close the dialog box.

Set Default: Click this button to set Start Time to zero, End Time to the total simulation length of the flow simulation, Time Interval to one tenth of the total simulation length, and then populate the table accordingly.



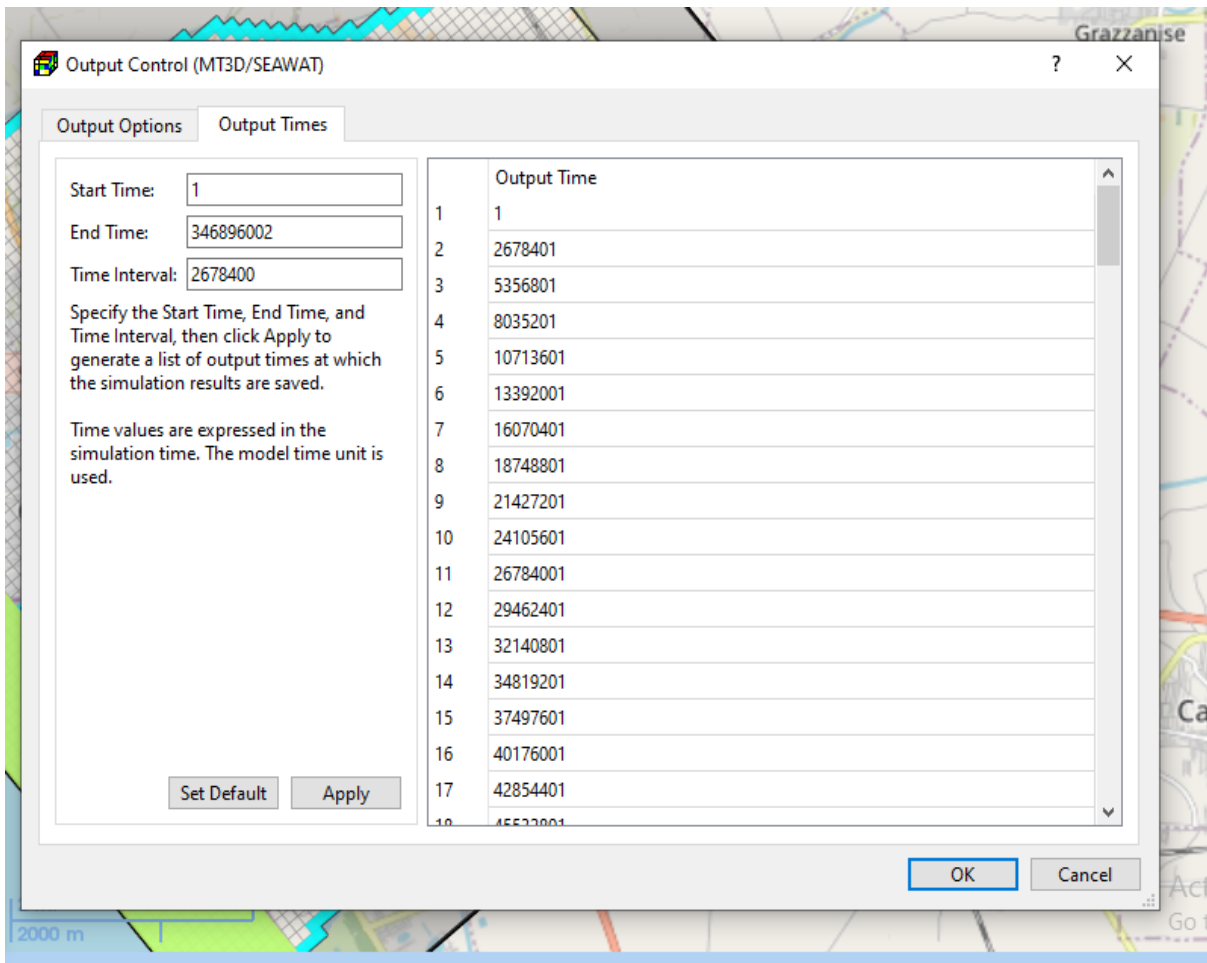


Figure 28 The Output Times tab of the Output Control (MT3D/SEAWAT) dialog box.

For the purposes of this study, SAVUCN was selected to save the calculated concentrations in binary files. CHKMAS was selected and NPRS was set to be greater than 0. Moreover, the Start Time, End Time, and Time Interval were set as 1s, 346896002 s, and 2678400 s respectively.

### 2.9.6 Run

Select this menu item to open the Run SEAWAT dialog box according to the transport model selected in the Transport Settings dialog box. The Run SEAWAT dialog box can be used to start a transport simulation or to build input files. The available settings of the dialog box are described below.

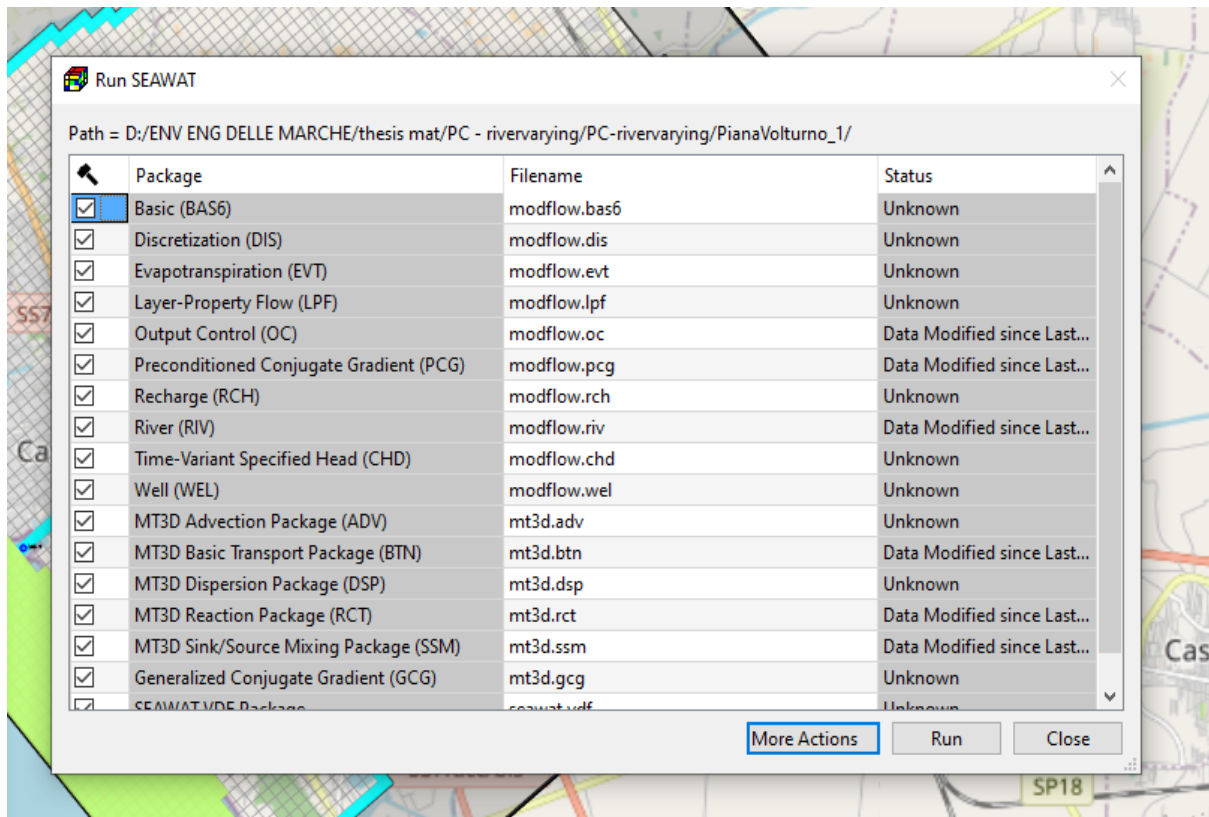


Figure 29 The Run SEAWAT dialog box.

1. Table:

- i. The build box. Prior to running a transport simulation, PM uses the user-specified data to build input files for SEAWAT. An input file will be built if its build box is checked. If an input file does not exist or the input data has been modified since the last build, its build box will be checked automatically.
- ii. Package is the name of the package of the flow model.
- iii. Filename is the name of the input file.

2. More actions

- i. Inspect Model Data: Select this to check the correctness and consistency of the model data.
- ii. Build Input Files: Select this to build the input files with the checked build boxes.
- iii. Rebuild All Input Files: Select this to rebuild all input files, except for existing input files that are marked as read-only.

3. Run: Click this button to build input files with the checked build boxes and the start the transport simulation.

- i. If Variable Density Flow and Transport (SEAWAT) is selected as the transport model, the simulation will be carried out the executable file of SEAWAT. The transport process can be density-dependent.

The transport simulation progress will be displayed in the SEAWAT Output window.

## 3.0 RESULTS AND DISCUSSIONS

In this section, results obtained from the HEC-RAS simulations of the VR from 2010 to 2020 are presented and discussed. Further, MODFLOW/SEAWAT results obtained from inputted salinities along the river from HEC-RAS simulations are presented and assessed. In addition, SEAWAT results considering paleo salinity is also presented and evaluated.

### 3.1 HEC-RAS Results

Results initially obtained from the HEC-RAS interpolations from inputted river stages at the river stations at CV and CA, and the sea levels at the estuary to determine the heads along the river reach are already presented in Section 2.3.8 in figure (16) which were used as input data for the River package in MODFLOW.

### 3.2 River Salinization by Tidal Forcing and Seawater Ingression

From the HEC-RAS simulations obtained for the river heads interpolations, and the salinity for the Tyrrhenian Sea and for freshwater according to Sorgente et al., (2020) and ARPAC (2023) indicates that, the maximum salinity is 38 g/L for the sea boundary condition whereas the minimum salinity is 0.4 g/L also at the river section at CA. Generally, the months of June, July, August, and September (summers) mostly had the peak salinity, whereas the months of November, December, January, February, and March (winters) had the minimum salinity along the river sections as shown in the figure below. Meanwhile, the salinity generally decreases along the river reach with the mid-section to the river station at CA recording low salinity and particularly for the months of February and March.

To further assess the salinity distribution along the river reach, the accuracy of the HEC-RAS simulation was investigated. Two snapshots within the winter and summer weeks were chosen to assess the SWI during periods of high river discharges (21st January 2014) and low discharges (12th July 2014). The profiles were sketched in red, including the profiles occurring after 6 and 12 hours (blue and green dashed lines) to depict the influence of tidal oscillation. It can be noticed from the salinity profile and schematic plot in the figure below that, salinity

distribution along the river reach varies as already indicated by both river discharges and tidal fluctuations, with high river salinization at the river mouth during low river discharges (summer) and tends to reduce gradually while moving upstream. In addition, it can be depicted from the figure (30) below that, during periods of high river discharges (winter), the tidal oscillations cannot be detected because of superiority of the river discharge, which indicates high river discharge is an inhibiting factor for SWI.

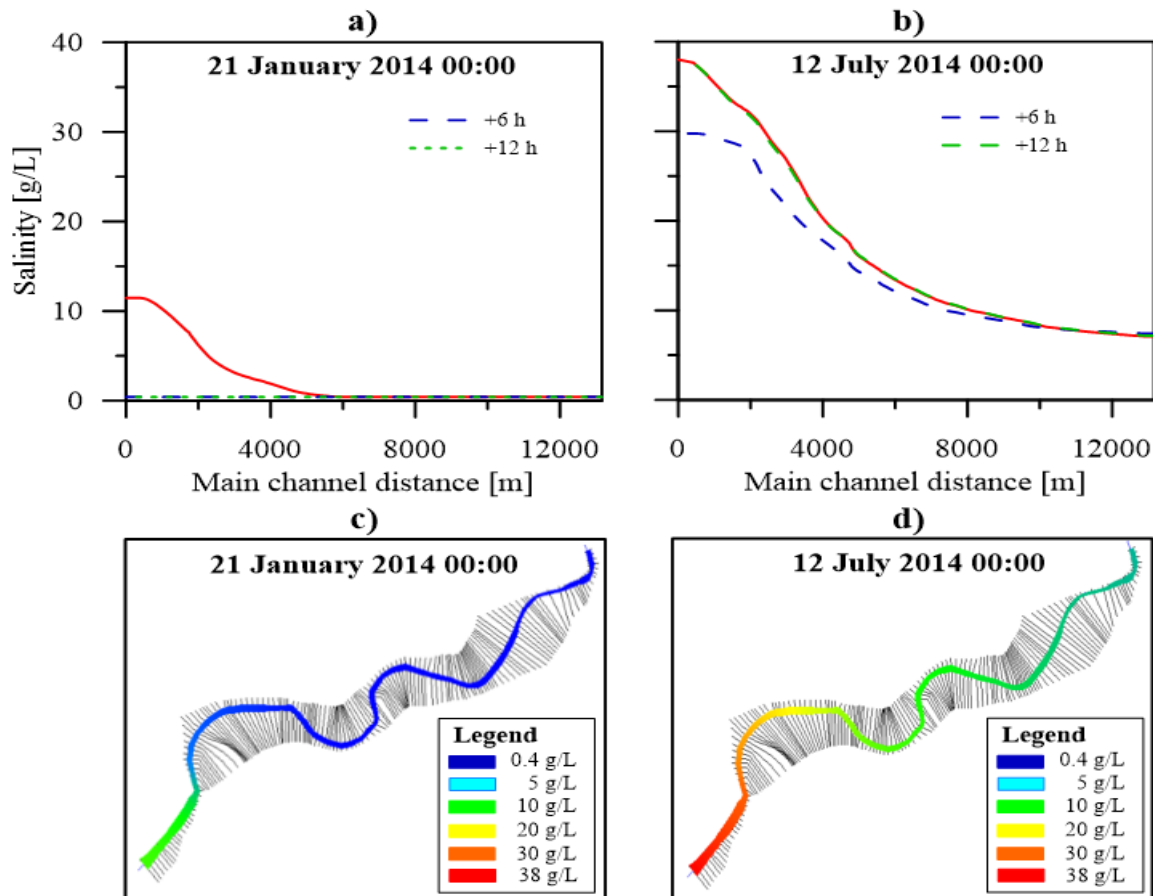


Figure 30 Salinity Profile and its associated snapshot (High Salinity (red) & Low Salinity (blue)) [Source: Gaiolini et al., 2023].

Furthermore, it can be noticed that the years 2010, 2011, 2013, and 2014 recorded averaged low salinities with values ranging between 18.6 to 22.5 g/L and 3 to 3.7 g/L at the river mouth and the river station at CA respectively, whereas the years 2012, 2015, 2016, 2017, 2018, 2019, and 2020 recorded averagely high salinities with concentrations ranging between 23 to 31 g/L and 3.3 to 4.4 g/L at the estuary and at CA respectively. It can be also noticed that the river mouth salinity is gradually on the ascendency from 2010 to 2020 from an annual average of 18.6 to 31 g/L although 2012 had high concentration and slight drop, as indicated in the figure (31) below which it can be attributed to progressing low discharges of the river and sea level

rise. The orange line shows the salinities at river mouth whereas the blue line indicates concentrations of the CA river station.

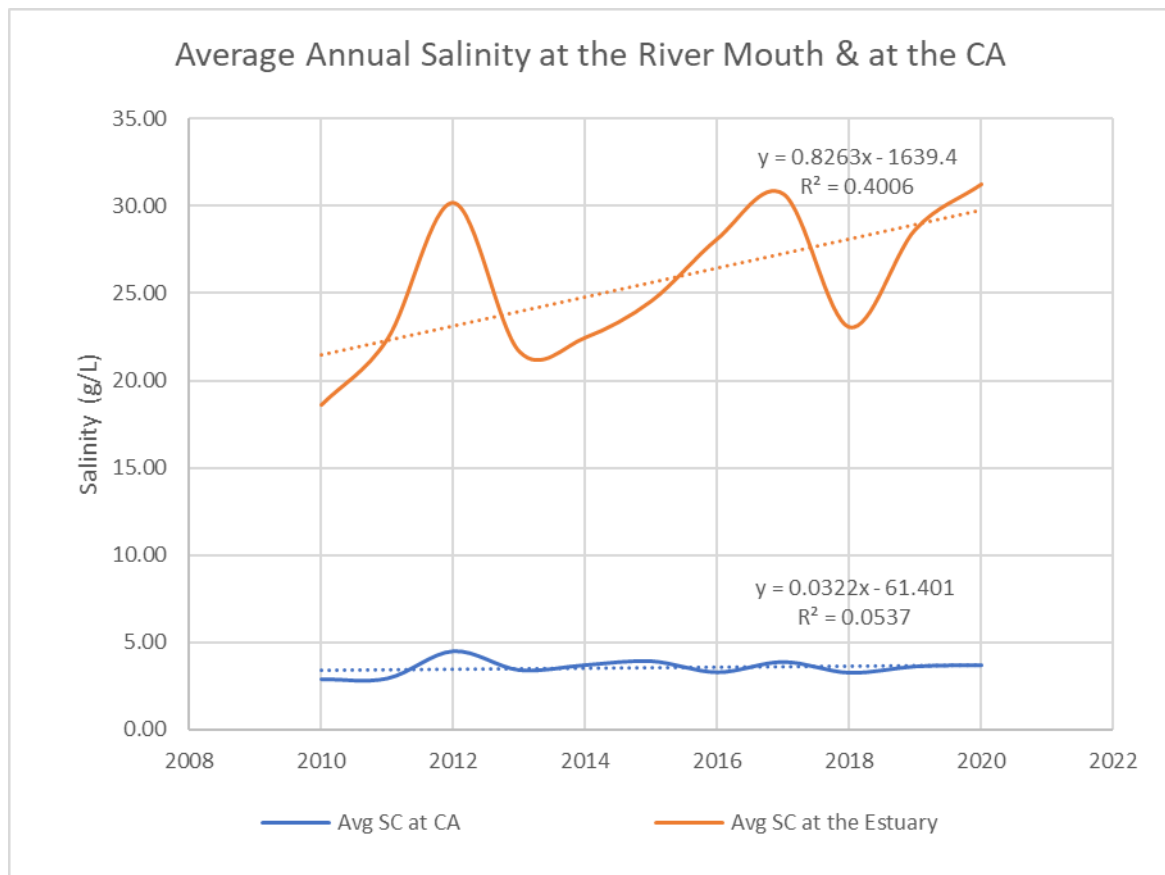


Figure 31 Salinity at the River Mouth and at CA.

Furthermore, it can be limned from the results of the HEC-RAS simulations in the figure (32) that the seasonal variation by meteoritic showers coupled with tidal fluctuations are influential in the variations of the salinity across the river reach. Moreover, all these salinities obtained from the HEC-RAS simulations indicates river salinization at selected distances from the estuary with the brown curve (peak salinization) indicating the salinity at 166.9 m to the light blue curve (lowest salinization) at 13.158 km from the estuary were imported as initial concentrations into SEAWAT for further simulations.

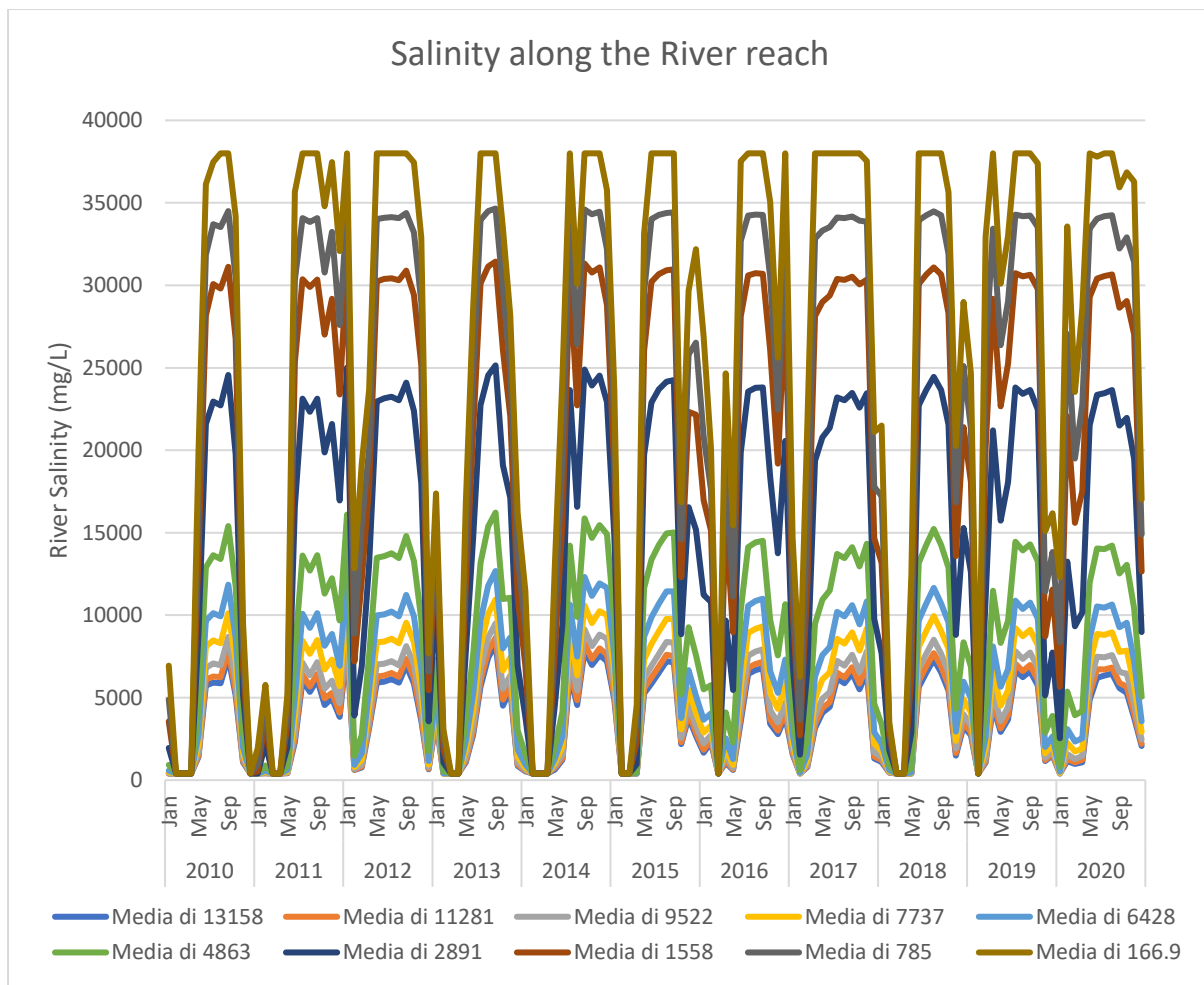


Figure 32 Initial River Salinity from HEC-RAS Simulations.

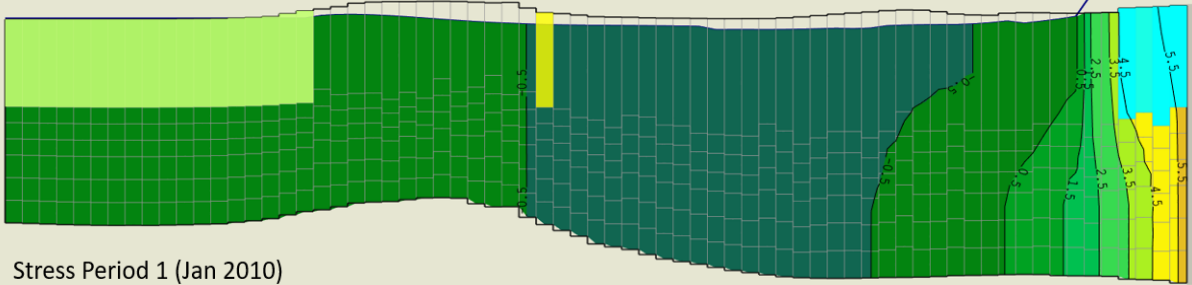
### 3.3 SEAWAT Results

Results obtained from MODFLOW/SEAWAT simulations after the modelling are presented and discussed in this section. SWI by paleo salinity and actual seawater intrusion are discussed to determine the dominating parameters controlling the aquifer salinization.

### 3.4 Heads contours results

To visualize the flow direction in the aquifer during the period of simulation, different cells located at different areas are selected to characterize flow trend in the aquifer since the area under study is geologically complicated and characterized by different depositional environments dunes, marshes and wetlands. Four different parallel cells are selected (row 25, 55, 40 & 65) with rows 25 and 40 within the river channel and Canale Agnena, whereas rows 55 and 65 are within the river channel and Regi Lagni canal. Moreover, different stress periods in sequential order were selected to clearly determine trend and direction of flow within the aquifer.

(a) Head contour for row 25



(b) Head contour for row 25

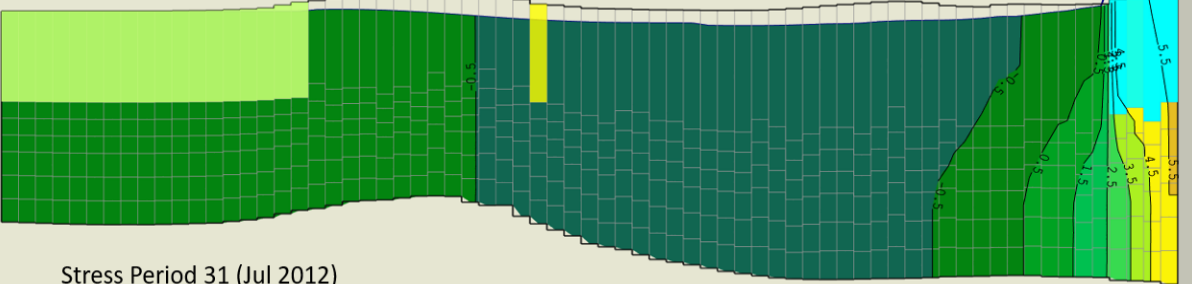
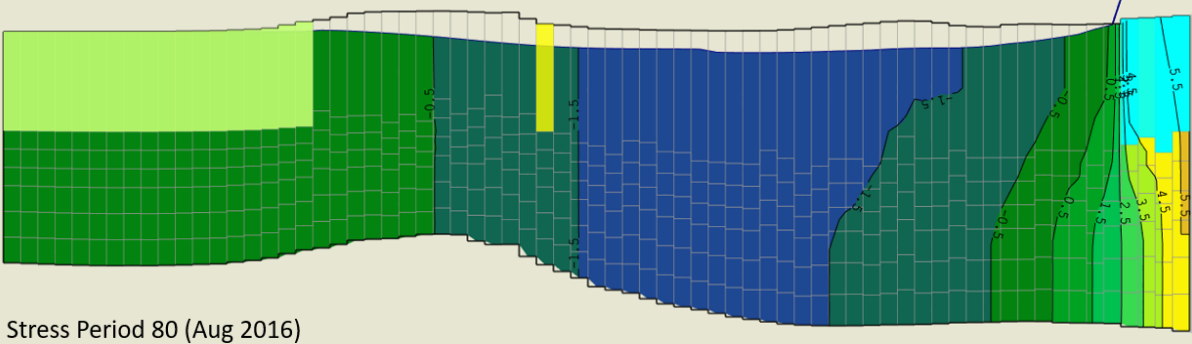


Figure 33 Head contour for row 25.

(c) Head contour for row 25



(d) Head contour for row 25

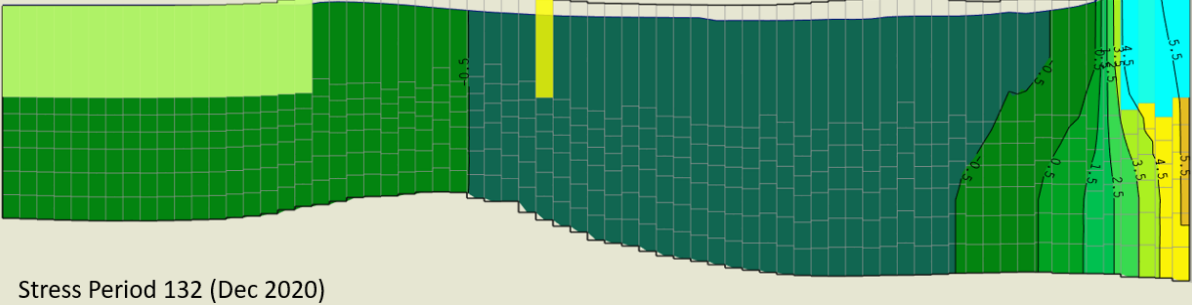


Figure 34 Head contour for row 25.



From the figures (33 & 34), with the uppermost area coloured yellow representing the location of the selected cell, it could be portrayed that the direction of flow is towards the teal to blue area (with the surface occupied by the wetlands within the river channel and the Canale Agnena) with the winters [(a) Jan 2010 & (d) Dec 2020] having high Heads whereas the summers [(b) Jul 2013 & (c) Aug 2016] are characterised by comparatively low heads which was due to high evapotranspiration and low precipitation. It could also be noticed from sections (a) and (d) [Jan 2010 & Dec 2020] that there is a marginal reduction in the Heads, considering contour [Head] (-0.5 m a.s.l.).

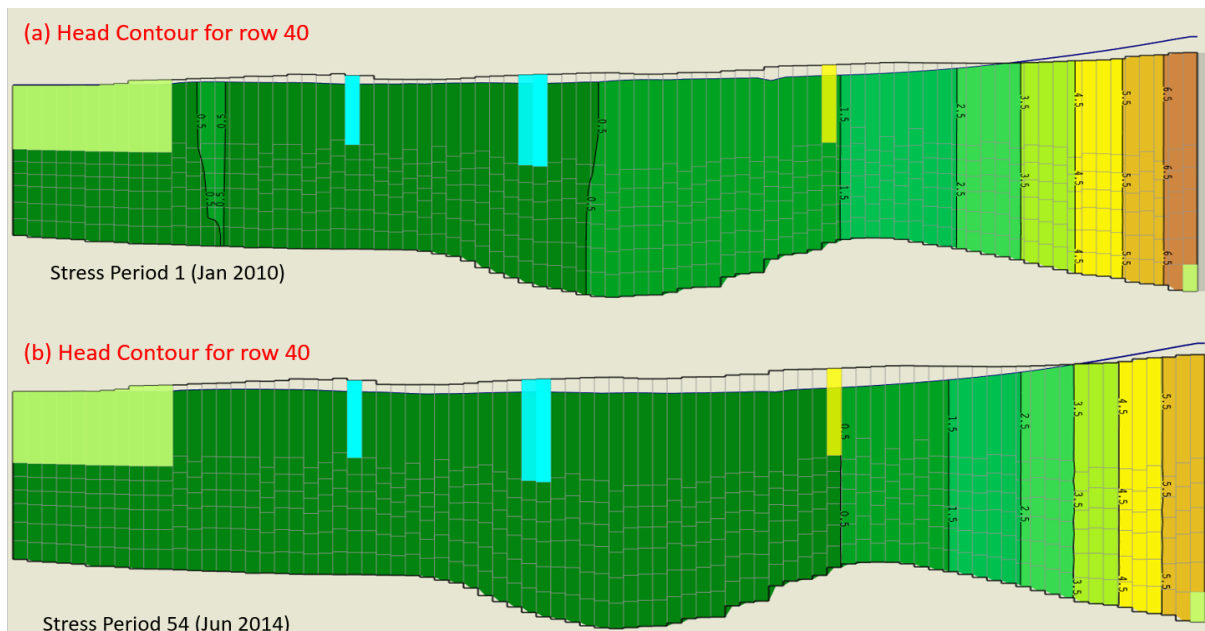


Figure 35 Head contour for row 40.

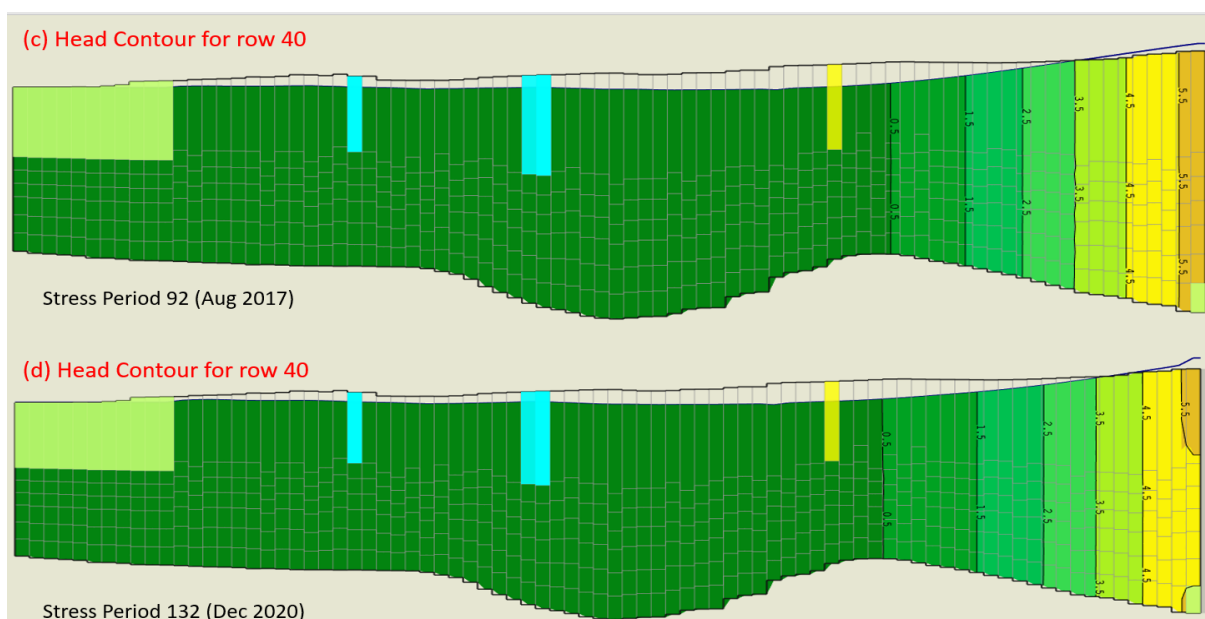


Figure 36 Head contour for row 40.

The figures (35 & 36) the depict the flow direction considering row 40, the uppermost yellow area represents the selected cell. It could be identified from the sections, the gentle propagation of the contours toward the bowl-shaped area (with the surface characterized by the wetlands and swamps) and signifying a gentle flow in the direction of the wetlands. Comparatively, stress period 1 (Jan 2010) recorded higher Heads in the direction of the wetlands with stress period 92 (Aug 2017) recording low Heads towards the wetlands signifying very low flows. It can be portrayed that there is a significant reduction in Heads towards the wetlands from stress period 1 to 132 considering the locations of contours (Heads) [0.5 & 1.5 m a.s.l.] which might be due to droughts or high evapotranspiration within the period under consideration.

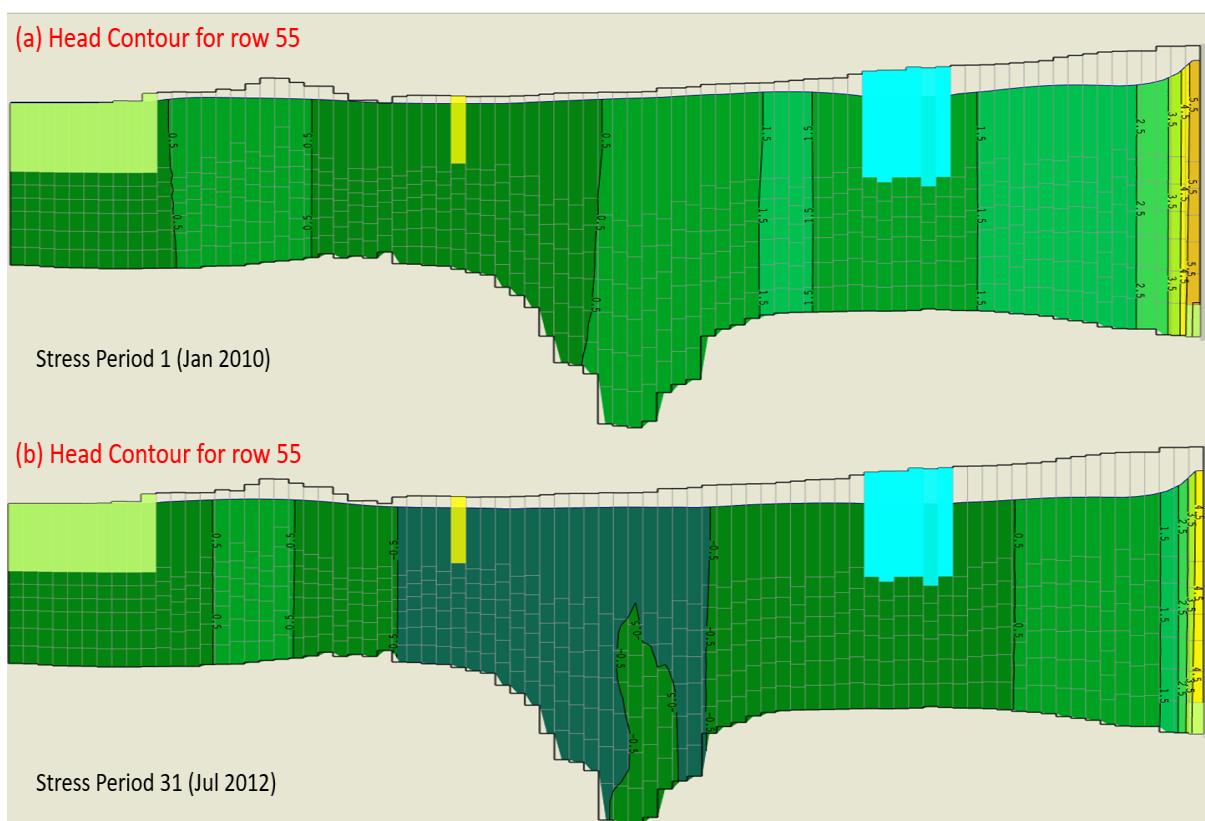


Figure 37 Head contour for row 55.

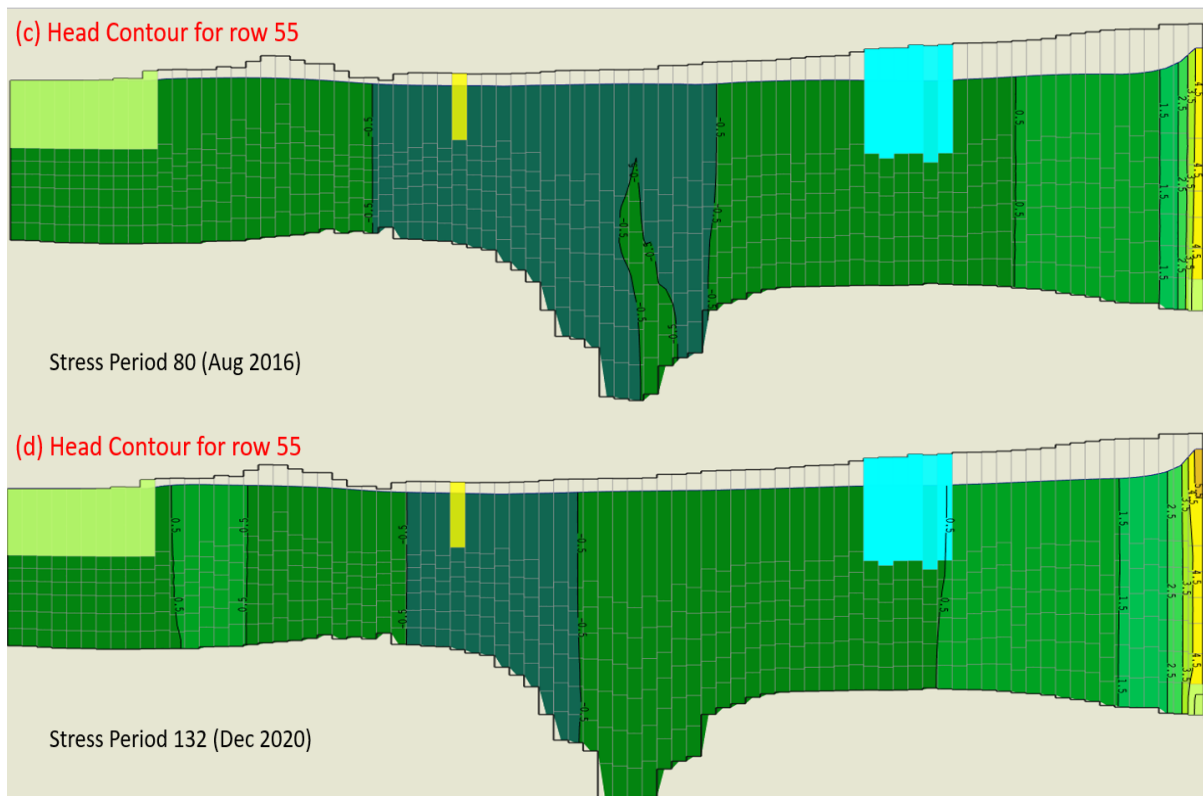


Figure 38 Head contour for row 55.

The figures (37 & 38) depict the Heads and flow direction within aquifer between the river channel and Regi Lagni canal. It's evident that the direction of flow is towards the wetlands between the river channel and canal with stress period 1 (Jan 2010) recording the high Heads signifying high flows into the wetlands during the winters. However, Heads recorded for the summers (stress period 31 [Jul 2012] & stress period 80 [Aug 2016]) are very low within the wetland even below m.s.l. indicating drought conditions coupled with evapotranspiration. It could be noticed that there is high reduction in Heads within the wetland comparing the Heads of stress period 1 (Jan 2010) to stress period 132 (Dec 2020).

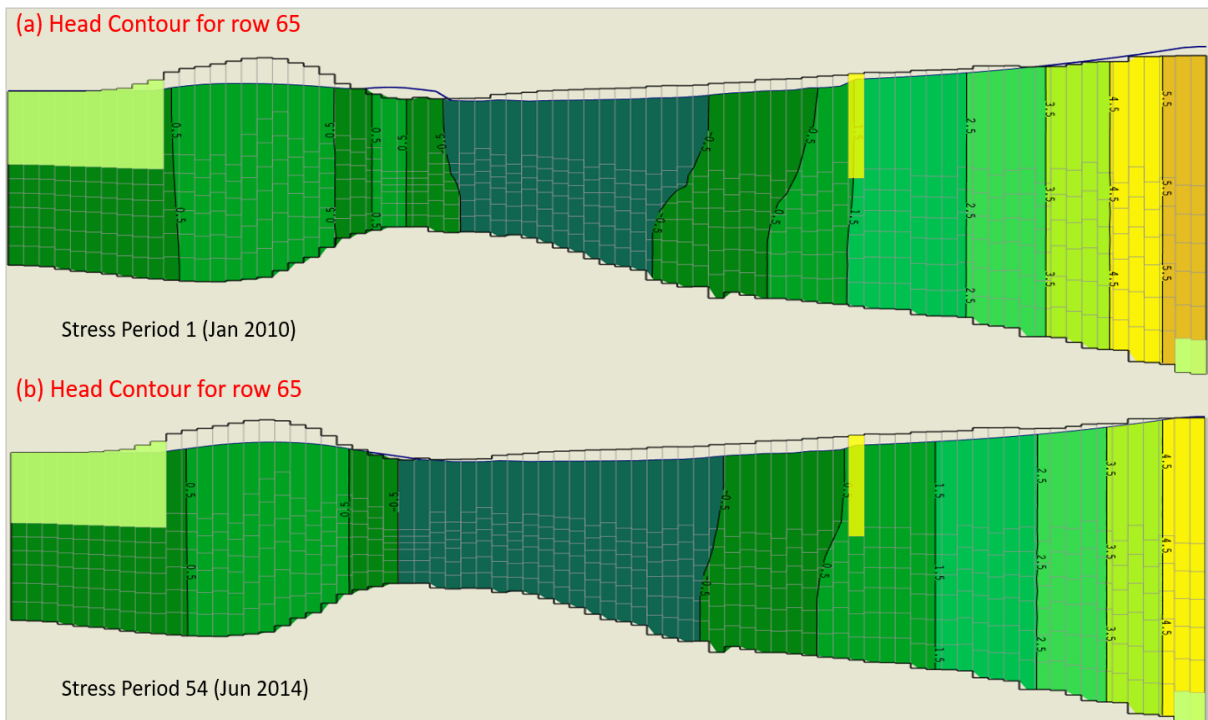


Figure 39 Head contour for row 65.

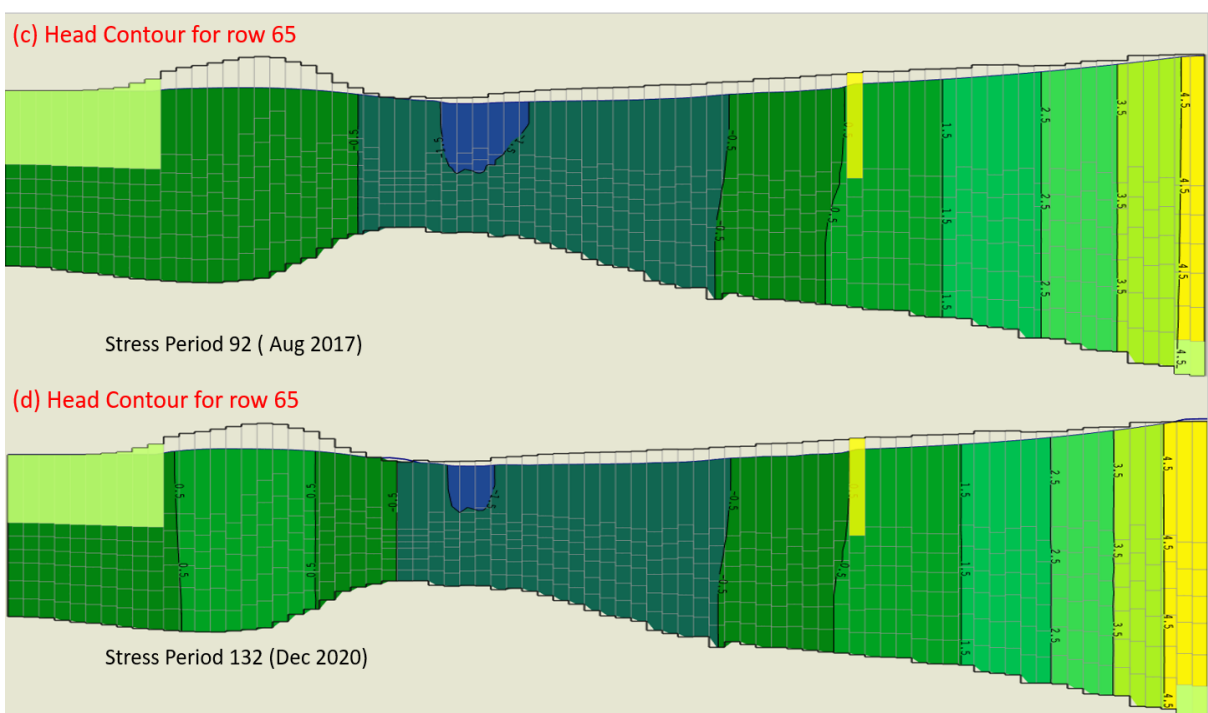


Figure 40 Head contour for row 65.

The figures (39 & 40) portray the Heads and flow direction within the aquifer between the river channel and Regi Lagni canal. It could be showed that the direction of flow is towards the teal area (with wetlands on the surface) with the stress period 1 (Jan 2010 in section [a]) recording high Heads. The Heads gradually decreases in the summers with stress period 92 (Aug 2017 in

section [c]) recording low Heads. And can be noticed that there's a reduction in the Heads from stress period 1 to 132 as already noted for other scenarios.

Furthermore, it can be affirmed that the direction of flow in the aquifer is towards the wetlands at both sides of the river channel with the winters having comparatively high Heads than the summers. In addition, it can be confirmed that there is a gradual reduction in Heads during the period under consideration with some periods (summers) recording Heads below m.s.l. in the wetlands.

### 3.5 Maps and Heads in selected piezometers

To confirm the findings illustrated in the previous section (3.4) to determine the direction of flow within the aquifer and the time evolution of Hydraulic Heads during the period of simulation, snapshots for four different stress periods (1, 54, 92 & 132) as used in the previous section were made at the mid-section of the (layer 4). Graphs depicting the piezometric heads of the selected observation points to characterize the Heads within the aquifer are presented below.

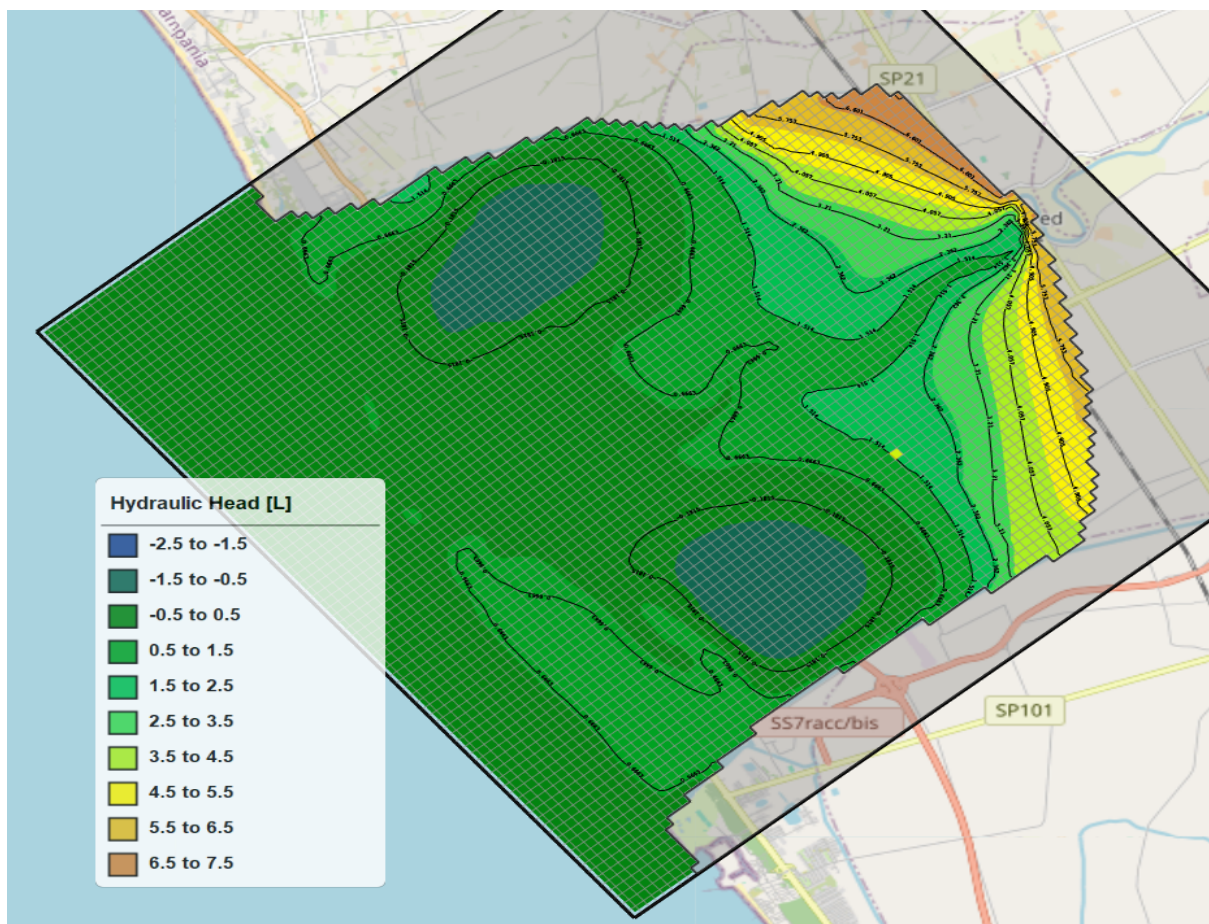


Figure 41 Piezometric map for Stress Period 1 [Jan 2010] (layer 4).



From the figure (41), the direction of flows is towards the blue coloured areas (with the surface characterized by the wetlands) with majority of heads ranging from -0.5 to 0.5 m a.s.l., with marginal heads difference between the wetlands and the seabed signifying low flows from the direction of the sea towards the wetlands.

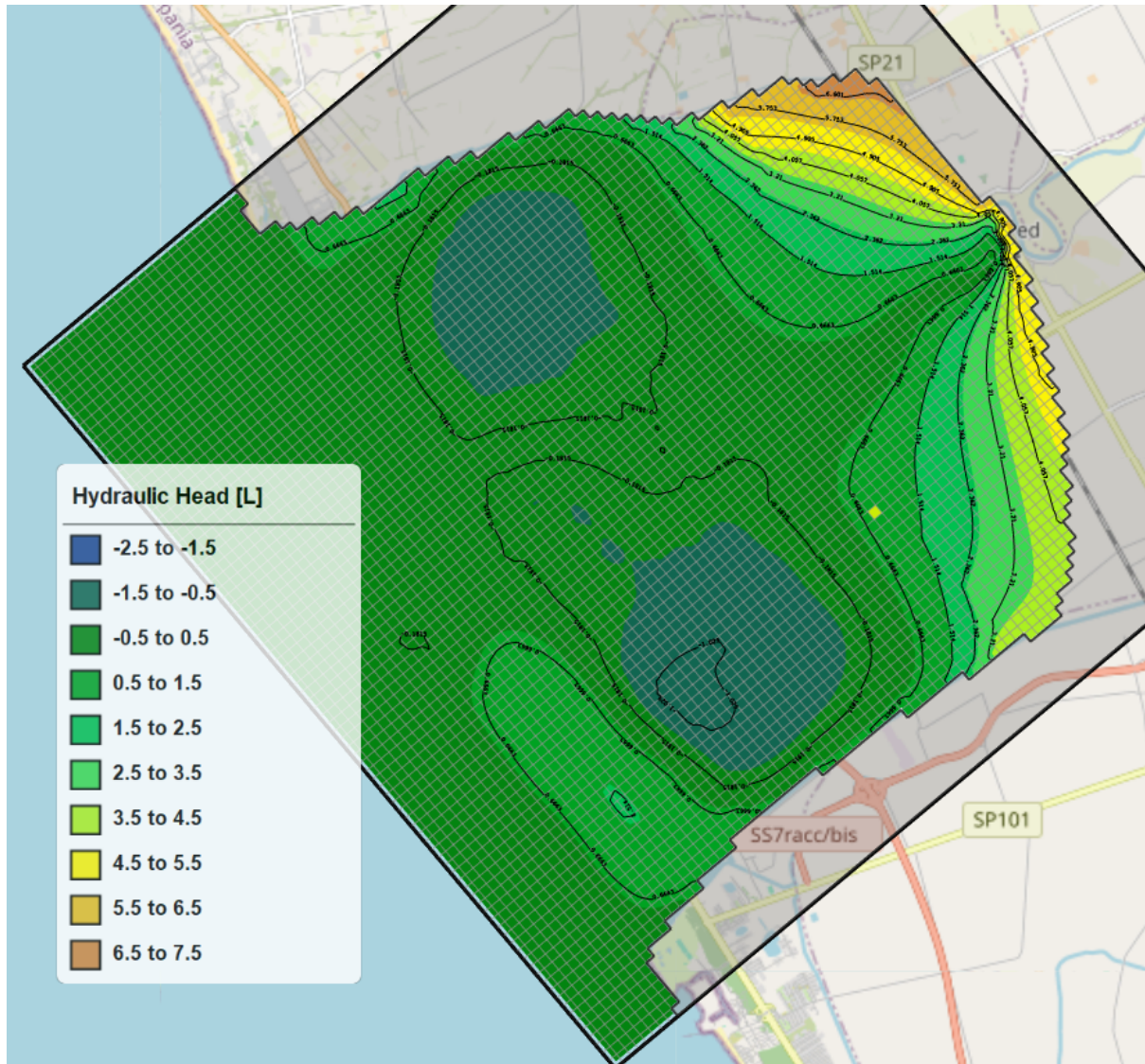


Figure 42 Piezometric map for Stress Period 54 [Jun 2014] (layer 4).

The figure above (42) is quite similar to the previous figure (40). However, the wetlands (surface of the blue areas) compared to the previous figure (40) is quite wide signifying a drop in Heads during the summers. During stress period 54, majority of the aquifer is characterized by Heads ranging from -1.5 to 0.5 m a.s.l.

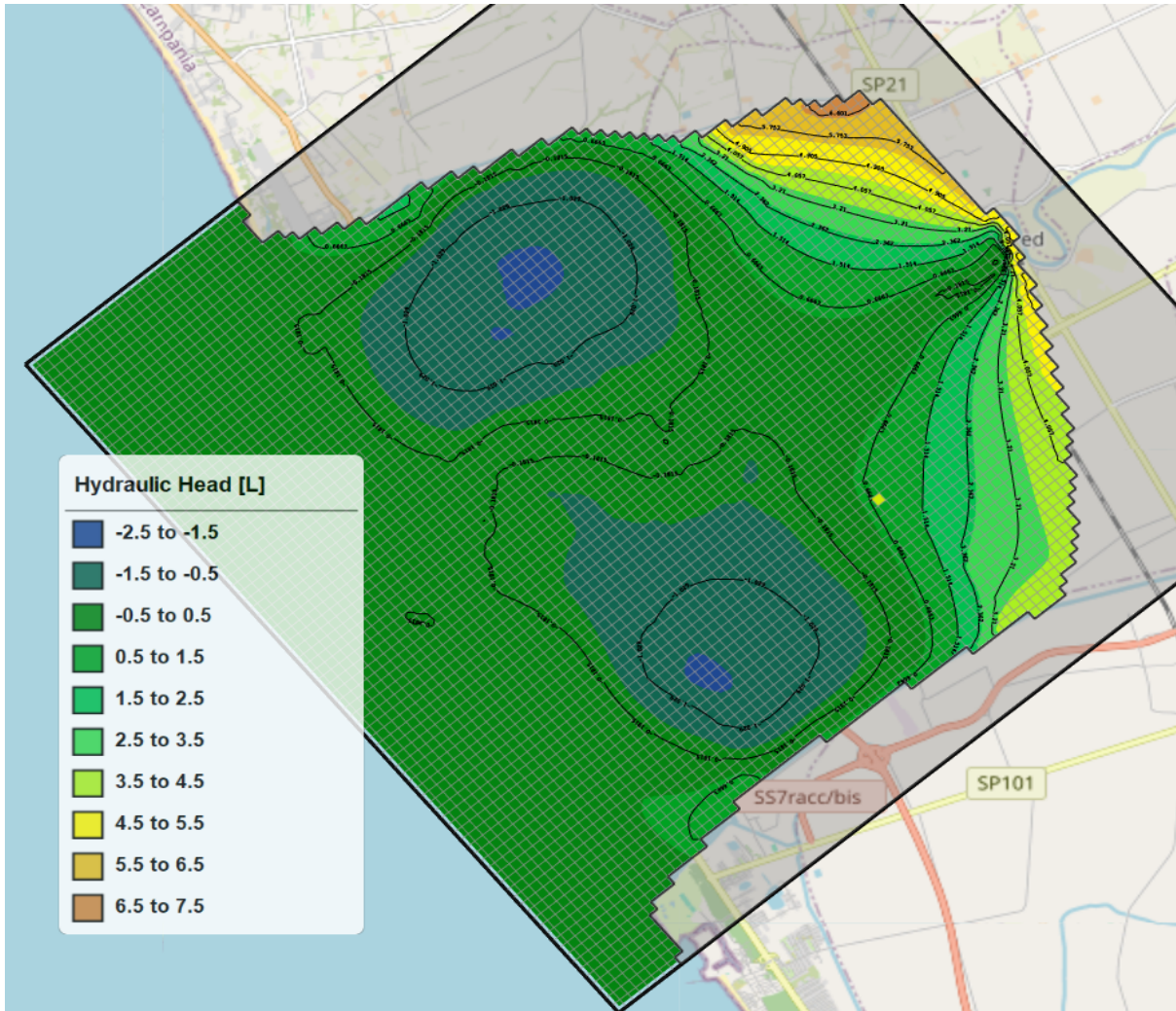


Figure 43 Piezometric map for Stress Period 92 [Aug 2017] (layer 4).

It can be identified from the above figure (43) that the flow is towards the direction of the blue areas as already noted in the previous figures (41 & 42). However, the spaces occupied the blue areas have increased significantly when compared to the previous figures (41 & 42) implying a higher drop in Heads from stress period 1 to 92 indicating gradual reduction of water in the aquifer which might be due to low precipitation and high evapotranspiration. Moreover, majority of the aquifer during stress period 92 is characterized by Heads between -2.5 to 0.5 m a.s.l. which confirms the drop in Heads.



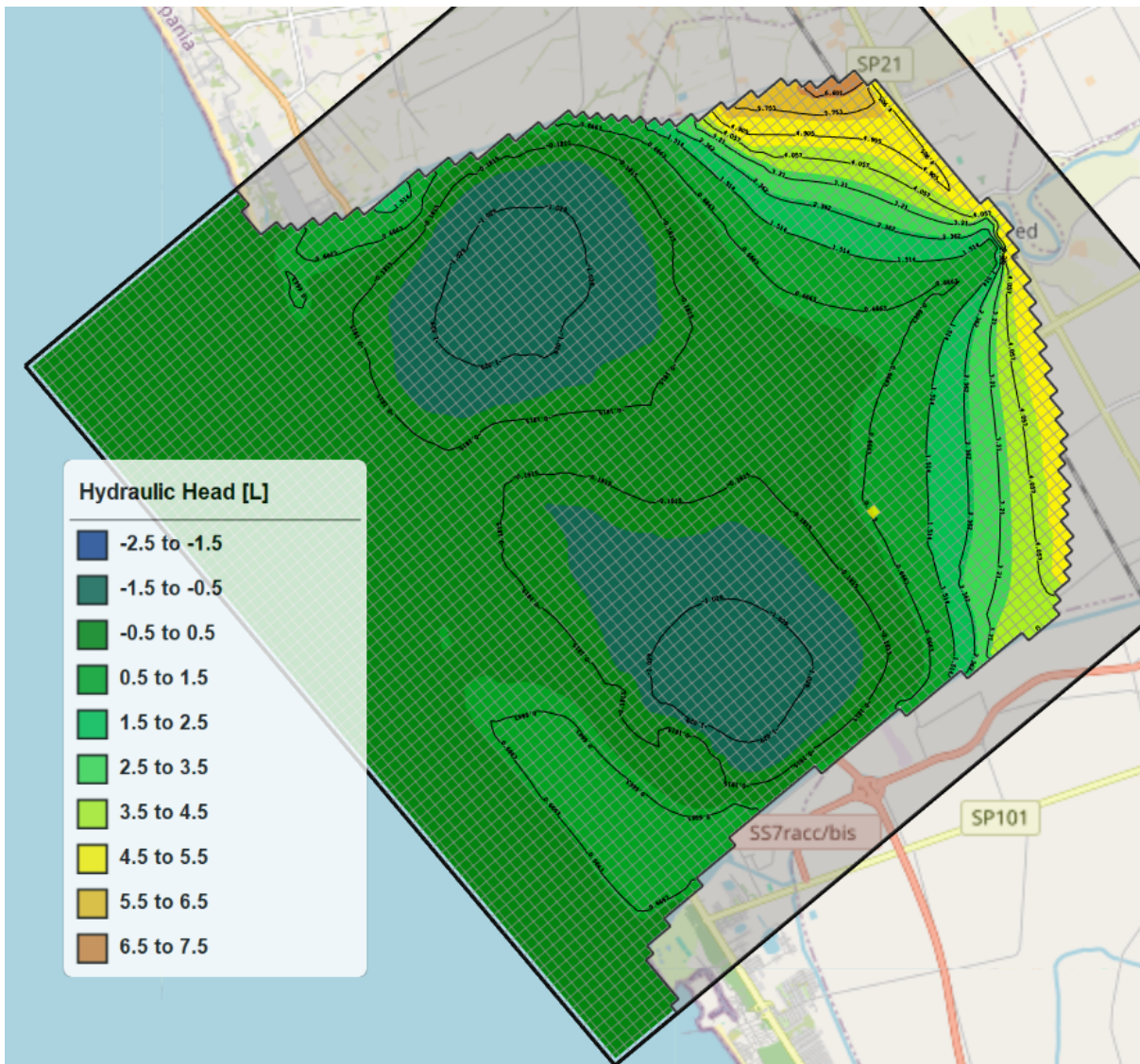


Figure 44 Piezometric map for Stress Period 132 [Dec 2020] (layer 4).

The figure (43) above is similar to the figures (41, 42, & 43) which are already discussed and confirm the direction of flow is towards the wetlands (surface of the blue areas). Although stress period 132 (Dec 2020) occurred in winter, there are wide areas in the figure characterized by Heads between -2.5 to 0.5 m a.s.l. It can be identified that the spaces occupied by the blue areas (Heads between -2.5 to -1.5 m a.s.l.) have increased during the period under consideration indicating a gradual decline in Hydraulic Heads within the aquifer.

To confirm these findings, the time evolution of the Hydraulic Heads during the period of simulation were assessed by evaluating the piezometric heads at specific observation points (Piezometers) with the results obtained presented below.

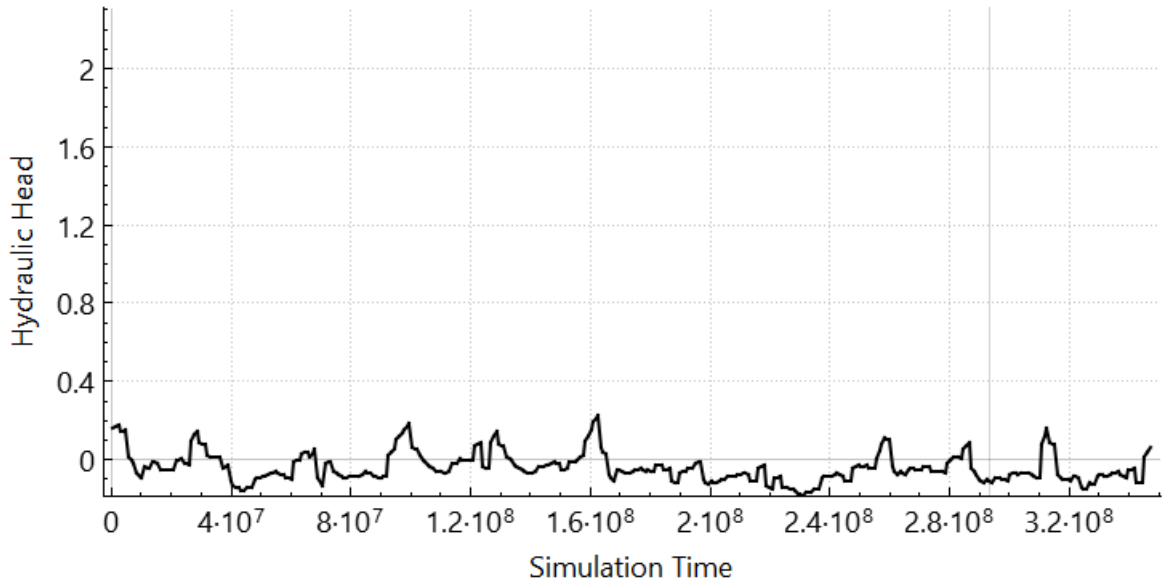


Figure 45 Hydraulic Head evolution of observation point (JAREX).

The figure (45) above shows the time evolution of the Hydraulic Head of observation point Piezometer JAREX), it can be noted that the Head oscillates in relation to seasonal variations of recharge and discharge with most period during the simulation recording Heads below the sea level, indicating the gradual decrease in Heads within the aquifer during the period of study.

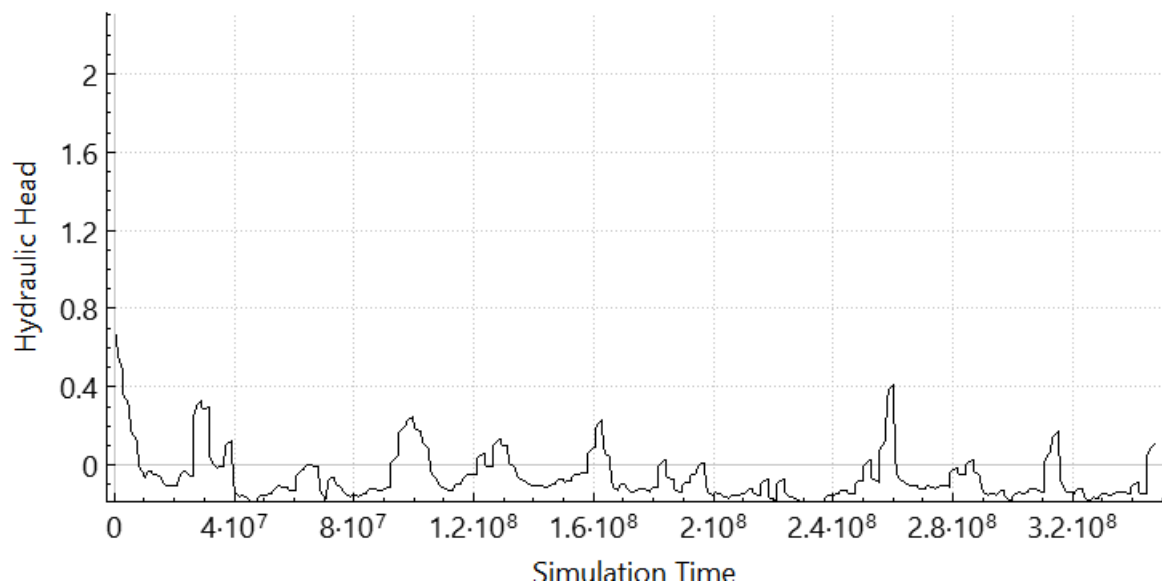


Figure 46 Hydraulic Head evolution of observation point (OWXWS).

The figure (46) above portrays the time evolution of the Hydraulic Head of observation point (Piezometer OWXWS), the evolution of the Head of this observation point with time is in relation to seasonal variations with recharge and discharge. Moreover, there is a significant

reduction in Head from the beginning to end of the simulation (from 0.7 to 0.3 m a.s.l.) with many periods within the time of simulation recording Heads below the sea level similar to the previous piezometer.

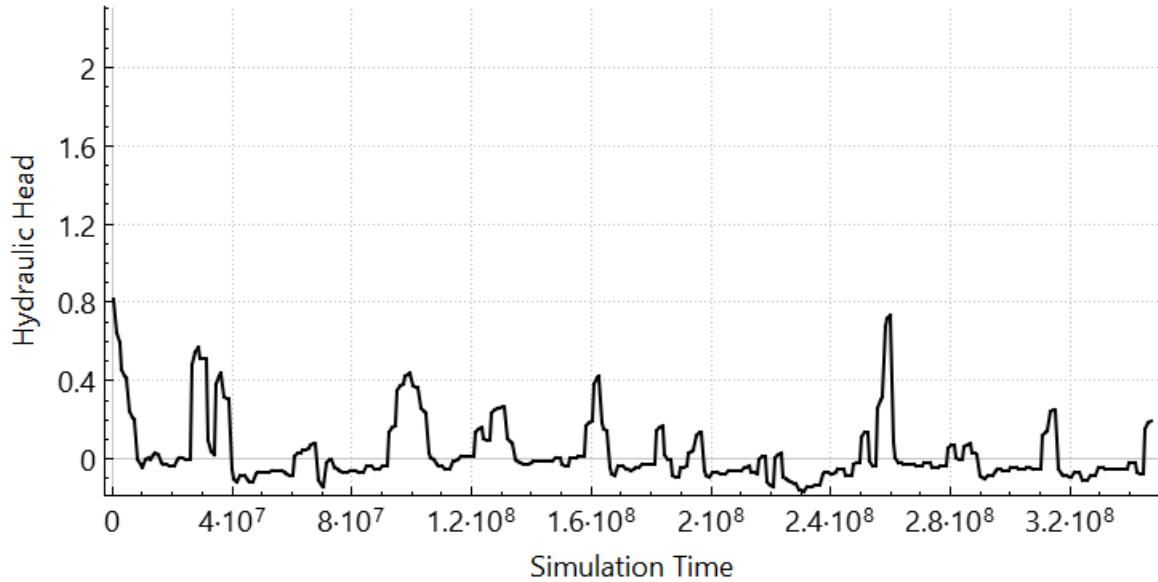


Figure 47 Hydraulic Head evolution of observation point (VFI1E).

The figure (47) above depicts the time evolution of the Hydraulic Head of observation point (Piezometer VFI1E), the evolution of the Hydraulic Head of this observation point is quite similar to the previous observation point discussed in figure (46). However, this observation point is characterized by periods recording Heads mostly above the sea level although there is a reduction in Head from the beginning to the end of the simulation period.

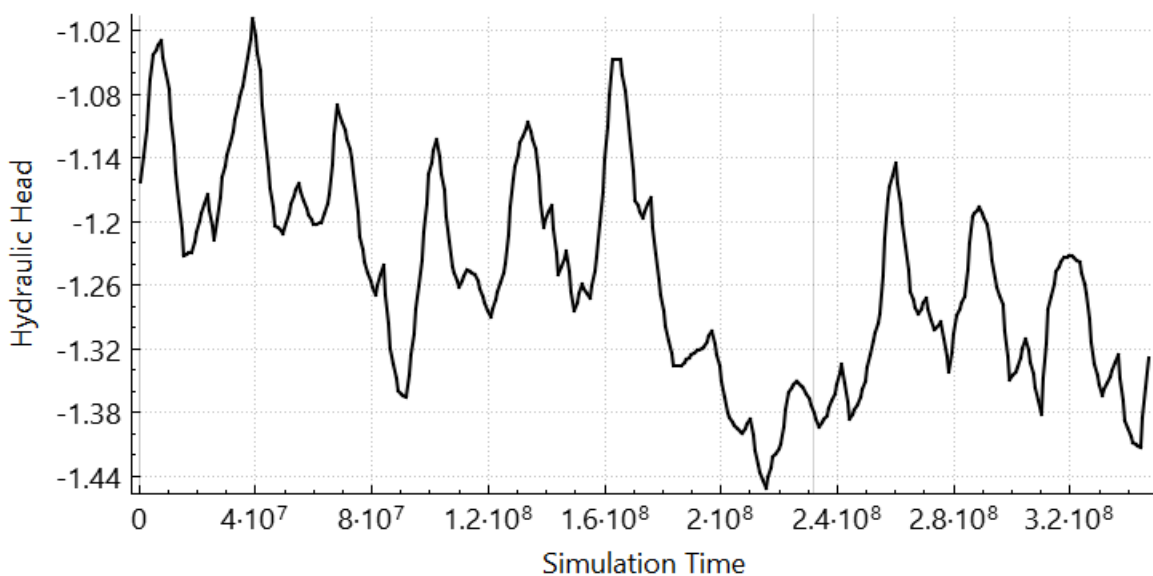


Figure 48 Hydraulic Head evolution of observation point (XAD2U).

The figure (48) above describes the time evolution of the piezometric height at observation point (Piezometer XAD2U). The evolution of the Head depicts an oscillating decreasing trend representing periods of recharge and discharge, and the gradual decline in Heads of the aquifer at this location (from -1.14 to -1.32 m a.s.l).

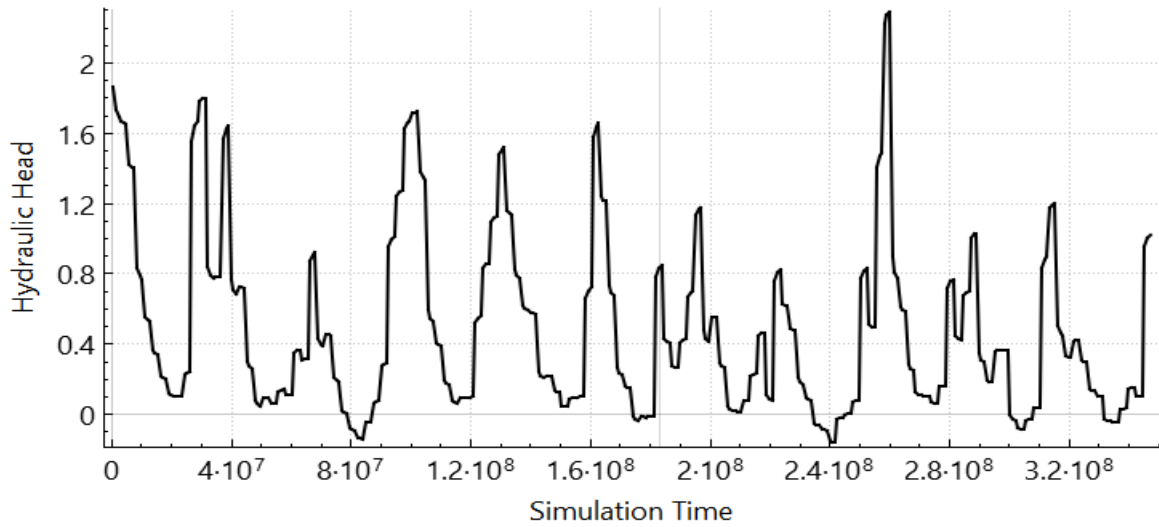


Figure 49 Hydraulic Head evolution of observation point (13158).

The figure (49) above shows the time evolution of the Hydraulic Head of observation point (Piezometer 13158), clearly representing periods of recharge and drought and its impacts on the river flow and its relationship with the aquifer, with few periods recording Heads below the sea level. However, it can be noticed that there is a decline in Head from the beginning to the end of the simulation (1.9 to 1.1 m a.s.l.) indicating gradual decline in discharge of the aquifer during the period of the study.

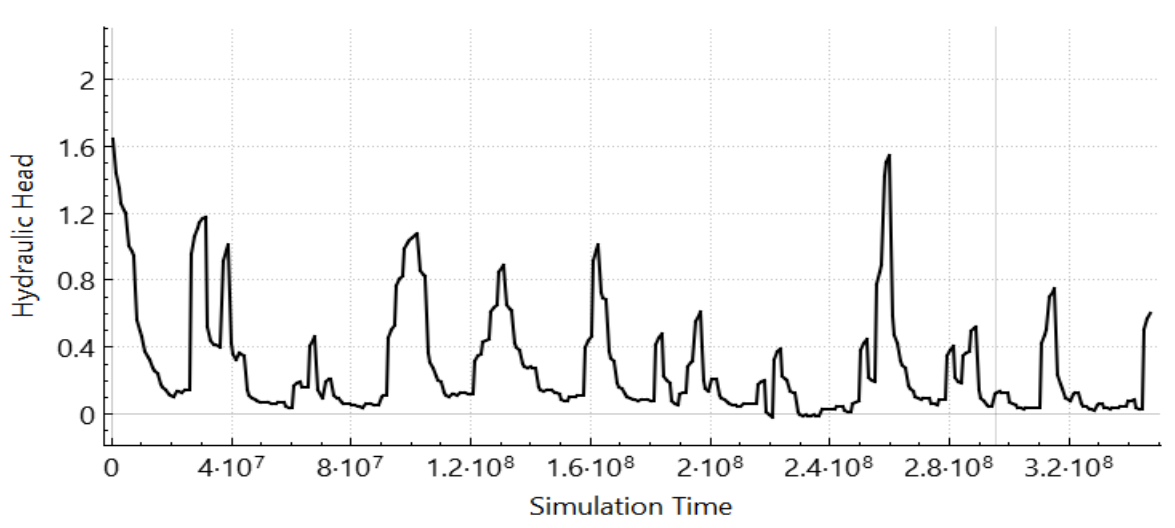


Figure 50 Hydraulic Head evolution of observation point (11281).

The figure (50) above is quite similar to the previously discussed figure (49). The Piezometric Head evolution with time portrays seasonal variations with periods of precipitation and drought. Similarly, to previously discussed observations points (Piezometers), there is a progressive decline in Head from the start of the simulation to the end (from 1.6 to 0.8 m a.s.l.), also indicating the gradual decline in Hydraulic Heads within the aquifer.

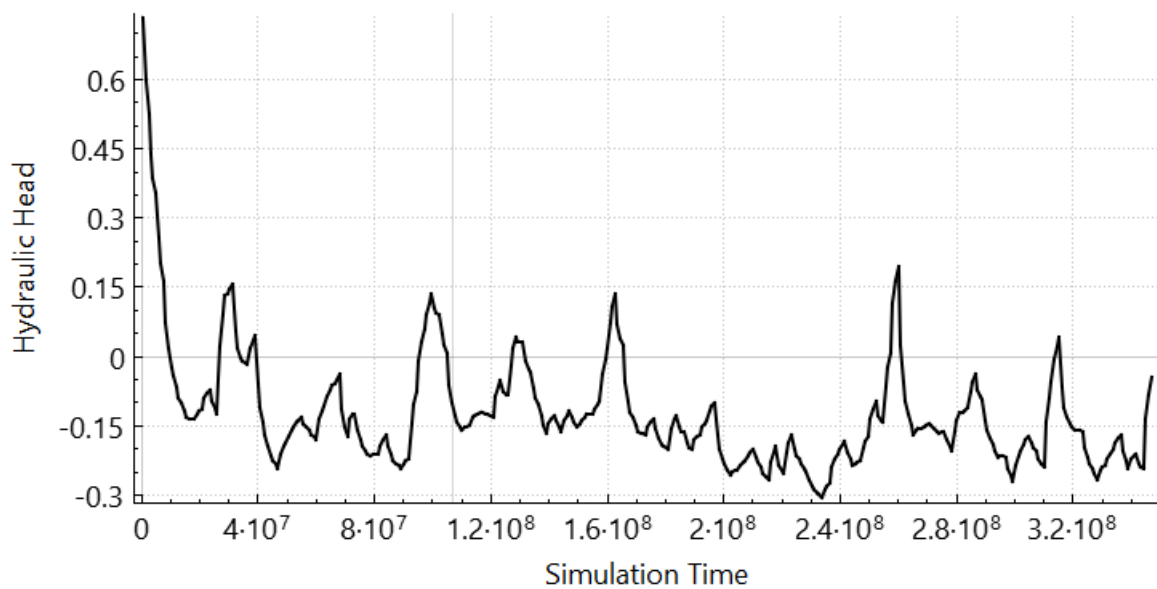


Figure 51 Hydraulic Head evolution of observation point (PTIRM).

The figure (51) above describes the time evolution of piezometric level within observations point (Piezometer PTIRM). This Piezometer has Head declining sharply and resuming stability within -0.15 to 0.15 m a.s.l. It can also be noticed that many periods within this Piezometer recorded Heads below sea level, signifying gradual decline Heads within the aquifer as already indicated.

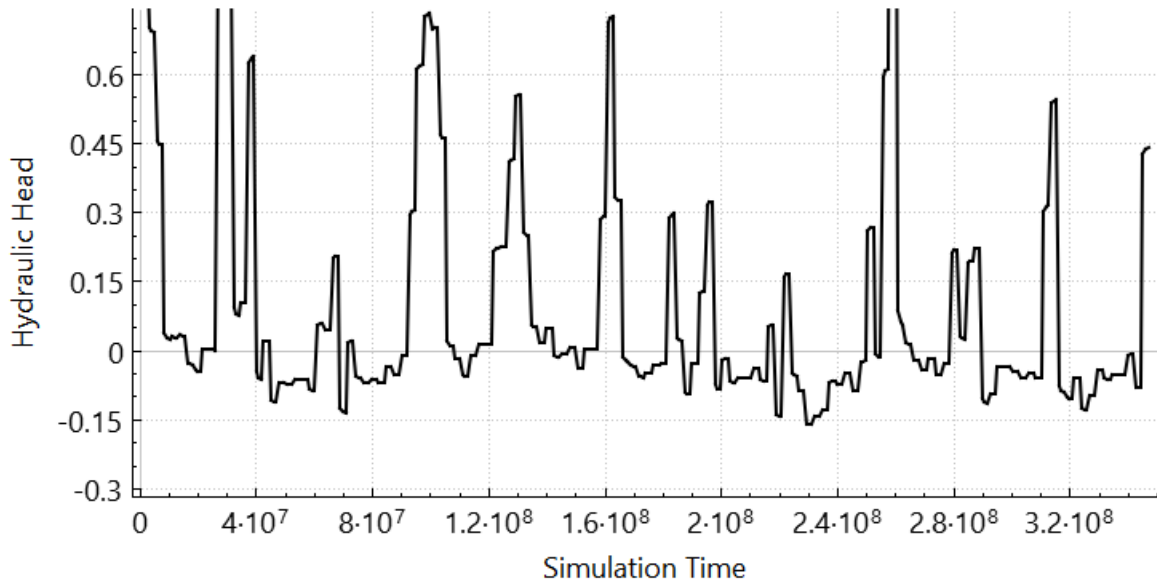


Figure 52 Hydraulic Head evolution of observation point (ZGV7V).

The figure (52) describes the time evolution of the Hydraulic Head in observation point (Piezometer ZGV7V). This Piezometer is characterized by oscillating Head in response to recharge and discharge and has majority of the periods within the simulation time recording Heads above the sea level. The slopes of the Head within this point in the aquifer indicates rapid recharge and discharge events.

### 3.6 Water Fluxes

With the aid of PM 11 ZoneBudget routine by assigning a defined zone number, the surface-ground-water interactions and their importance in relation to the overall model domain was assessed in terms of water budget component.

Groundwater storage refers to the storing abilities of the aquifer over a period, thus the difference between recharge and discharge. In MODFLOW, the net inflow of water into the groundwater system is denoted by the phrase "storage in". The computation involves adding up the recharge, surface inflow, and any additional water sources that enter the system, deducting the pumping, and then figuring out the remaining water sinks. Whereas "storage out" refers the net outflow of water from the groundwater system, occurring through processes such as pumping and evapotranspiration. It can be identified that storage into the aquifer was high between April and September, with flowrates ranging between 0.61 to 1.24 m<sup>3</sup>/s and the peak flowrate in April 2018. The storage out refers to the discharge from the aquifer, which ranged between 0.61 to 2.17 m<sup>3</sup>/s from November to March, and the peak flowrate occurring in

November 2019. Based on the differences in flowrates for the storage in and out, it is quite evident that the aquifer might be feeding the river.

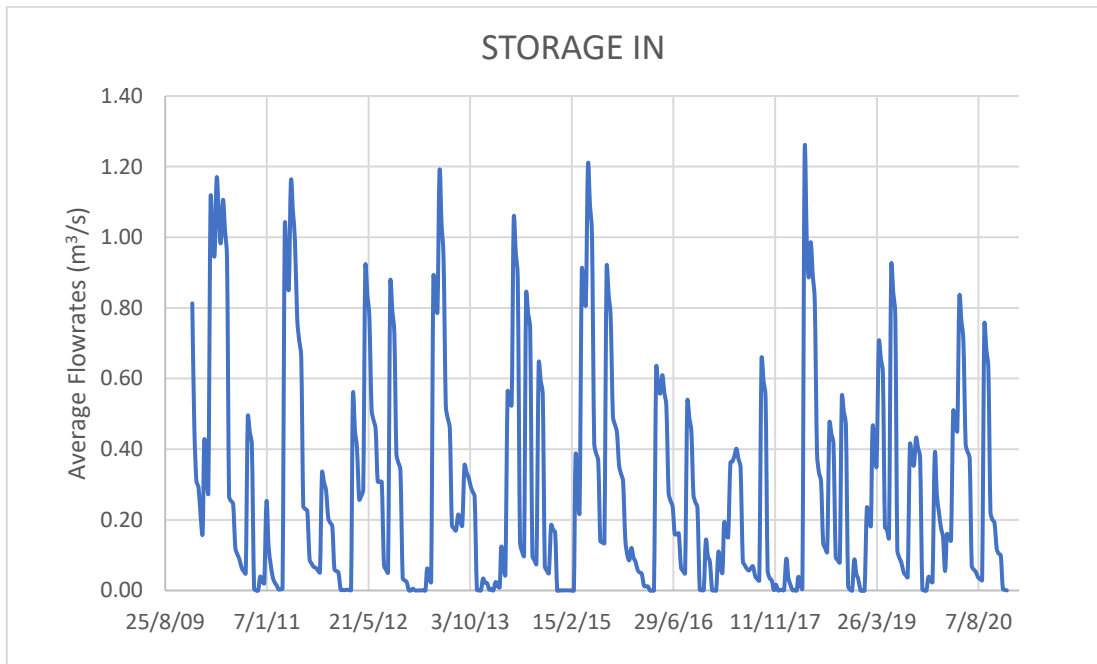


Figure 53 Storage In.

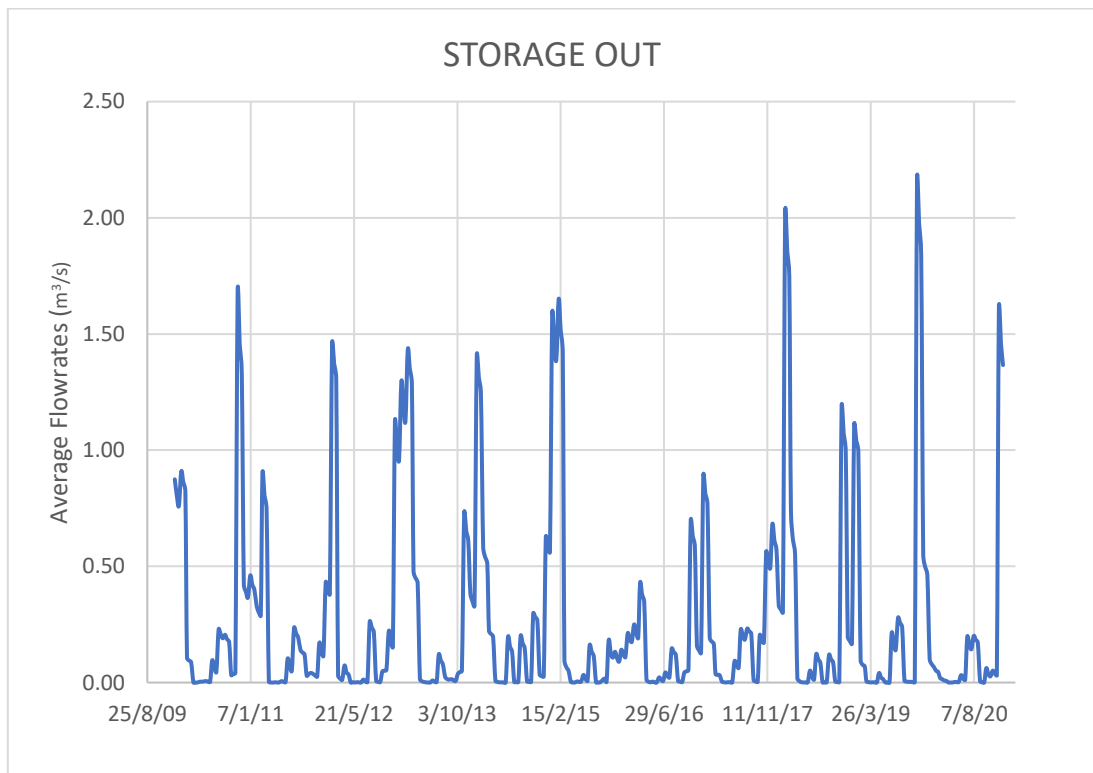


Figure 54 Storage Out.



River leakage is the river inflow into the aquifer, and depends on the riverbed conductance and elevation, and the river stage, determining the interaction between the aquifer and the river. It can be noticed that the leakage in from the river into the aquifer occurs mostly between the months of May to October with maximum flowrates between 0.35 to 0.48 m<sup>3</sup>/s with the peak value occurring in June 2019. Whereas the river leakage out of the groundwater into the river occurred mostly for the months of January to April with flowrates ranging from 0.8 to 1.2 m<sup>3</sup>/s with the maximum flowrate recorded in January 2010. Moreover, from the figures (55 & 56) below, it could be noted that river leakage in varies significantly across the seasons although it is gradually on the ascendancy during the period under consideration whilst the river leakage out is also gradually on the decrease although the outflow flowrates slightly exceed the inflow flowrates. Indicating that the rate at which the aquifer is contributing to the river flow is gradually decreasing, yet the rate at which the aquifer is feeding the river is higher than the rate at which the river is feeding the aquifer.

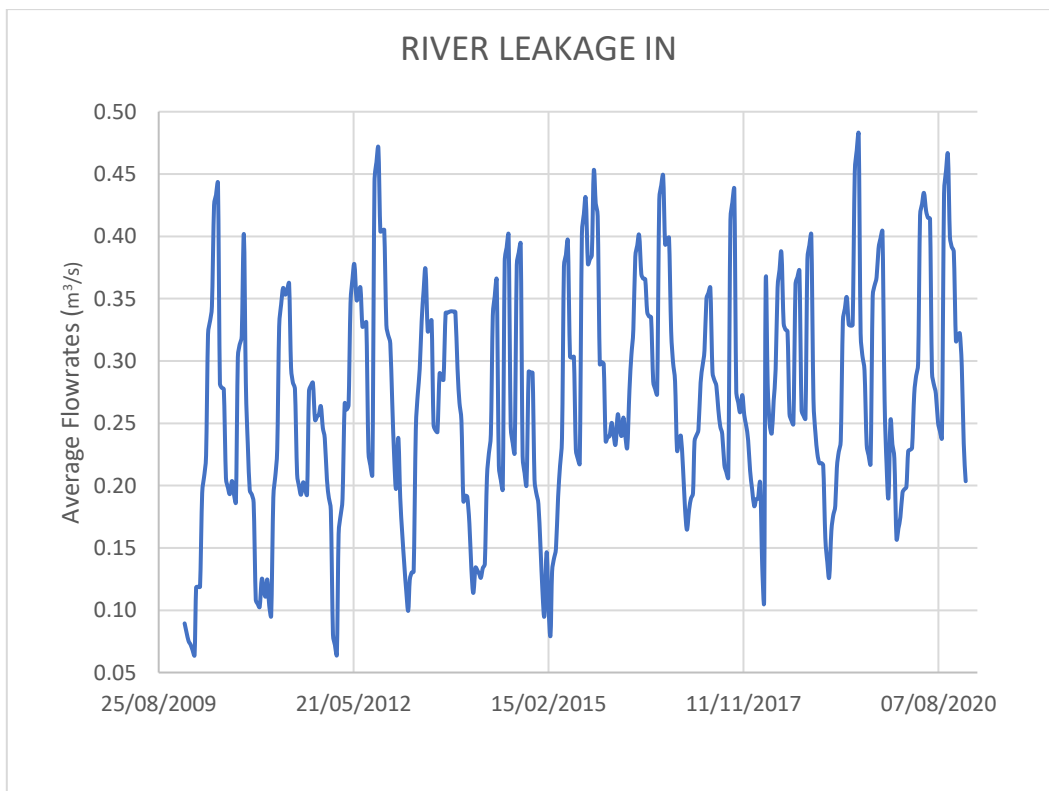


Figure 55 River leakage In.

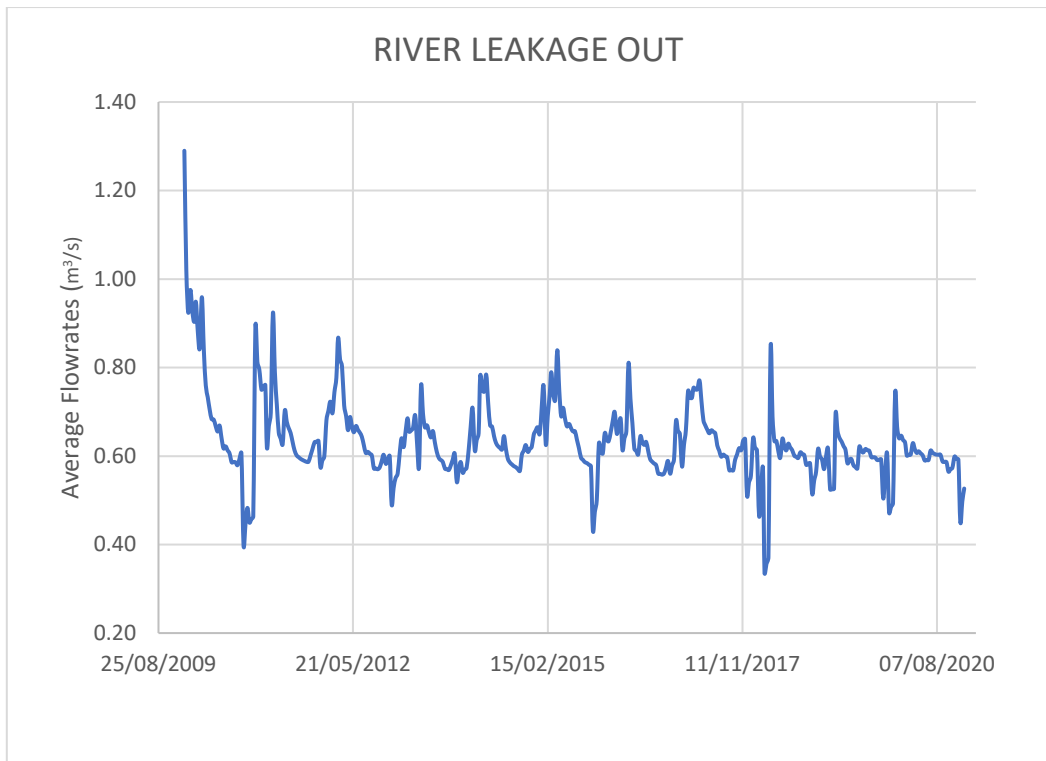


Figure 56 River leakage out.

Evapotranspiration variations greatly depending on the location of the study area, time of year, and vegetation type. Its rates are greatly accelerated during warm temperatures coupled with droughts whereas at cold temperatures with precipitations, its rates decline massively. Maximum evapotranspiration rates occurred within the months of April to October with rates between 0.80 to 1.62 m<sup>3</sup>/s with the peak rate recorded in June 2010, indicating that in the summers, the evapotranspiration is quite high. From the figure (57) below, the seasonal variation of the evapotranspiration rates is clearly shown, it can also be noted that seasonal variation during the period under study is quite steady below 1.5 m<sup>3</sup>/s.

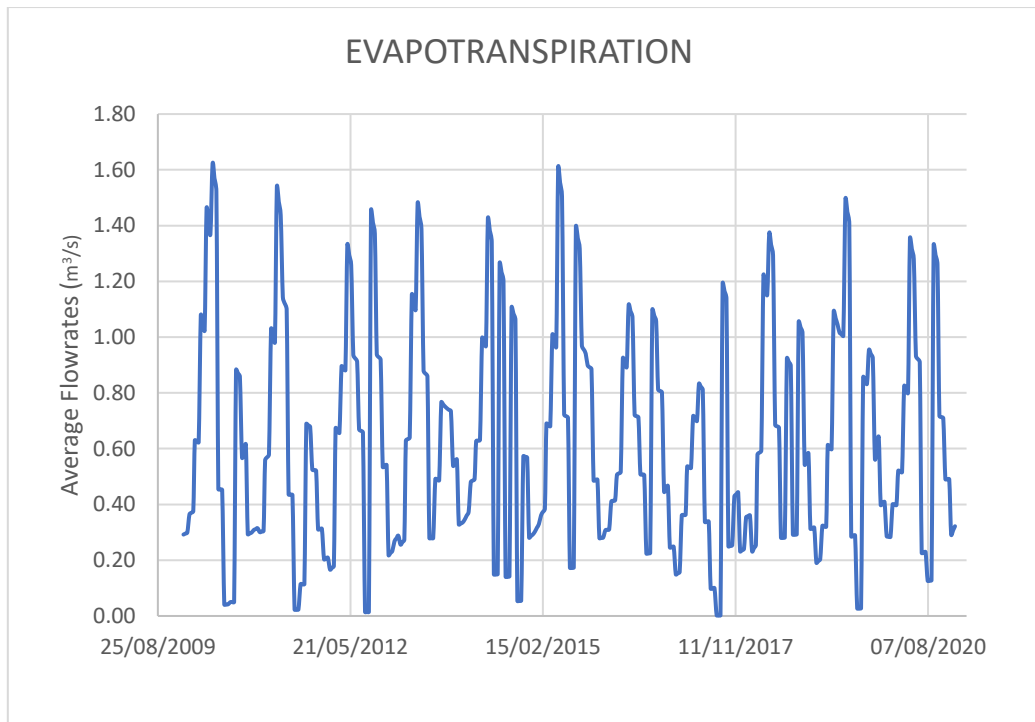


Figure 57 Evapotranspiration.

In MODFLOW, the term "constant head" refers to a boundary condition that specifies that the head at a given location will remain constant throughout the simulation. This means that there is no flow of water into or out of the cell at that location. The term "constant head out" represents the total amount of water that is flowing out of the cell at that location whilst "constant head in" represents the total amount of water that is flowing into the cell at that location.

When a diffusing-convective transport (DCDT) boundary is used in a water budget calculation, the term "DCDT out" represents the total amount of dissolved constituents (salinity) that are leaving the cell at that location. This water can be transported out of the cell by diffusion, convection, or a combination of both. Whilst the term "DCDT in" also represents the total amount of dissolved constituents (salinity) that are entering the cell at that location. The DCDT in occurred mostly for the months of November to March with flowrates ranging between 300 to 860 m<sup>3</sup>/s, with the maximum flowrate recorded for the month February 2018. In contrast, the DCDT out occurred throughout the months with the peak flowrate 283 m<sup>3</sup>/s for the month October 2012.

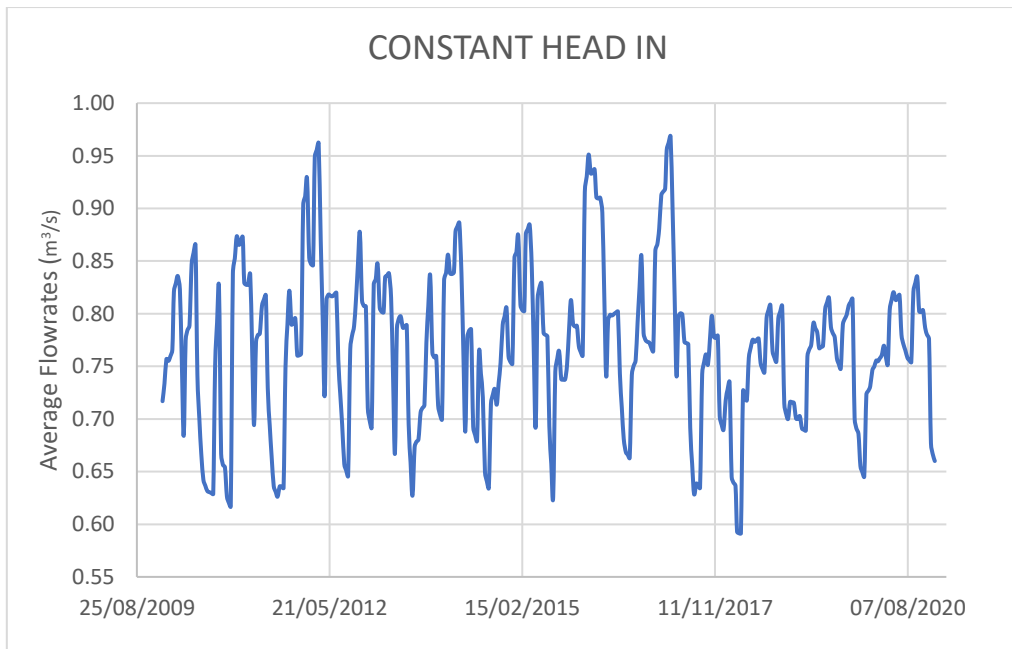


Figure 58 Constant Head In.

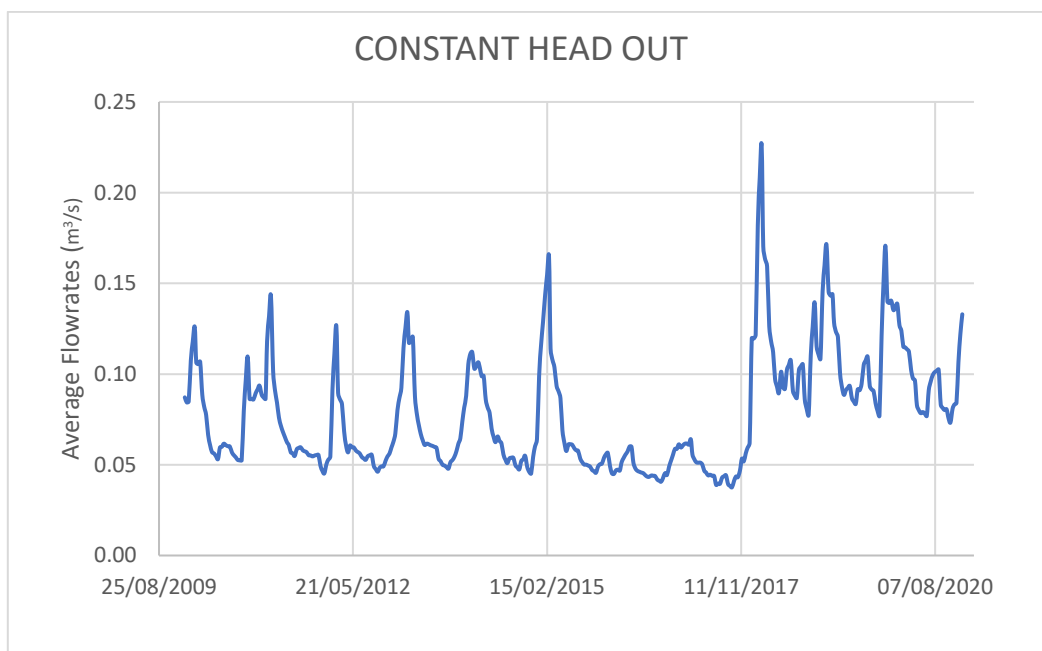


Figure 59 Constant Head out.

Well represents the extraction of water from the groundwater system usually by pumping indicating the groundwater depletion. The well was employed in June to August at a constant pumping rate of approximately  $0.015 \text{ m}^3/\text{s}$  probably for irrigation purposes.

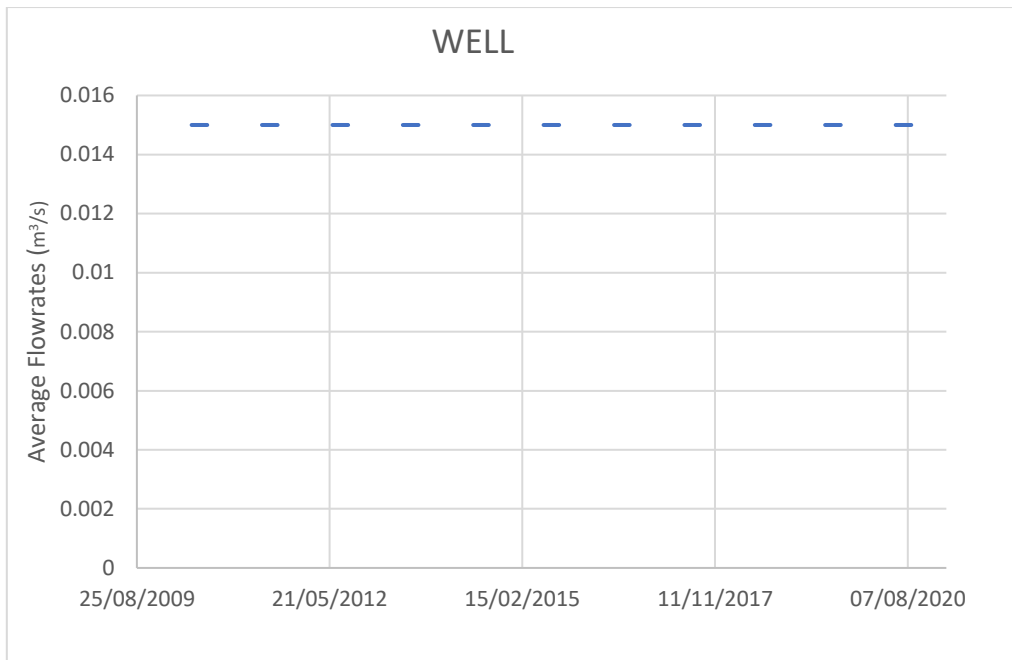


Figure 60 Well.

The total inflows into and out of the aquifer were compared to determine peak seasons when flows were into the aquifer occurred and vice versa. It was observed that flowrates into the aquifer occurred mostly between November to March with maximum flowrates between 202 to 863 m<sup>3</sup>/s whereas flowrates out of the aquifer occurred virtually throughout the seasons.

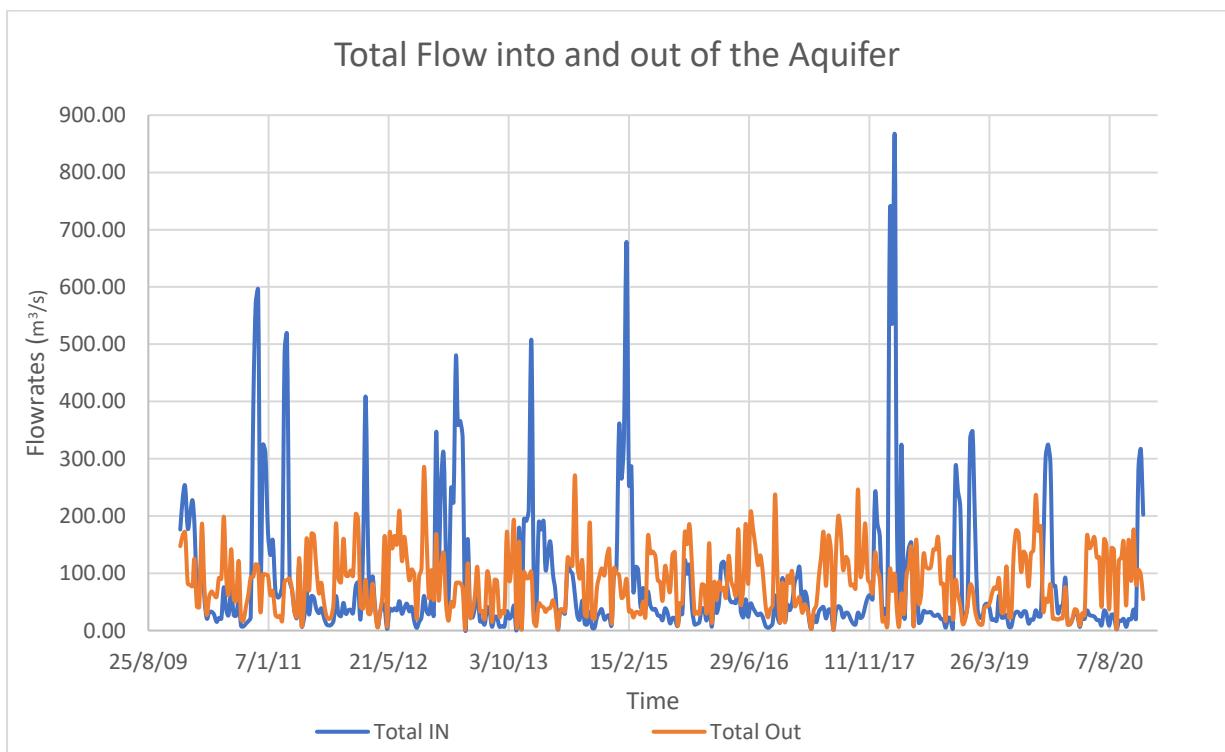


Figure 61 Flows into and out of the aquifer.

### 3.7 Seawater Intrusion Assessment

To attain a better understanding of the salinization of the VR aquifer by SWI using the river channel as a pathway, further assessments were made by comparing the salinity from different stress periods from the MODFLOW/SEAWAT simulations coupled with their concentrations across different layer (depth of the aquifer) at the river mouth for cell (14, 16). Snapshots for each stress period were made for 3 different layers to assess the salinity across the layers.

The first stress period (January 2010), the sixty first stress period (January 2015), and the one hundred and thirty second stress period (December 2020) were considered. It could be identified that the salinity for all the stress periods decrease marginally across the layers (vertically along the aquifer) with the first stress period (January 2010) recording approximately 14.08 g/L, 14.09 g/L, and 8.23 g/L for layer 1, 4 and 7 respectively. For the sixty first stress period (January 2015), the salinities were approximately 20.37 g/L, 15.65g/L and 11.66 g/L for layer 1, 4 and 7 respectively, and lastly, for the one hundred and thirty second stress period (December 2020), the concentrations were 26.20 g/L, 21.05 g/L and 14.63 g/L for the layer 1, 4 and 7 respectively. It therefore indicates the significance of SWI along the river channel is minimal across the aquifer although for the first layers the salinization is quite evident but vertically across the aquifer the impacts of SWI by actual seawater intrusion is minimal.

Furthermore, since all the previously selected stress periods occurred in winter, two different stress periods from summer were also observed (stress periods 44 and 79) for August 2014 and July 2016 to better characterise the aquifer salinity. Stress period 44 recorded 20.15 g/L, 14.96 g/L and 10.85 for layer 1, 4, and 7 respectively. Whereas stress period 79 recorded 21.27 g/L, 16.96 g/L and 12.93 g/L for layer 1, 4 and 7 respectively, thereby illustrating the findings already observed.



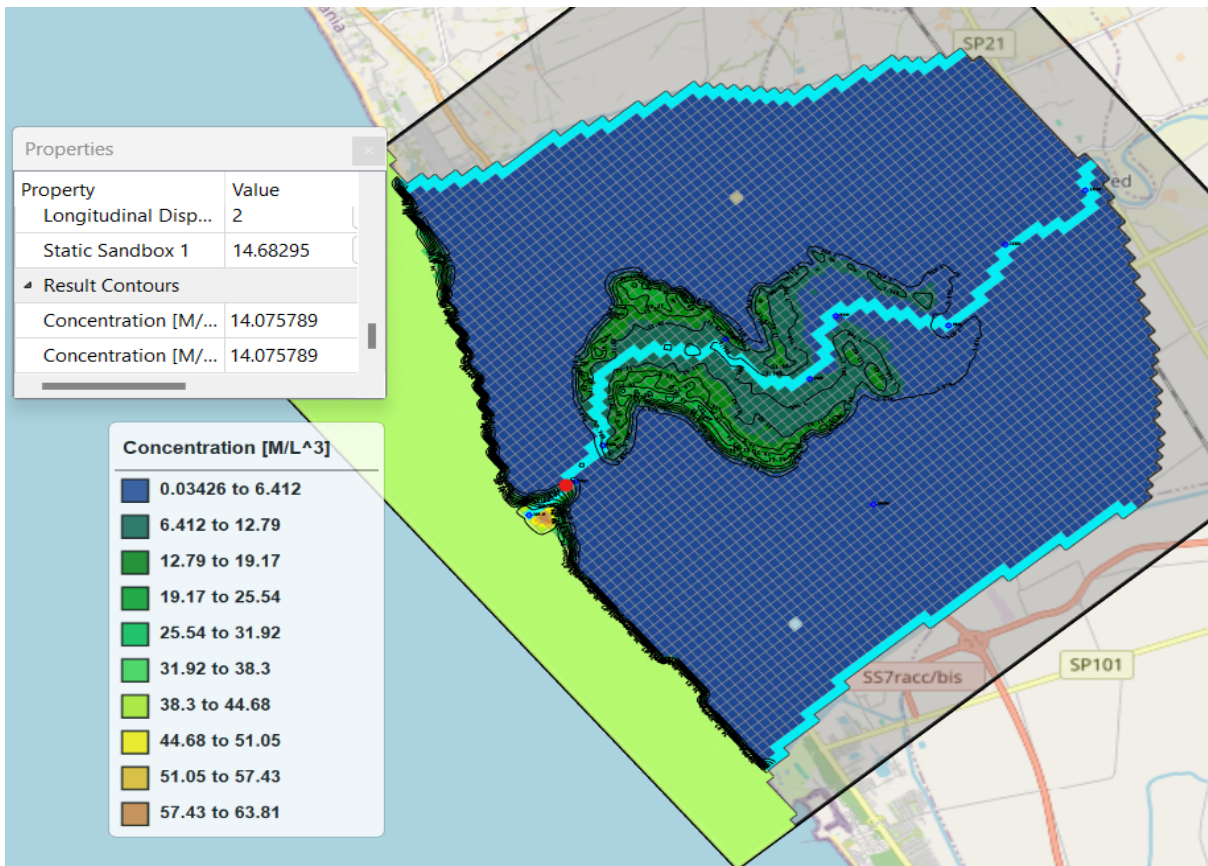


Figure 62 Salinity Concentrations of Stress Period 1 layer 1 (with selected cell in red)

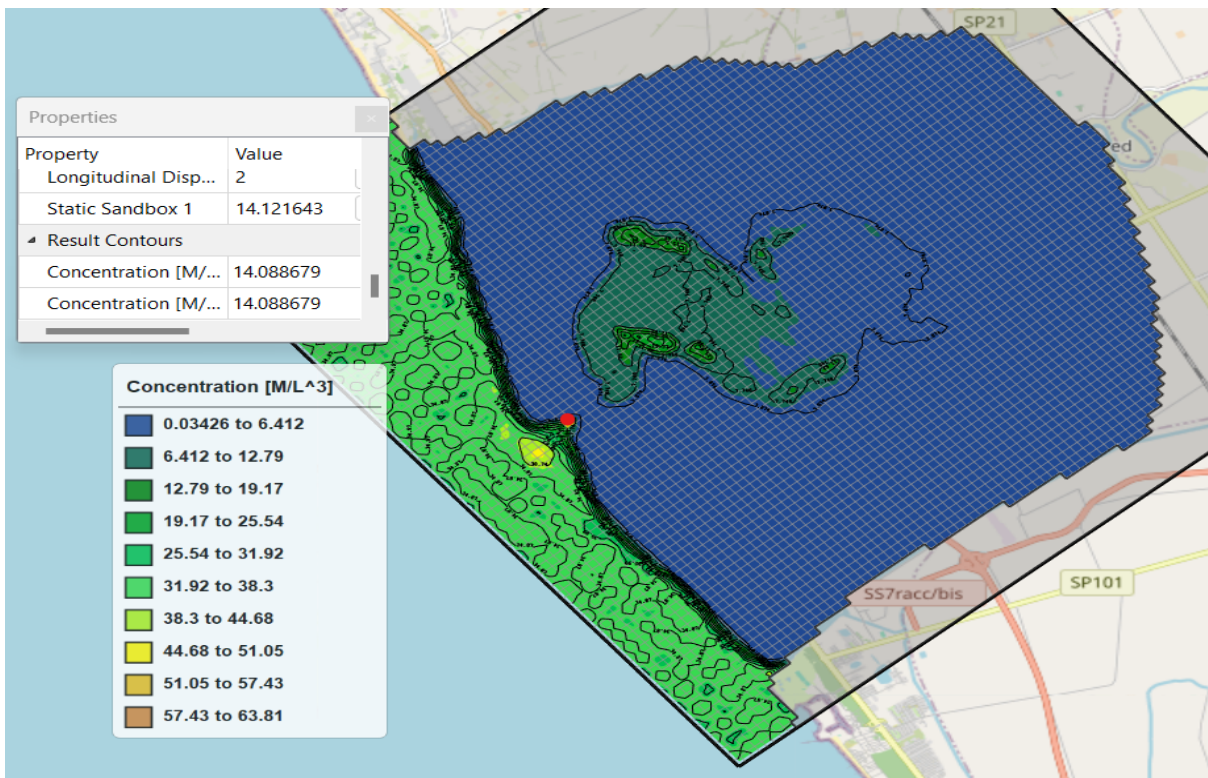


Figure 63 Concentrations of Stress Period 1 layer 4 (with selected cell in red)

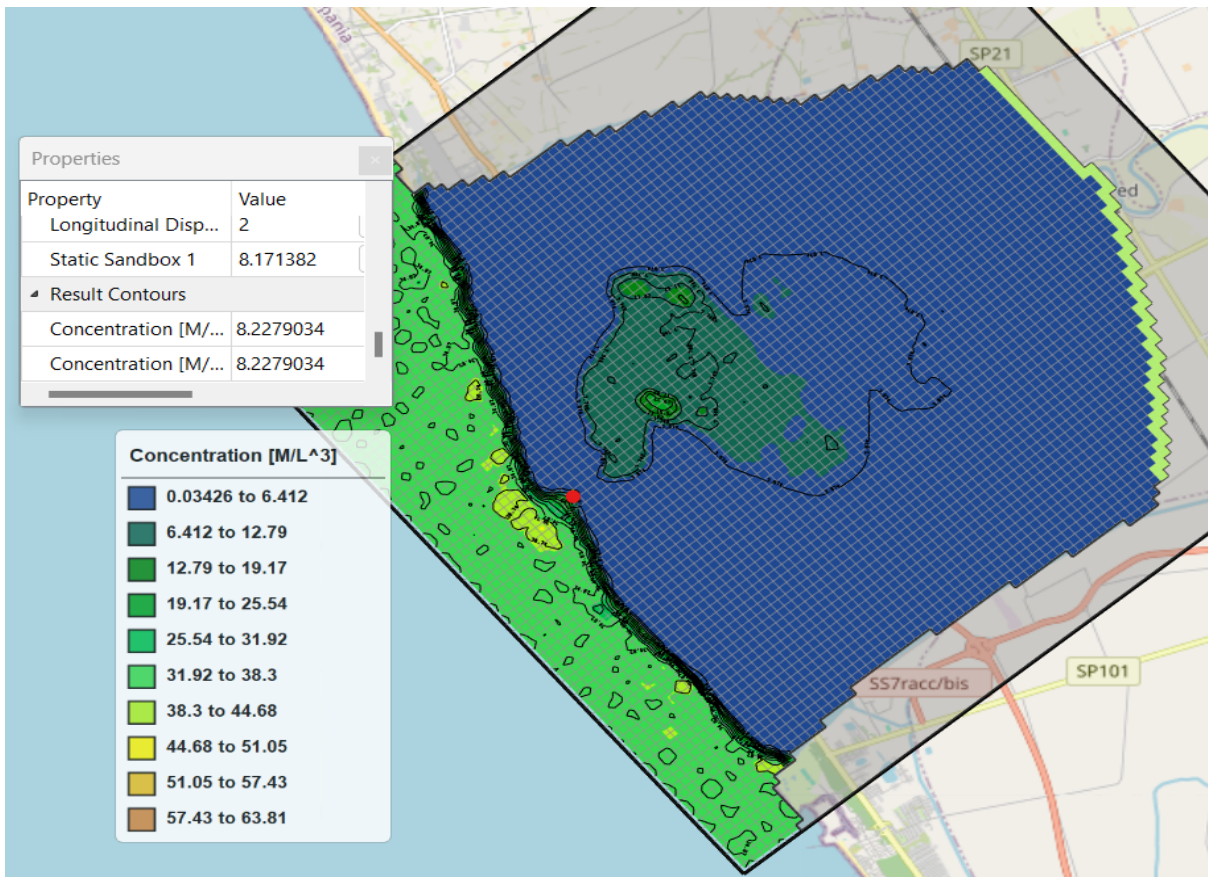


Figure 64 Concentrations of Stress Period 1 layer 7 (with selected cell in red)

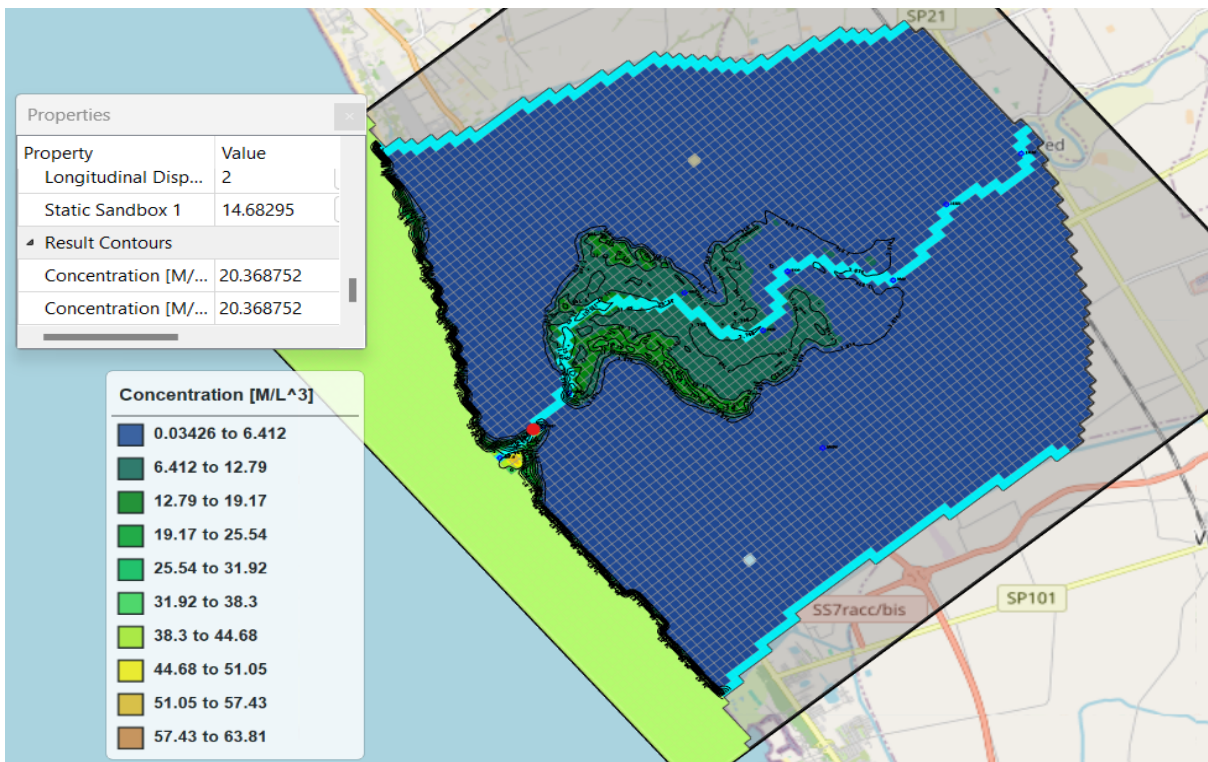


Figure 65 Salinity Concentrations for Stress Period 61 layer 1 (with selected cell in red)



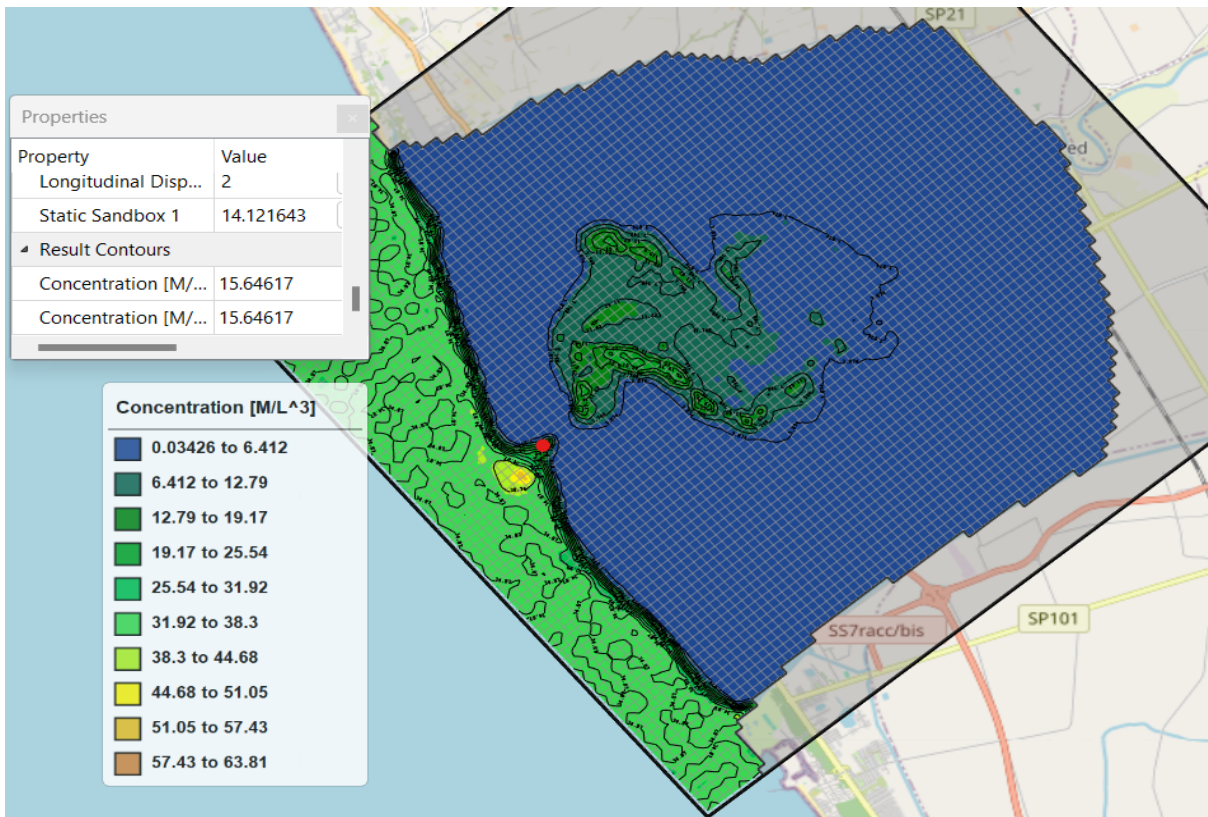


Figure 66 Salinity Concentrations for Stress Period 61 layer 4 (with selected cell in red).

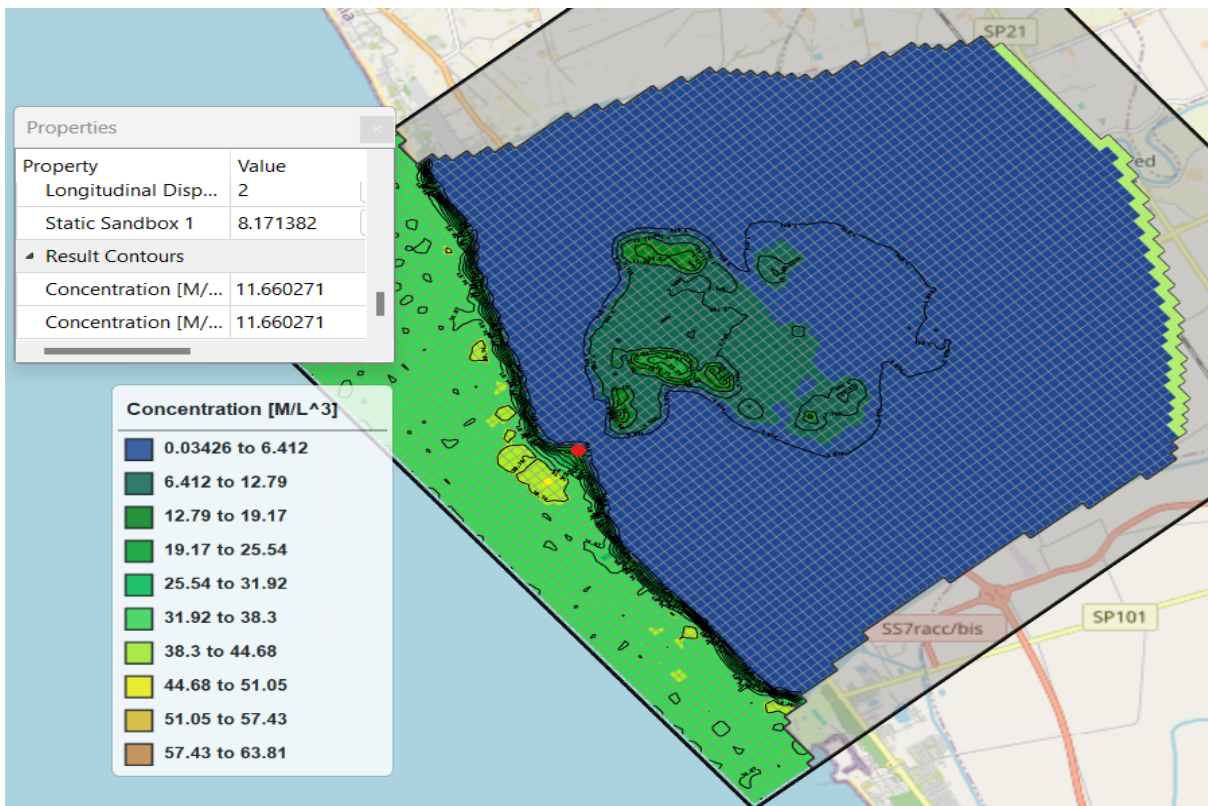


Figure 67 Salinity Concentrations for Stress Period 61 layer 7 (with selected cell in red).

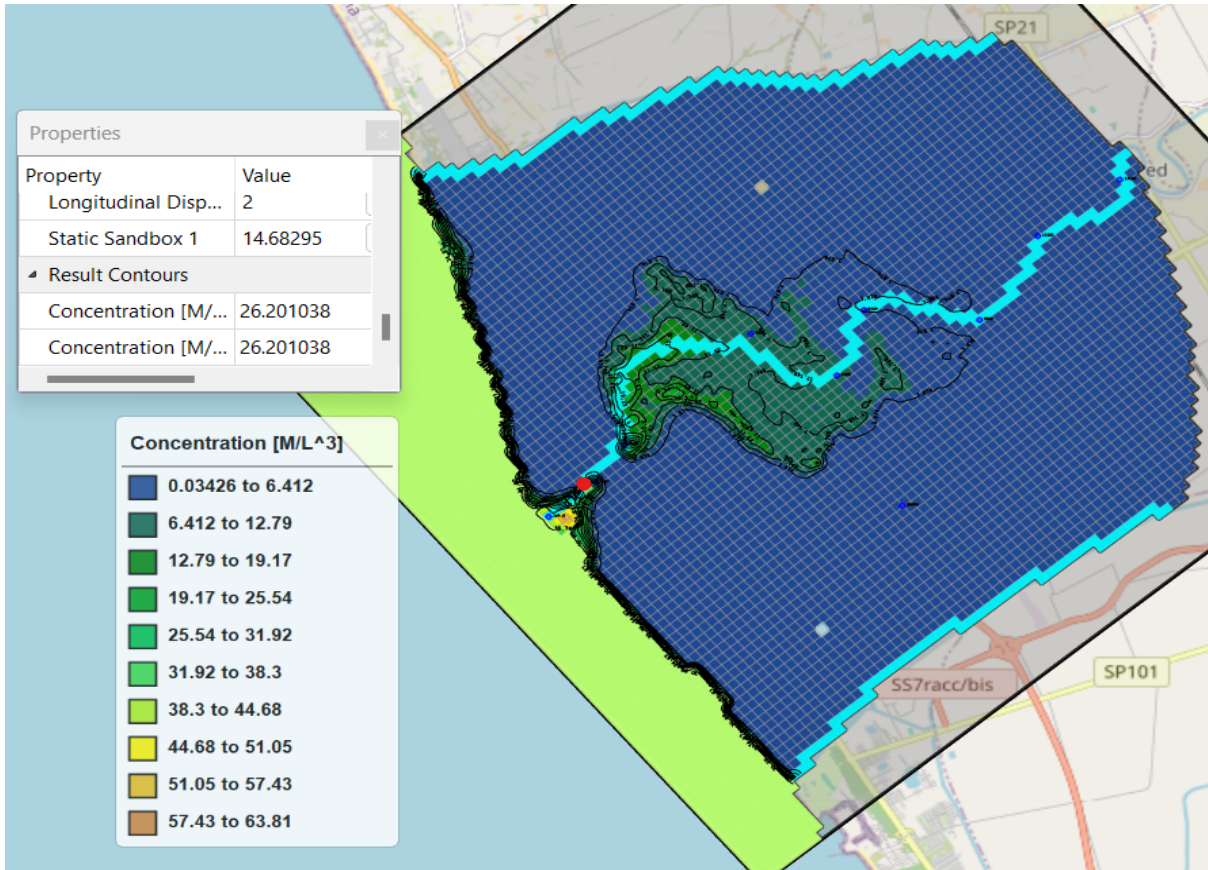


Figure 68 Salinity Concentrations for Stress Period 132 layer 1 (with selected cell in red).

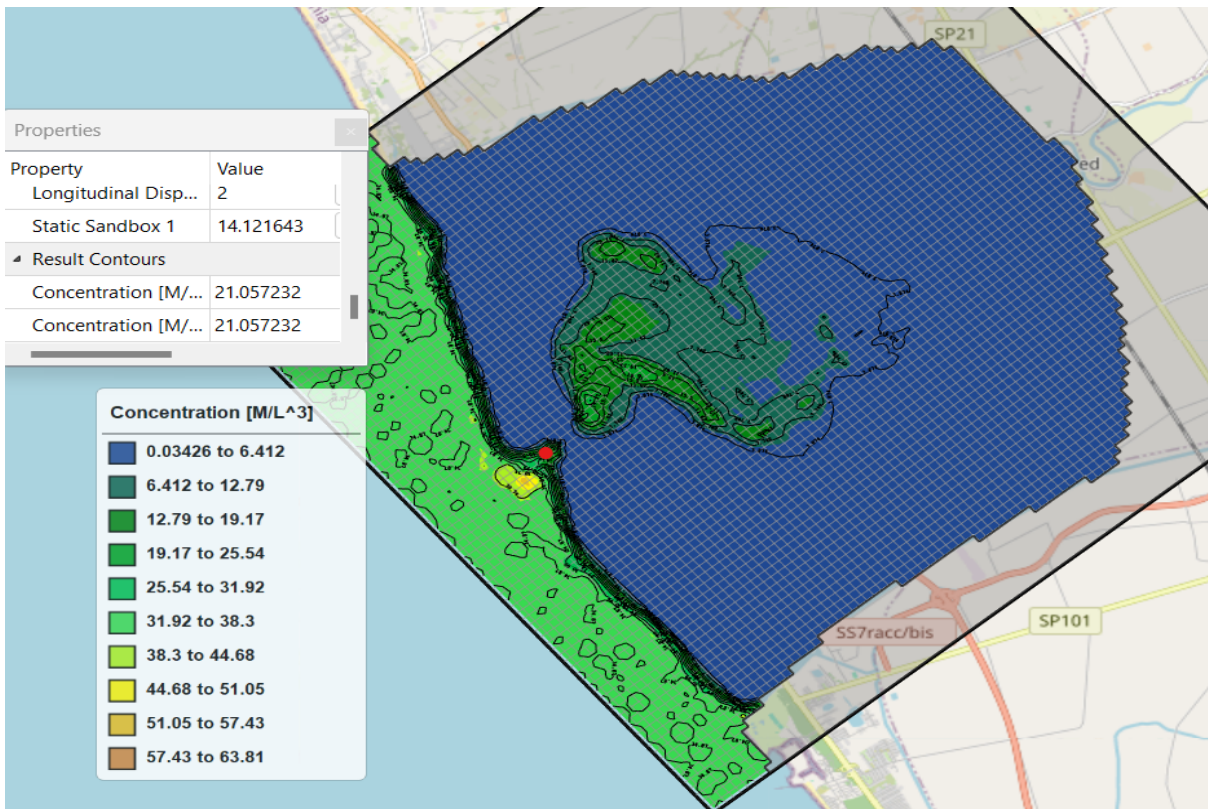


Figure 69 Salinity Concentrations for Stress Period 132 layer 4 (with selected cell in red).



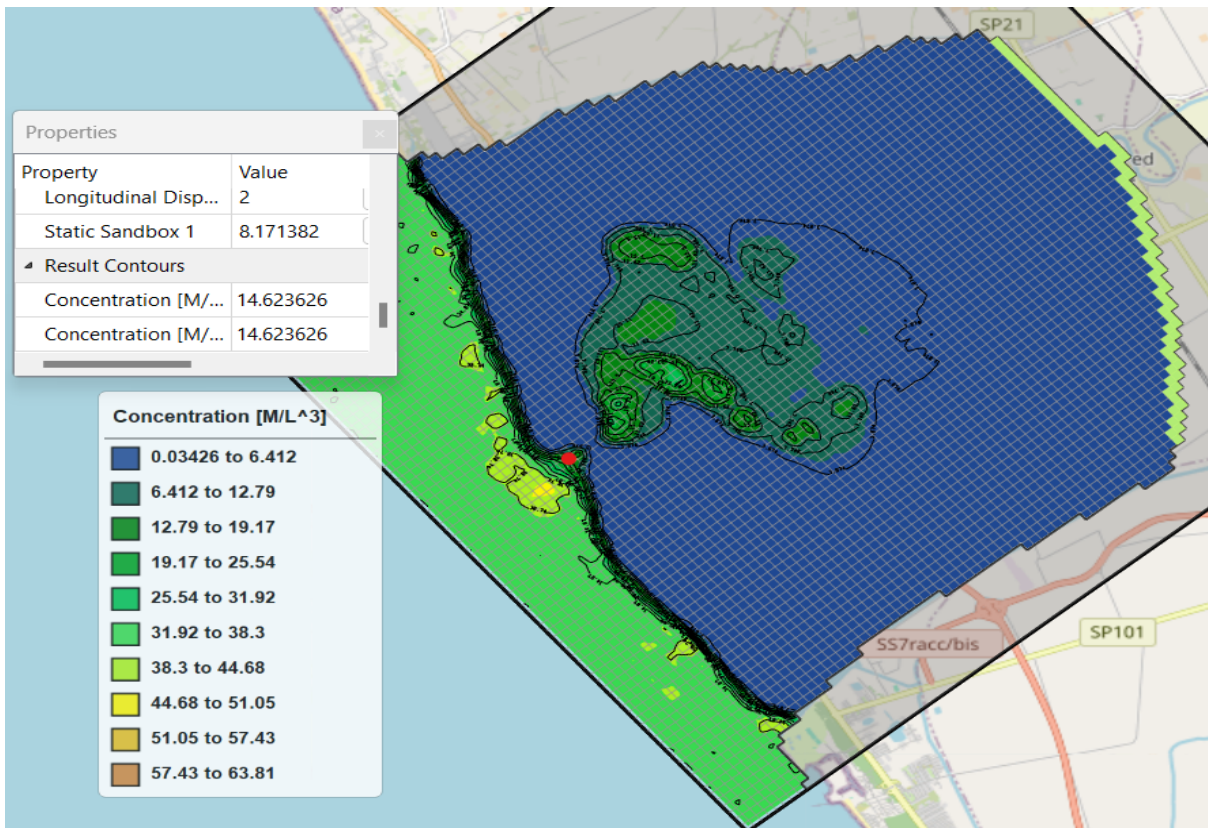


Figure 70 Salinity Concentrations for Stress Period 132 layer 7 (with selected cell in red).

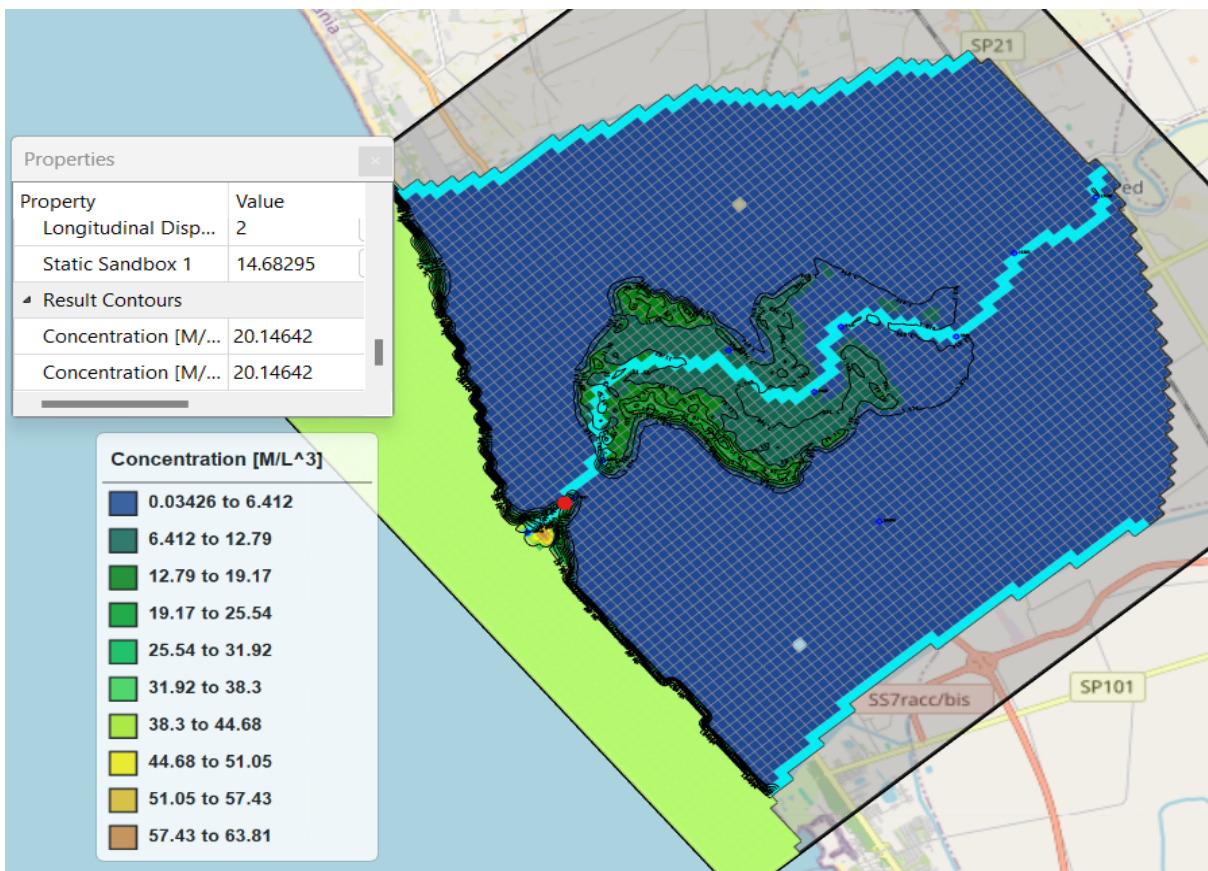


Figure 71 Concentrations for Stress Period 44 layer 1 (with selected cell in red).



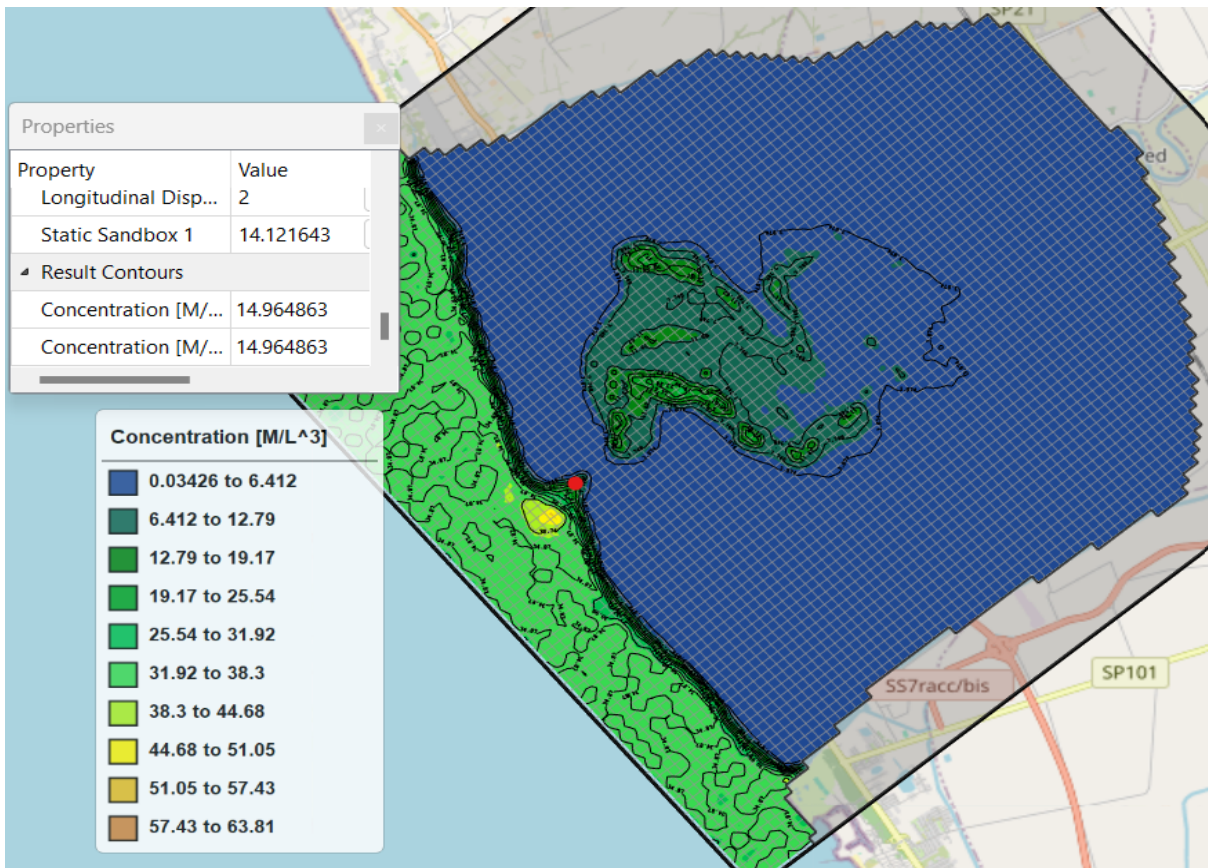


Figure 72 Concentrations for Stress Period 44 layer 4 (with selected cell in red).

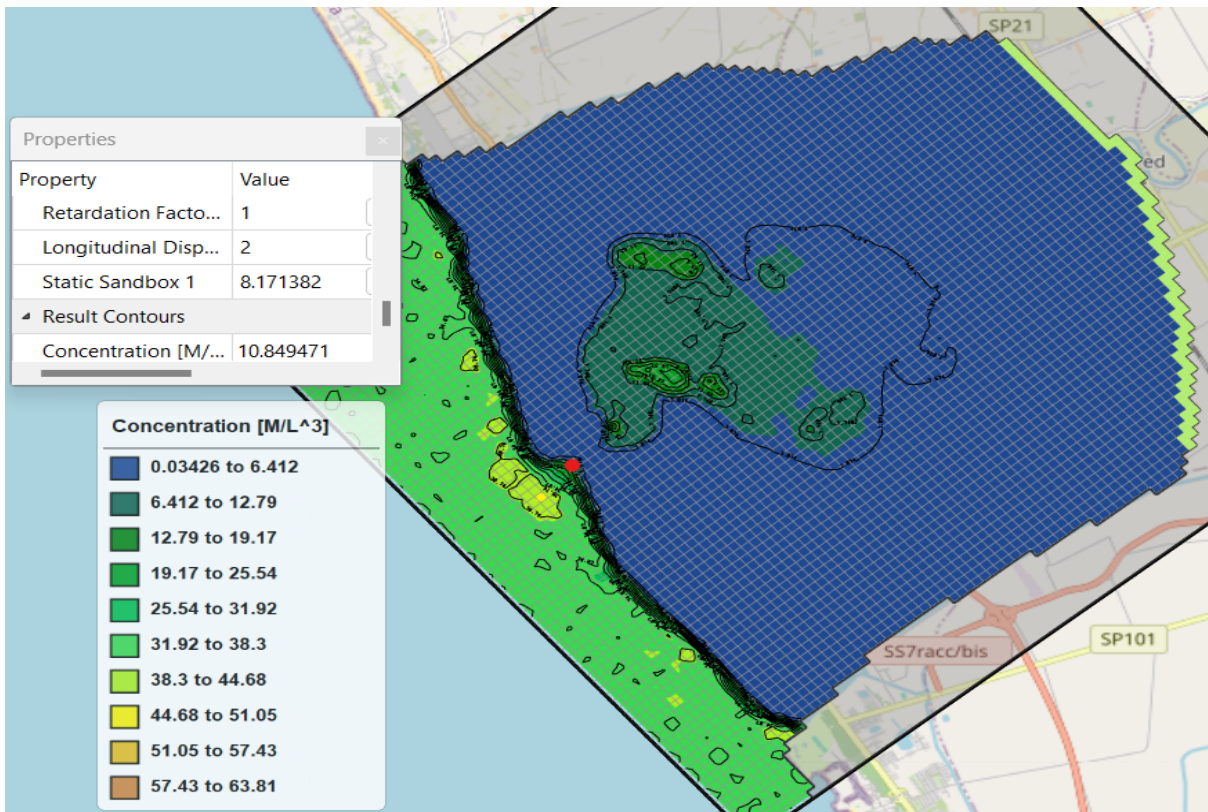


Figure 73 Concentrations for Stress Period 44 layer 7 (with selected cell in red).



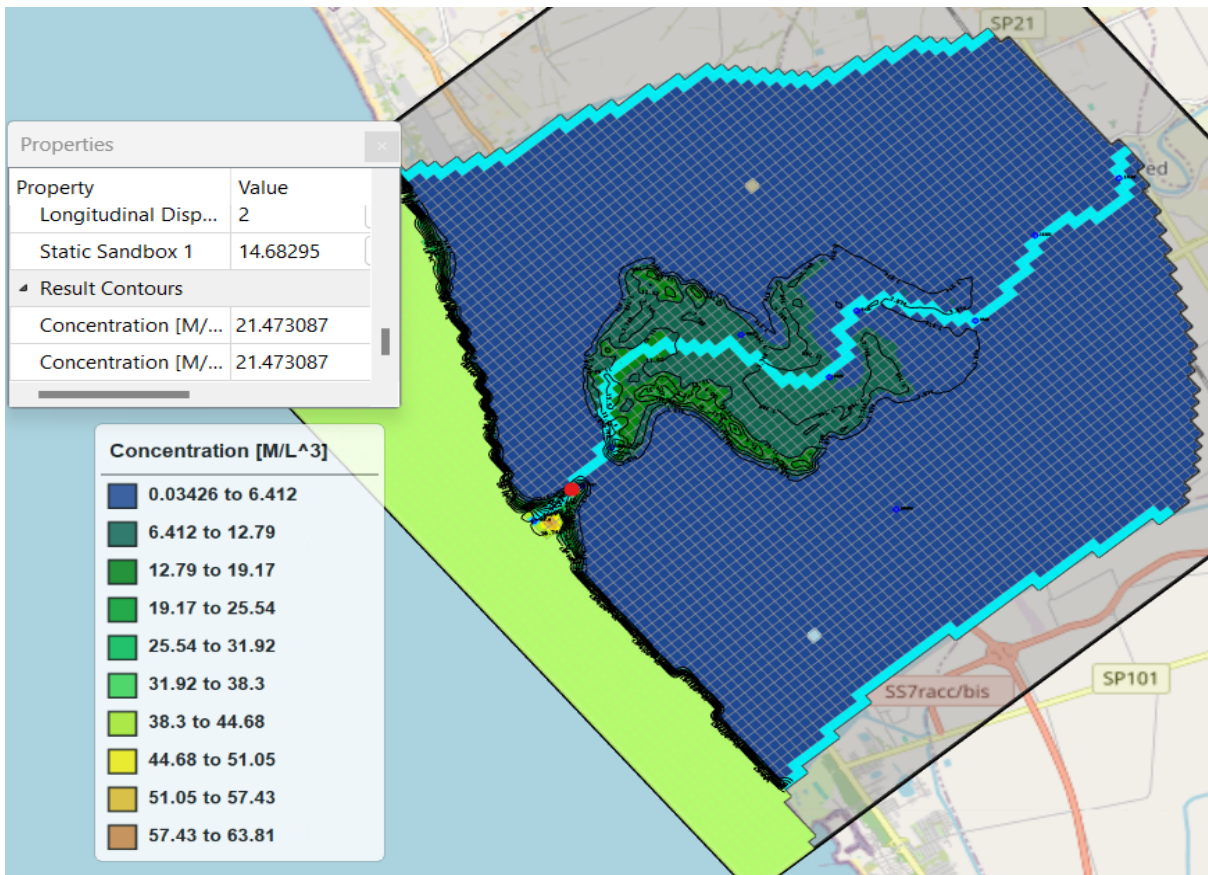


Figure 74 Concentrations for Stress Period 79 layer 1 (with selected cell in red).

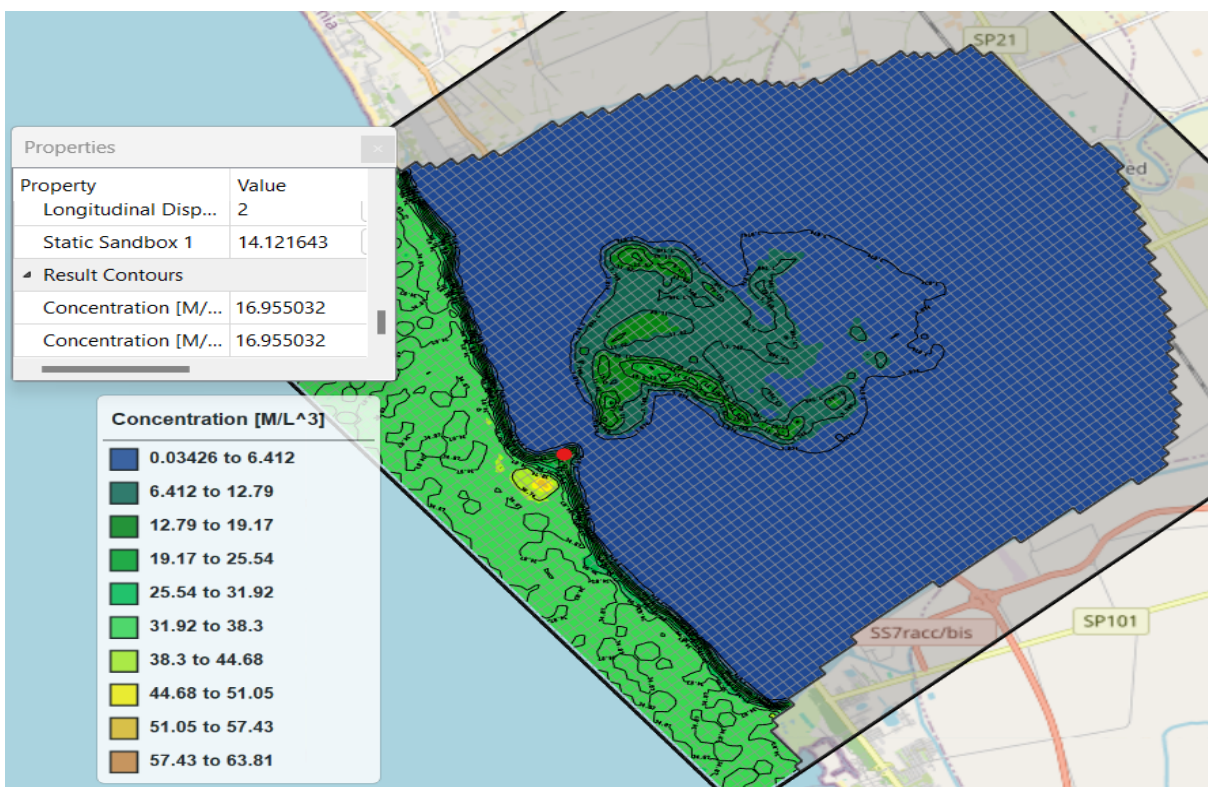


Figure 75 Concentrations for Stress Period 79 layer 4 (with selected cell in red).

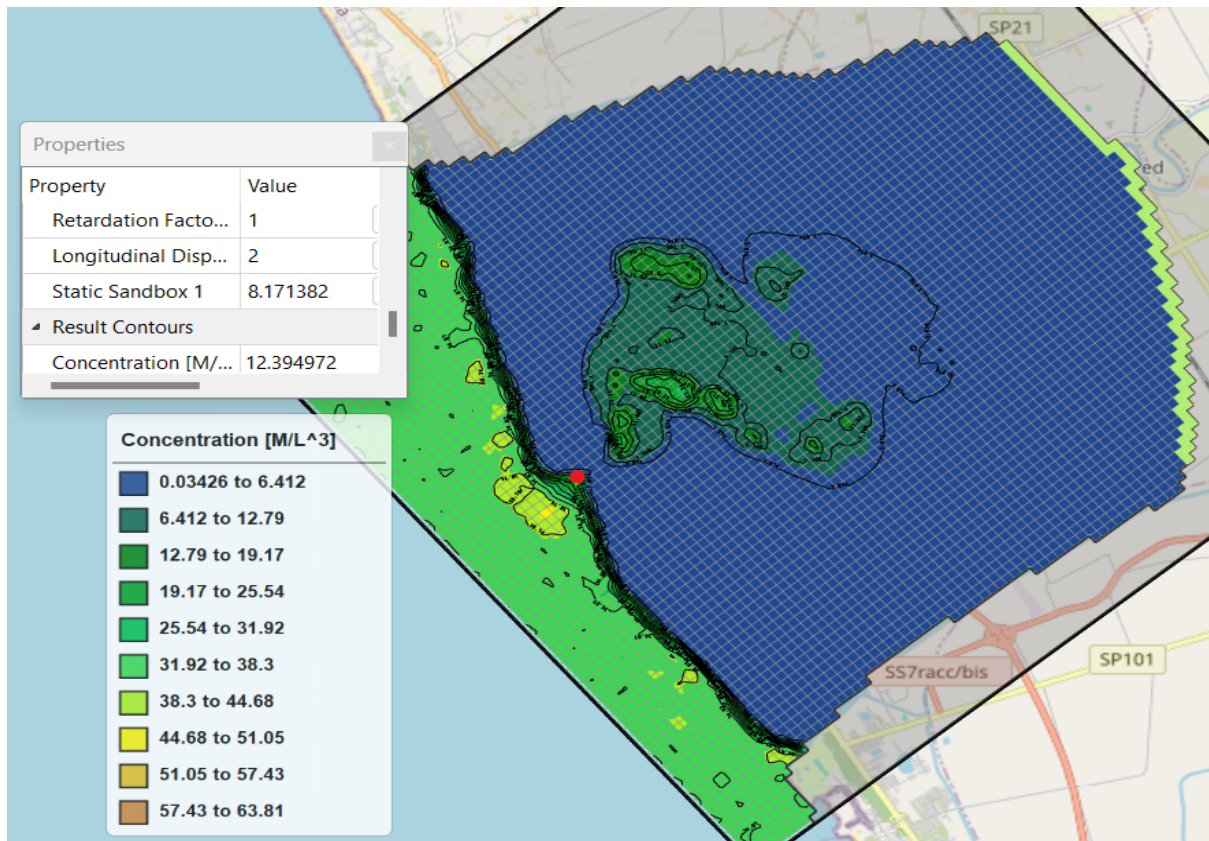


Figure 76 Concentrations for Stress Period 79 layer 7 (with selected cell in red).

Furthermore, comparisons were made between SWI using the river channel as a pathway and SWI by paleo salinity into the aquifer to ascertain the major cause of the salinization of the aquifer. Snapshots were made for rows 25 (in red) and 50 (in magenta) which are close to river mouth and rows 35 (in pastel pink) and 60 (in red-orange) near the mid-section of the river reach as shown in the figure (77) below, considering the longitudinal direction for better comparison. Moreover, rows 25 and 35 are within the river channel and Canale Agnena whereas rows 50 and 60 are within the river channel and Regi Lagni Canale.



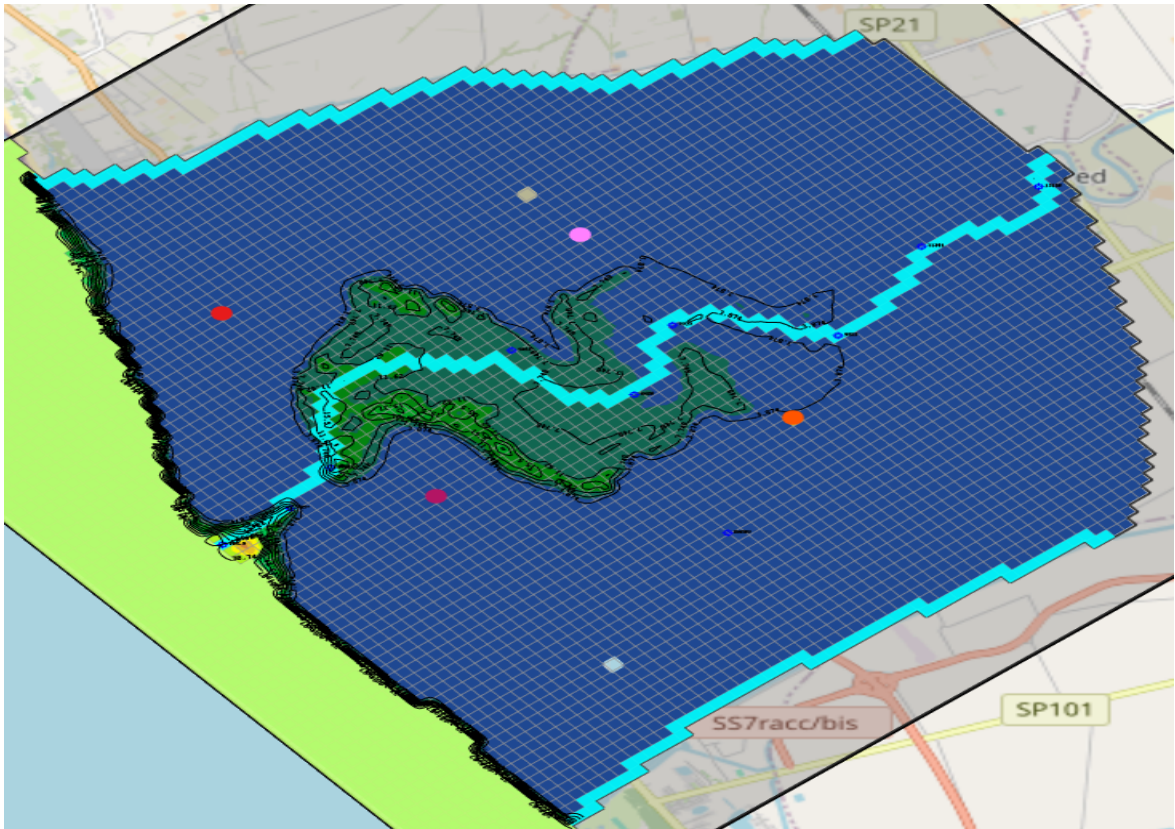


Figure 77 Observed cells for the comparison between paleo salinization and actual seawater intrusion.

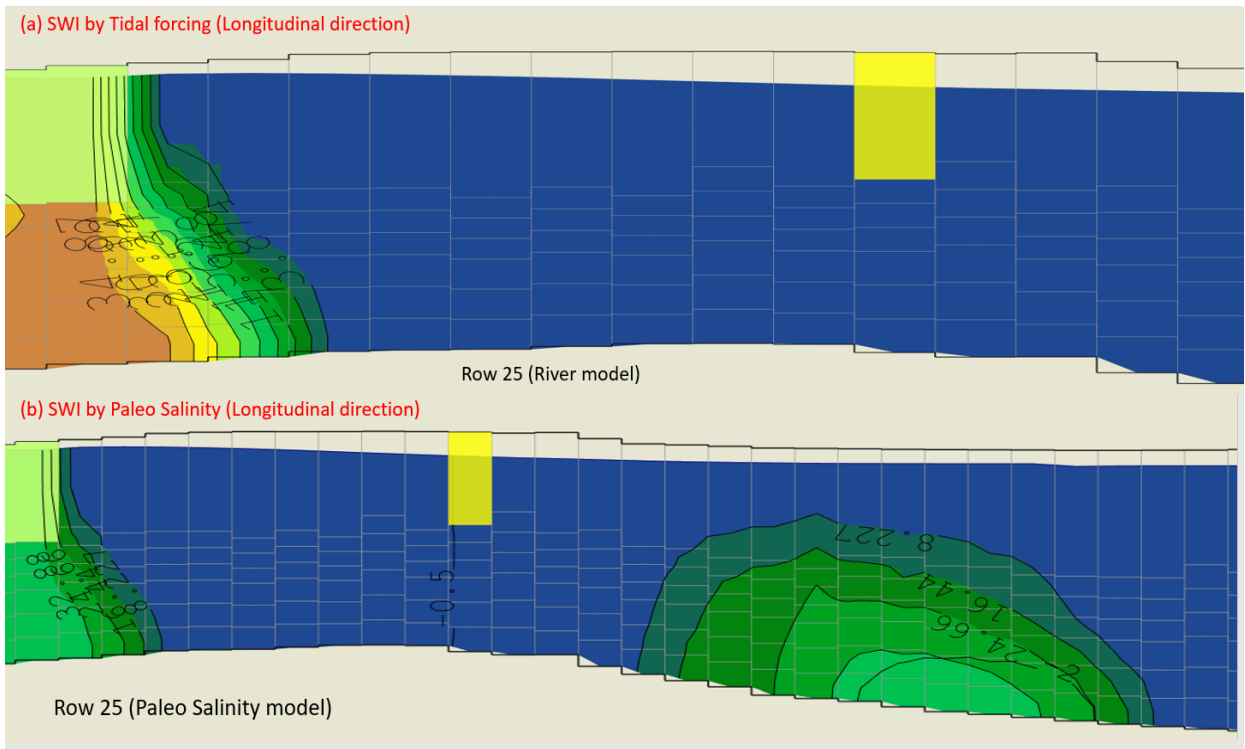


Figure 78 Comparison between actual seawater intrusion & paleo salinity SWI for row 25.

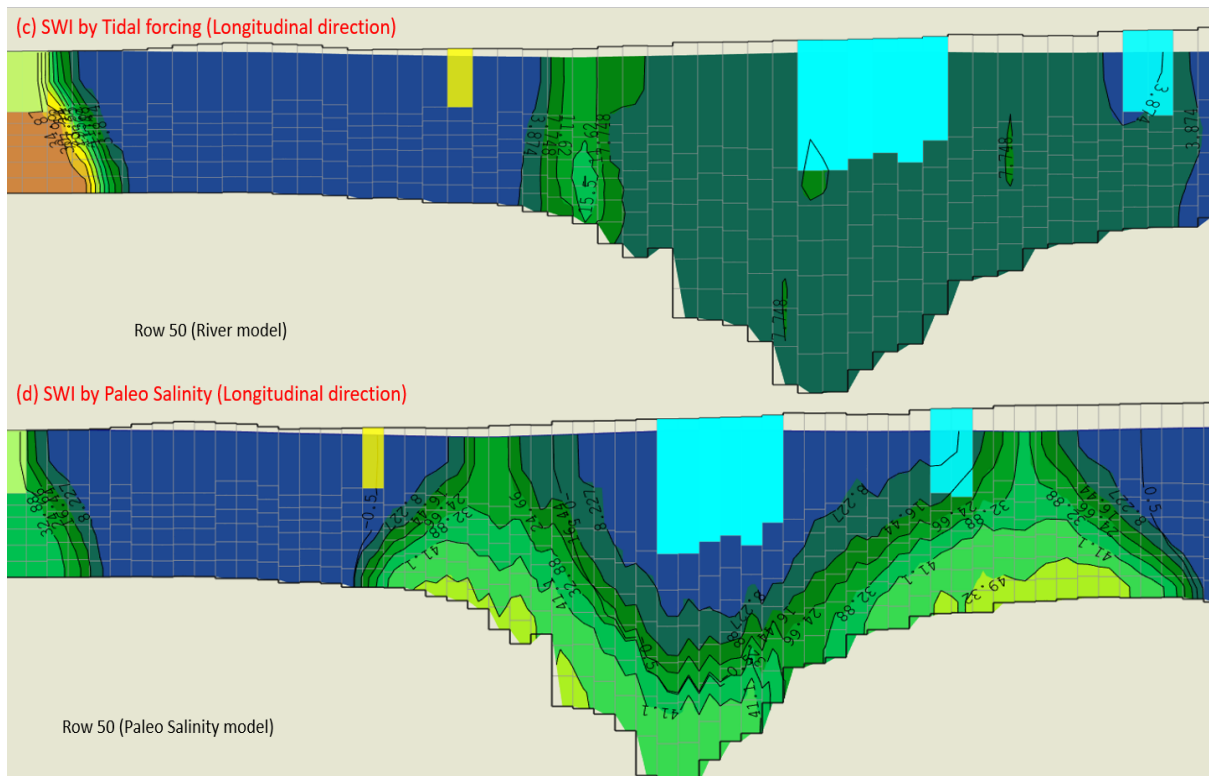


Figure 79 Comparison between actual seawater intrusion & paleo salinity SWI for row 50.

From the figures (78 & 79) above, the selected cells are in yellow at the uppermost part of the sections with the non-saline part of the aquifer in deep blue. It can be noticed from the coloured (light green to green) area in section (a) the propagation of the seawater wedge by actual seawater intrusion during the period of simulation, the propagation approximately covered a cell, with each cell representing 146.67 m, then the propagation of seawater wedge for the period under consideration will be approximately 150 m from the estuary using the river channel as a pathway into the aquifer, a similar situation can be identified for section (c).

Comparatively for the SWI by paleo salinization in section (b) and (d) respectively, the area covered by the paleo salinity plume (green area) in sections (b) and (d) are wide within the aquifer and certainly will be the cause of the salinization of the aquifer. To further clarify these findings, another comparison is made in the figures (80 & 81) below.

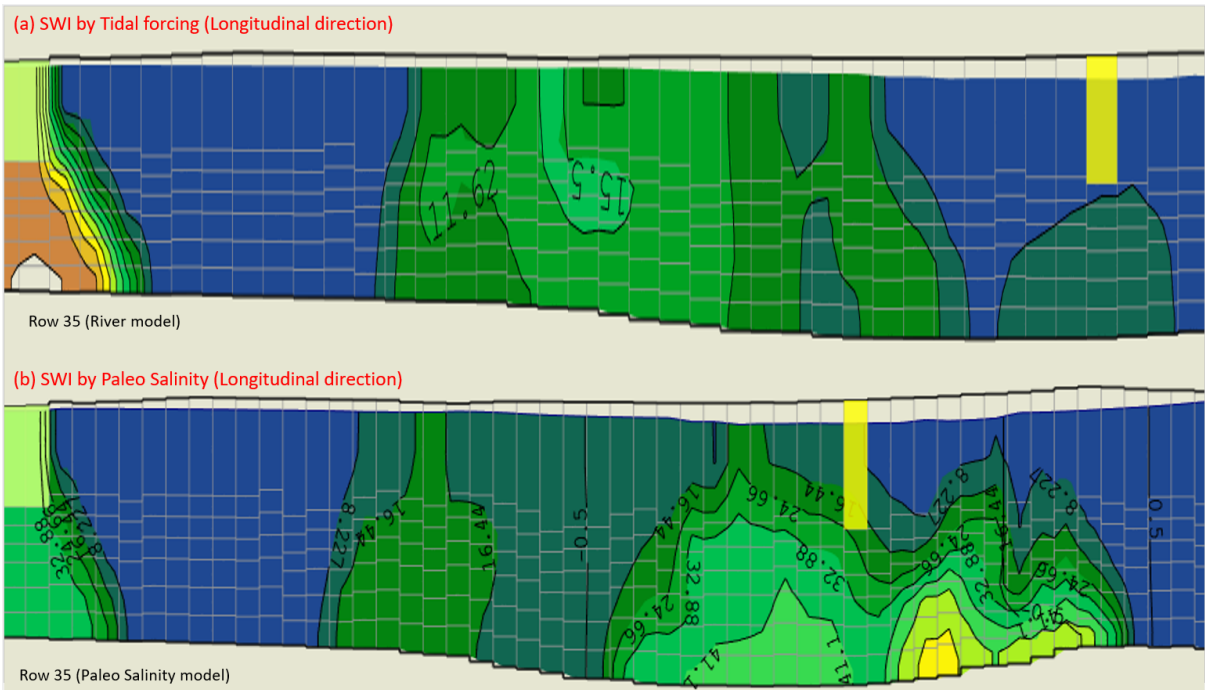


Figure 80 Comparison between actual seawater intrusion & paleo salinity SWI for 35.

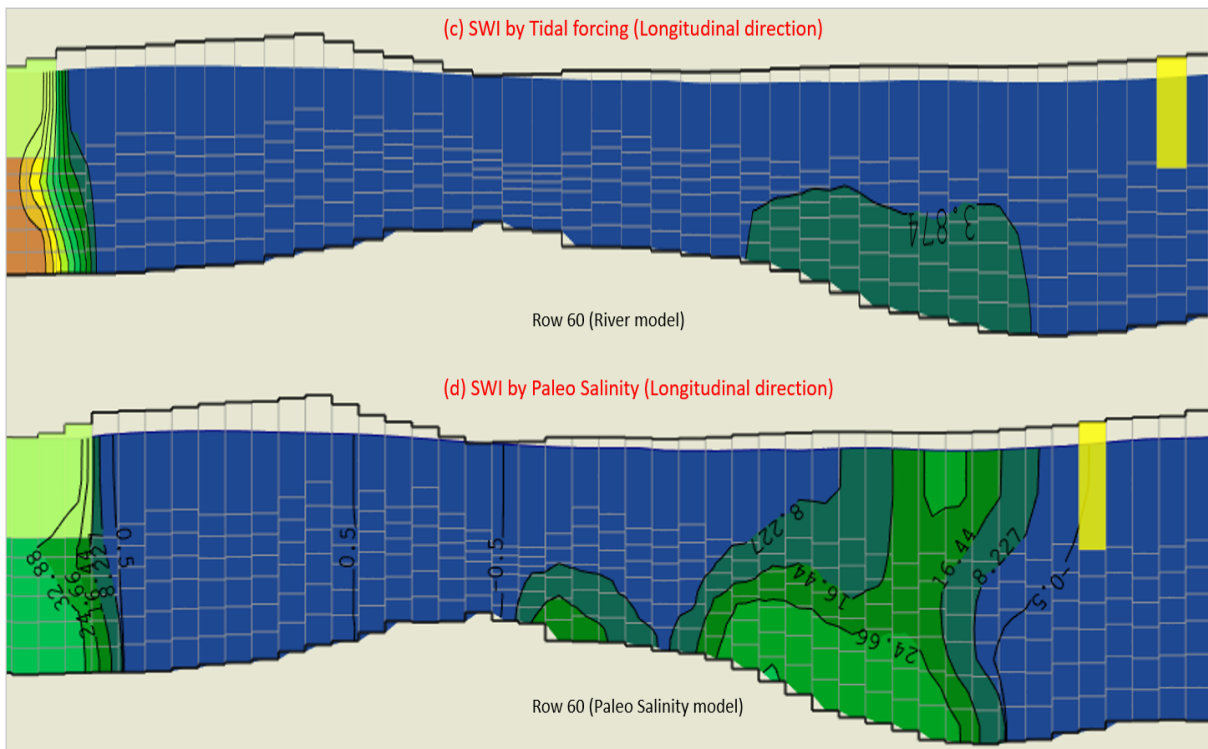


Figure 81 Comparison between tidal forcing & paleo salinity SWI for 60.

The figures (80 & 81) above depict the salinization of the aquifer near the mid-section of the river reach with the location of the selected cells in yellow at the uppermost part of the sections. Section (a) and (c) represents the salinization by actual seawater intrusion using the river channel as a pathway whereas the section (b) and (d) represents the salinity by paleo

salinization. Similarly, the green to teal area at the left side in section (a) and (c) represent SWI by actual seawater intrusion through the river channel, and its significance to the total salinization of the aquifer seems very minimal whereas the green- teal area (within the mid-sections) portrays the paleo salinity in sections (b) and (d) and are comparatively large within the aquifer and affirms that the paleo salinity is the major cause of the aquifer salinization.

To further quantify the SWI by actual seawater intrusion and paleo salinity in the aquifer and to confirm the impacts and dominant salinity activity in the aquifer, a mass balance of both paleo salinity and actual seawater intrusion in the aquifer was simulated with SEAWAT and the results obtained are presented and discussed in the figures below.

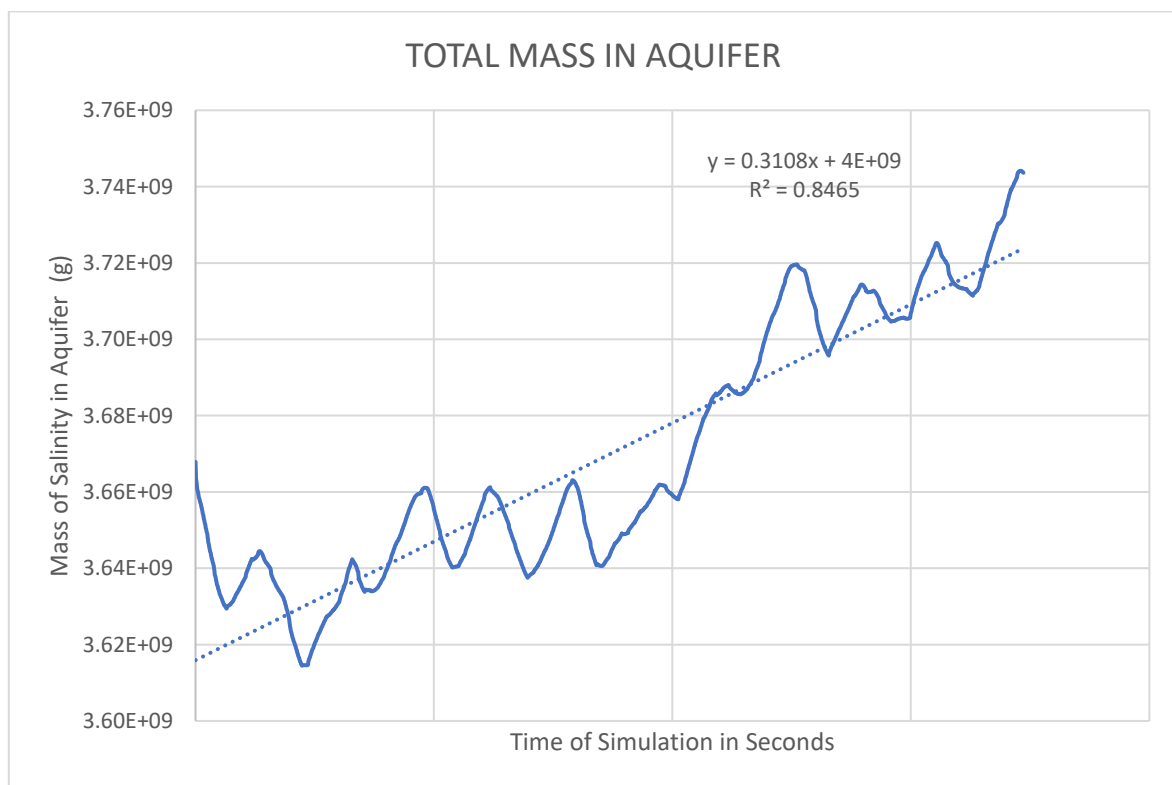


Figure 82 Mass of Salinity by actual seawater intrusion.

In the figure (82), it can be identified that after the period of simulation with SEAWAT, the total amount of salinity accumulated in the aquifer due to actual seawater intrusion is  $3.67 \times 10^3$  tons whereas the total amount of salinity in the aquifer by paleo salinization is  $6.53 \times 10^3$  tons as represented in figure (83). It is evident in figure (82) that, the rate of salinization of the aquifer by actual intrusion gradually increases, whereas in figure (83), the rate of paleo desalination is also gradually increasing.

Moreover, from the mass balance evaluation, it can be estimated that the paleo salinization of the aquifer exceeds the actual seawater intrusion salinization by approximately  $2.86 \times 10^3$  tons

of salinity. Although paleo desalination is on the increase as already indicated in figure (83), yet from the mass balance simulations there exist huge paleo salinity in the aquifer.

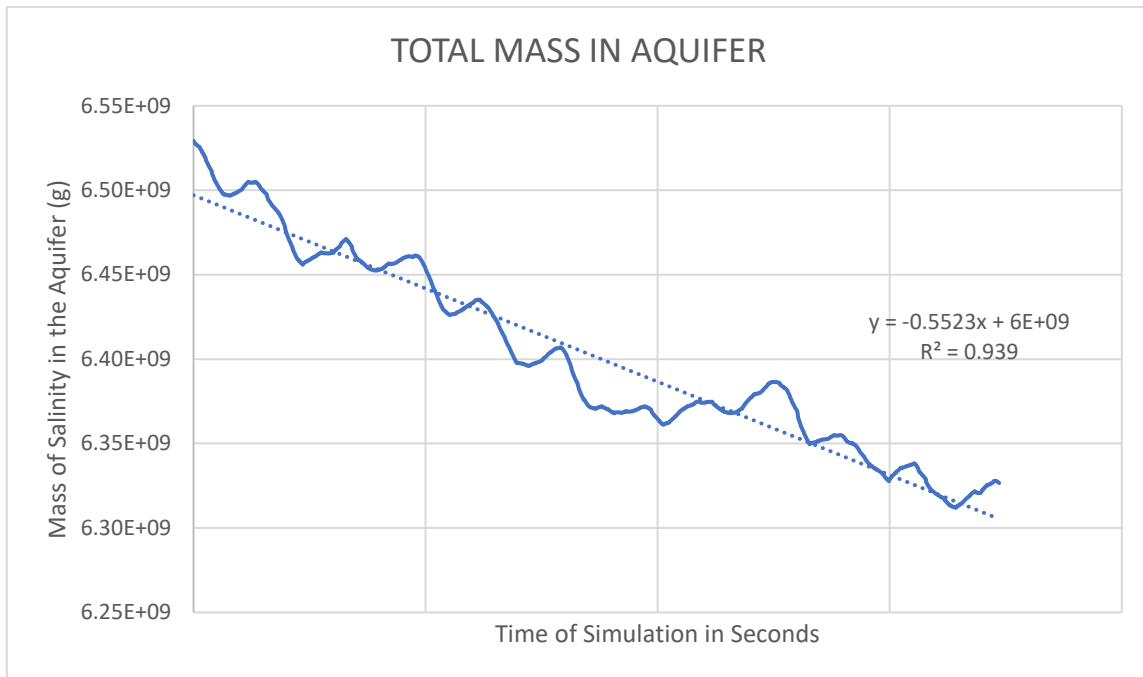


Figure 83 Mass of Paleo Salinity in the aquifer.

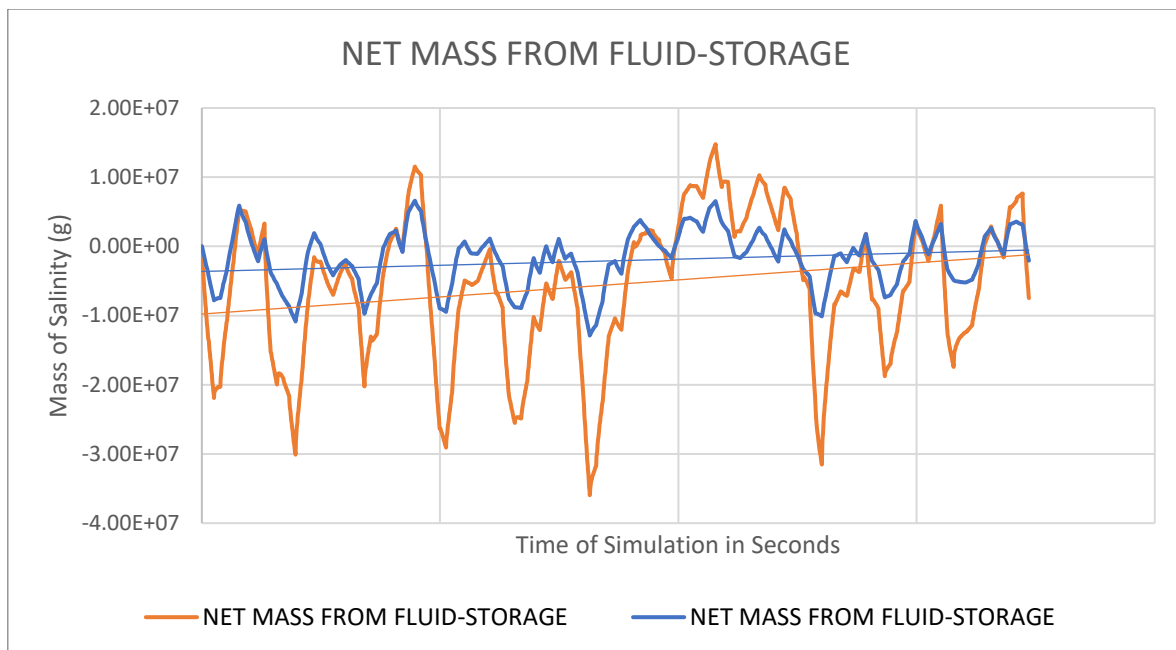


Figure 84 Net Salinity from Fluid-Storage.

The graph above (figure 76) shows the net salinity mass from fluid-storage with the orange line indicating net salinity mass induced by paleo salinity, whilst the blue line indicates the net salinity induced by actual seawater intrusion in the aquifer. The orange line exceeds the blue



line because paleo salinization within the aquifer is higher than salinization due to actual seawater intrusion.

## 4.0 CONCLUSIONS

This thesis started with the numerical modelling of surface water with HEC-RAS to determine the river stages and salinity along the final reach of the Volturno river for the decade 2010-2020. A large scale MODFLOW numerical model covering the entire porous aquifer of the Campania region was downscaled and used to determine the direction of flow within the final reach of the Volturno river aquifer which were towards the wetlands and swamps beside the river channel. The numerical model was capable to capture the Piezometric Heads variations in relation to seasonal recharge and discharge patterns. The results highlighted a gradual decline in the Heads within the aquifer with time.

The SEAWAT numerical model was capable to determine that the salinization of the aquifer by actual seawater intrusion was prevailing along the Volturno river channel, which acted as a preferential pathway. While the seawater wedge along the coast was not pronounced, usually within 100 and 200 m inland, due to the elevated freshwater discharge.

By using the FLOWBUDGET routine, it was determined that the rate at which the aquifer is feeding river has declined in the last decade, due to a lack of recharge. While the Volturno river leakage is gradually on the ascendancy, enhancing the aquifer salinization during drought periods when the Volturno river waters are mainly saline or brackish.

The scenario modelling exercise confirmed that the salinization of the aquifer is prevalently imputable to paleo salinity respect to the actual seawater intrusion salinization mechanisms. The scenario modelling exercise enable to quantify the paleo salinity and actual seawater intrusion salinity patterns as well as it was determined that actual seawater intrusion is gradually increasing in the last decade. It can be concluded that, with such a complex tridimensional and variable density numerical modelling the major salinization mechanisms within a coastal aquifer can be estimated in the following order: paleo seawater presence>>seawater ingression in the Volturno river>>seawater wedge along the coast>evapoconcentration via evapotranspiration processes.

## 5.0 REFERENCES

- Aeschbach-Hertig, W., Gleeson, T. (2012). Regional strategies for the accelerating global problem of groundwater depletion. *Nature Geoscience* 5(12), 853-861. <https://doi.org/10.1038/ngeo1617>
- Ackerman, C.T., Jensen, M.R., Brunner, G.W. (2010). Geospatial capabilities of HEC-RAS for model development and mapping. In Proceedings of the 2<sup>nd</sup> Joint Federal Interagency Conference, Las Vegas, NV, USA (Vol. 27).
- Anderson, M.P., Woessner, W.W., Hunt, R.J. (2015) Applied groundwater modelling: simulation of flow and advective transport. Academic press, Elsevier, London.
- ARPAC (2023). Online database on surface water quality of Campania Region. <https://dati.arpacampania.it/dataset/monitoraggio-acque-superficiali-s07> Dataset identify number: ARPA: <https://dati.arpacampania.it/dataset/monitoraggio-acque-superficiali-s07> Last access at 13/03/2023.
- Autorità di Bacino del Fiume Volturno (2018). Piano d'azione per la gestione del rischio alluvioni nel bacino del fiume Volturno. Autorità di Bacino del Fiume Volturno.
- Bear, J., Cheng, A.H.D. (2010). Modelling groundwater flow and contaminant transport (Vol. 23, pp. 89-103). Dordrecht: Springer.
- Bonumà, N.B., Reichert, J.M., Rodrigues, M.F., Monteiro, J.A.F., Arnold, J.G., Srinivasan, R. (2015). Modelling surface hydrology, soil erosion, nutrient transport, and future scenarios with the ecohydrological swat model in Brazilian watersheds and river basins. *Tópicos em ciência do solo*. Viçosa, MG: Sociedade Brasileira de Ciência do Solo 9, 241-90.
- Brunner, G.W. (2010). HEC-RAS River Analysis System. Hydraulic Reference Manual. Version 4.1. U.S. Army Corps of Engineers, Hydrologic Engineering Centre, Davis CA
- Busico, G., Buffardi, C., Ntona, M.M., Vigliotti, M., Colombani, N., Mastrociccio, M., Ruberti, D. (2021). Actual and forecasted vulnerability assessment to seawater intrusion via GALDIT-SUSI in the Volturno river mouth (Italy). *Remote Sensing* 13(18), 3632. <https://doi.org/10.3390/rs13183632>
- Buddemeier, R. W., Schloss, J. A. (2000). Groundwater Storage and Flow, [Accessed on 2014 August 22]. Available from <http://www.kgs.ku.edu/HighPlains/atlas/apgengw.htm>
- Cao, T., Han, D., Song, X., Trolle, D. (2020). Subsurface hydrological processes and groundwater residence time in a coastal alluvium aquifer: Evidence from environmental tracers ( $\delta^{18}\text{O}$ ,  $\delta^2\text{H}$ , CFCs,  $^3\text{H}$ ) combined with hydrochemistry. *Science of the Total Environment* 743, 140684. <https://doi.org/10.1016/j.scitotenv.2020.140684>
- Corrado, G., Amodio, S., Aucelli, P.P., Pappone, G., Schiattarella, M. (2020). The subsurface geology and landscape evolution of the Volturno coastal plain, Italy: Interplay between tectonics and sea-level changes during the Quaternary. *Water* 12(12), 3386. <https://doi.org/10.3390/w12123386>
- Eswar, D., Karuppusamy, R., Chellamuthu, S. (2021). Drivers of soil salinity and their correlation with climate change. *Current Opinion in Environmental Sustainability* 50, 310-318. <https://doi.org/10.1016/j.cosust.2020.10.015>

- Ferris, L. (2020). Ocean\_data\_tools: A MATLAB toolbox for interacting with bulk freely-available oceanographic data. *Journal of Open Source Software* 5(54), 2497. <https://doi.org/10.21105/joss.02497>
- Ferguson, G., Gleeson, T. (2012). Vulnerability of coastal aquifers to groundwater use and climate change. *Nature climate change* 2(5), 342-345. <https://doi.org/10.1038/nclimate1413>
- Gaiolini, M., Colombani, N., Busico, G., Rama, F., Mastrocicco, M. (2022). Impact of Boundary Conditions Dynamics on Groundwater Budget in the Campania Region (Italy). *Water* 14(16), 2462. <https://doi.org/10.3390/w14162462>
- Gaiolini, M., Colombani, N., Mastrocicco, M., Postacchini, M. (2023). Seawater intrusion assessment along the Volturno River (Italy) via numerical modelling and spectral analysis. *Journal of Hydrology* 626, 130289. <https://doi.org/10.1016/j.jhydrol.2023.130289>
- Gossel, W., Sefelnasr, A., Wycisk, P. (2010). Modelling of paleo-saltwater intrusion in the northern part of the Nubian Aquifer System, Northeast Africa. *Hydrogeology Journal* 18, 1447-1463. <https://doi.org/10.1007/s10040-010-0597-x>
- Guo, W., Langevin, C.D. (2002). User's guide to SEAWAT; a computer program for simulation of three-dimensional variable-density ground-water flow (No. 06-A7). <https://doi.org/10.3133/twri06A7>
- Harbaugh, A. W., Banta, E.R., Hill, M.C., Mc Donald, M.G. (2000). MODFLOW-2000, the U.S. geological survey modular ground-water model-user guide to modularization concepts and the ground-water flow process. U.S. geological survey. Open-File Report 00-92
- Hussain, M.S., Abd-Elhamid, H.F., Javadi, A.A., Sherif, M.M. (2019). Management of seawater intrusion in coastal aquifers: A review. *Water*, 11(12), 2467. <https://doi.org/10.3390/w11122467>
- Johnson, T. (2007). Battling seawater intrusion in the central & west coast basins. WRD Technical Bulletin, 13. TB13\_Fall07\_Seawater\_Barriers
- Kourgialas, N.N., Dokou, Z., Karatzas, G.P., Panagopoulos, G., Soupios, P., Vafidis, A., Manoutsoglou, E., Schafmeister, M. (2016). Saltwater intrusion in an irrigated agricultural area: combining density-dependent modelling and geophysical methods. *Environmental Earth Sciences* 75, 1-13. <https://doi.org/10.1007/s12665-015-4856-y>
- Lal, M., Sau, B.L., Patidar, J., Patidar, A. (2018). Climate change and groundwater: impact, adaptation and sustainable. *International Journal of Bio-resource and Stress Management* 9(3), 408-415. <https://doi.org/10.23910/IJBSM/2018.9.3.3C0671b>
- Lu, W., Yang, Q., Martín, J.D., Juncosa, R. (2013). Numerical modelling of seawater intrusion in Shenzhen (China) using a 3D density-dependent model including tidal effects. *Journal of Earth System Science* 122, 451-465. <https://doi.org/10.1007/s12040-013-0273-3>
- Manfreda, S., Messina, M., Avino, A., Pizzolla, T., Bonelli, R., Giuzio, L., Totaro, V., Iacobellis, V., Fiorentino, M. Corbelli, V. (2023). Updating flood annual maxima in Southern Italy. In Italian Conference on Integrated River Basin Management.

- Matano, F., Sacchi, M., Vigliotti, M., Ruberti, D. (2018). Subsidence trends of Volturno river coastal plain (northern Campania, southern Italy) inferred by SAR interferometry data. *Geosciences* 8(1), 8. <https://doi.org/10.3390/geosciences8010008>
- Mirzavand, M., Sadatinejad, S. J., Ghasemieh, H., Imani, R., Motlagh, M. S. (2014). Prediction of ground water level in arid environment using a non-deterministic model. *Journal of Water Resource and Protection* 6 (7), e46179. <https://doi.org/10.4236/jwarp.2014.67064>
- Mirzavand, M., Ghazavi, R. (2015). A stochastic modelling technique for groundwater level forecasting in an arid environment using time series methods. *Water Resources Management* 29, 1315-1328. <https://doi.org/10.1007/s11269-014-0875-9>
- McLusky, D.S., Elliott, M. (2004). *The estuarine ecosystem: ecology, threats and management.* (third ed.), Oxford University Press, Oxford (2004).
- Paldor, A., Michael, H.A. (2021). Storm surges cause simultaneous salinization and freshening of coastal aquifers, exacerbated by climate change. *Water Resources Research* 57(5), e2020WR029213. <https://doi.org/10.1029/2020WR029213>
- Parisi, A., Monno, V., Fidelibus, M.D. (2018). Cascading vulnerability scenarios in the management of groundwater depletion and salinization in semi-arid areas. *International Journal of Disaster Risk Reduction* 30, 292-305. <https://doi.org/10.1016/j.ijdrr.2018.03.004>
- Rapporto sullo stato dell'ambiente (2020) “Ministero dell'Ambiente e della Tutela del Territorio e del Mare.”
- Richardson, C.M., Davis, K.L., Ruiz-González, C. Guimond, J.A., Michael, H.A., Paldor, A., Moosdorf, N., Paytan A. (2024). The impacts of climate change on coastal groundwater. *Nature Reviews Earth & Environment* <https://doi.org/10.1038/s43017-023-00500-2>
- Roy, M.P. (2015). Groundwater towards sustainable agriculture-a global challenge. *International Journal of Ecosystems* 5(3A), 86-88. <https://doi.org/10.5923/c.ije.201501.12>
- Ruberti, D., Buffardi, C., Sacchi, M., Vigliotti, M. (2022). The late Pleistocene-Holocene changing morphology of the Volturno delta and coast (northern Campania, Italy): Geological architecture and human influence. *Quaternary International* 625, 14-28. <https://doi.org/10.1016/j.quaint.2022.03.023>
- Simlandy, S. (2015). Importance of groundwater as compatible with environment. *International Journal of Ecosystem* 5(3), 89-92. <https://doi.org/10.5923/c.ije.201501.13>
- Sorgente, R., Di Maio, A., Pessini, F., Ribotti, A., Bonomo, S., Perilli, A., Alberico, I., Lirer, F., Cascella, A., Ferraro, L. (2020). Impact of freshwater inflow from the Volturno river on coastal circulation. *Frontiers in Marine Science* 7, 293. <https://doi.org/10.3389/fmars.2020.00293>
- Subedi, A.S., Sharma, S., Islam, A., Lamichhane, N. (2019). Quantification of the effect of bridge pier encasement on headwater elevation using HEC-RAS. *Hydrology* 6(1), 25. <https://doi.org/10.3390/hydrology6010025>

- Tamiru, H., Dinka, M.O. (2021). Application of ANN and HEC-RAS model for flood inundation mapping in lower Baro Akobo River Basin, Ethiopia. *Journal of Hydrology: Regional Studies* 36, 100855. <https://doi.org/10.1016/j.ejrh.2021.100855>
- Tarolli, P., Luo, J., Straffelini, E., Liou, Y.A., Nguyen, K.A., Laurenti, R., Masin, R., D'Agostino, V. (2023). Saltwater intrusion and climate change impact on coastal agriculture. *PLOS Water* 2(4), e0000121. <https://doi.org/10.1371/journal.pwat.0000121>
- Teatini, P., Gambolati, G., Gonella, M., Brunone, B., Ferrante, M., Marconi, S. (2001). Modelling Seawater Intrusion in the Porto Recanati Aquifer, Italy. In Proc. of the 1st Int. Conf. on 'Saltwater Intrusion and Coastal Aquifers. Monitoring, Modelling, and Management'. D. Quazar and AH-D. Cheng. [teatini-gambolati-gonella-paper-libre.pdf](https://doi.org/10.1016/j.jseaes.2021.104830)
- Thakur, J. K., Singh, S. K., Ekanthalu, V. S. (2017). Integrating remote sensing, geographic information systems and global positioning system techniques with hydrological modelling. *Applied Water Science* 7(4), 1595-1608. <https://doi.org/10.1007/s13201-016-0384-5>
- Vaux, H. (2011). Groundwater under stress: the importance of management. *Environmental Earth Sciences* 62, 19-23. <https://doi.org/10.1007/s12665-010-0490-x>
- Vengosh, A., Helvacı, C., Karamanderesi, İ. H. (2003). Reply to the comment on "Geochemical constraints for the origin of thermal waters from western Turkey" by Umran Serpen and Tahir Öngür. *Applied Geochemistry* 18(7), 1117-1119. [https://doi.org/10.1016/S0883-2927\(02\)00209-3](https://doi.org/10.1016/S0883-2927(02)00209-3)
- Wang, Q., Li, S., Jia, P., Qi, C., Ding, F. (2013). A review of surface water quality models. *The Scientific World Journal* 2013, 231768. <https://doi.org/10.1155/2013/231768>
- Xu, X., Xiong, G., Chen, G., Fu, T., Yu, H., Wu, J., Liu, W., Su, Q., Wang, Y., Liu, S., Shi, X. (2021). Characteristics of coastal aquifer contamination by seawater intrusion and anthropogenic activities in the coastal areas of the Bohai Sea, eastern China. *Journal of Asian Earth Sciences* 217, 104830. <https://doi.org/10.1016/j.jseaes.2021.104830>
- Yang, J., Townsend, R.D., Daneshfar, B. (2006). Applying the HEC-RAS model and GIS techniques in river network floodplain delineation. *Canadian Journal of Civil Engineering* 33(1), 19-28. <https://doi.org/10.1139/105-102>
- Yao, Y., Tian, Y., Andrews, C., Li, X., Zheng, Y., Zheng, C. (2018). Role of groundwater in the dryland ecohydrological system: A case study of the Heihe River Basin. *Journal of Geophysical Research: Atmospheres* 123(13), 6760-6776. <https://doi.org/10.1029/2018JD028432>
- Yoon, B. I., Woo, S. B. (2015). The along-channel salinity distribution and its response to river discharge in tidally-dominated Han River Estuary, South Korea. *Procedia Engineering* 116, 763-770. <https://doi.org/10.1016/j.proeng.2015.08.362>
- Yu, S., Jiao, J. J., Luo, X., Li, H., Wang, X., Wang, Q., Yao, M., Guo, Y., Deng, Z., Zuo, J. (2023). Vertical leaching of paleo-saltwater in a coastal aquifer-aquitard system of the Pearl River Delta. *Journal of Hydrology* 626, 130168. <https://doi.org/10.1016/j.jhydrol.2023.130168>
- Zhang, X., Hu, L., He, M. X. (2009). Scattering by pure seawater: Effect of salinity. *Optics Express* 17(7), 5698-5710. <https://doi.org/10.1364/OE.17.005698>

Zeng, Y., Huai, W. (2014). Estimation of longitudinal dispersion coefficient in rivers. Journal of Hydro-Environment Research 8(1), 2-8. <https://doi.org/10.1016/J.JHER.2013.02.005>